A STUDY OF THE EFFECT OF PERIODIC STRUCTURE ON THE ATTENUATION PERFORMANCE OF THE MUFFLERS

SHI XIAOFENG

Ph.D

The Hong Kong Polytechnic University

2016

The Hong Kong Polytechnic University

Department of Building Services Engineering

A Study of the Effect of Periodic Structure on the Attenuation Performance of the Mufflers

Shi Xiaofeng

A thesis submitted in partial fulfillment of the requirements for the Degree of Doctor of Philosophy

June, 2015

CERTIFICATE OF ORIGINALITY

I hereby declare that this thesis is my own work and that, to the best of my knowledge and belief, it reproduces no material previously published or written, nor material that has been accepted for the award of any other degree or diploma, except where due acknowledgement has been made in the text.

________________________________(Signed)

Shi Xiaofeng (Name of student)

Department of Building Services Engineering

The Hong Kong Polytechnic University

Hong Kong, China

June, 2015

Dedication

To my parents

Shi Youlu and Zhang Shilan

who always support me with warm care

Abstract

The use of multiple mufflers is often a way used to improve the sound attenuation performance of the mufflers. When the mufflers are periodically mounted on the duct, the transmission loss of the periodic mufflers is determined by the characteristics of both the muffler itself and the periodic structure. This thesis therefore provides a systematic investigation of the effect of the periodic arrangement on the transmission loss of the mufflers including the simple expansion chamber muffler and the micro-perforated muffler. The study on the wave propagation in such periodic structures provides how the periodic structure influences the performance of the mufflers which can contribute to the design of the periodic mufflers.

The theory of various mufflers is investigated. For resonator mufflers, the resonance frequency is mainly determined by its physical parameters. In order to adapt to the changes, a semi-active resonator via the control of the termination impedance of the resonator is used. A theoretical study is conducted to investigate the effect of flow on the semi active Helmholtz resonator in a low Mach number flow duct. To improve the attenuation of the Helmholtz resonator at lower frequencies, a Helmholtz resonator with a spiral neck is proposed and the theoretical results show that the resonance frequency can be effectively lowered by incorporating the spiral neck which have potential application of tonal noise control within a limited space.

The expansion chamber muffler is an effective device for noise reduction in duct systems. The transmission loss of the single expansion muffler has a periodic character that is often used for the periodic noise control. The Bloch wave theory and the transfer matrix method are used to study the wave propagation in periodic expansion chamber mufflers and the dispersion characteristics are examined. The theory is validated against finite element method simulation. Compared to a single expansion chamber muffler, the stopbands of the finite periodic structure is mainly due to its dispersion characteristics. With different configuration, the results indicate that the periodic structure can enhance the transmission loss within a narrower frequency range or change effective noise control frequency ranges with different distance between mufflers.

Because of the high acoustic resistance and low mass reactance due to the sub-millimeter perforation, the micro-perforated muffler can provide considerable sound attenuation of duct noise. The wave propagation in periodic micro-perforated mufflers is studied theoretically, numerically and experimentally. This study indicates that the combination of the Bragg reflection due to the periodic structure and the resonance of the micro-perforated muffler can result in different transmission loss. The proposed periodic placement of micro-perforated mufflers can provide lower frequency noise control within a broader frequency range or enhance transmission loss around the resonant frequency.

Publications Arising from the Thesis

Published papers

Xiaofeng Shi and Cheuk Ming Mak. Helmholtz resonator with a spiral neck. *Applied Acoustics* **99**, 68-71 (2015).

Xiaofeng Shi, Cheuk Ming Mak and Jun Yang. Attenuation Performance of a semi-active Helmholtz resonator in a grazing flow duct. *Open Journal of Acoustics* **3**, 25-29 (2013).

Conference paper

Xiaofeng Shi, Cheuk Ming Mak and Jun Yang. The effect of flow on semi active control of duct noise by a Helmholtz resonator. Proceeding of Inter-noise 2011, Osaka, Japan, 2011.

Xiaofeng Shi, Cheuk Ming Mak and Junfang Wang. Effect of a low mach number flow on a semi active Helmholtz resonator. 19th International Congress on Sound and Vibration, Vilnius, Lithuania, 2012

Paper under review

Xiaofeng Shi and Cheuk Ming Mak. Sound attenuation of a periodic array of micro-perforated tube mufflers. Submitted to *Journal of Sound and Vibration* (2015).

Xiaofeng Shi and Cheuk Ming Mak. Transmission loss of periodic expansion chamber mufflers. Submitted to *Acta Acustica united with Acustica* (2015).

Acknowledgements

First of all, I wish to express my sincerest appreciation to my chief supervisor, Prof. Mak Cheuk-ming, who always offered his thoughtful insight and warm encouragement throughout my studies. The study cannot be completed without his patient guidance and support.

I would also like to take this opportunity to thank my co-supervisor, Prof. Yang Jun, for his valuable advice and help during my study.

Furthermore, I would like to thank all the members in my research group. Their kind assistance and thoughtful advice helped me a lot in my studies and my life. I will treasure the friendship with them all my life. I would also like to thank all the staff and technicians for their kind support during the experimental works.

Finally, I would like to express my deepest appreciation to my mother, father and my sister. I could not have finished my work without their understanding, support and encouragement.

Table of Contents

Nomenclature

C_{HR}	Compliance of the Helmholtz resonator
c	Speed of sound
d	Distance between periodic mufflers
d_1	Diameter of the circular duct
d_2	Diameter of the single expansion chamber
d_h	Hole diameter of the micro-perforation
e^{-jqh}	Eigenvalue of the transfer matrix of the periodic mufflers
F	A factor representing the flow change as a result of the curvature in the duct
f_0	Resonance frequency of the Helmholtz resonator
h	Periodic distance of the periodic mufflers
I_n	Amplitude of the incident plane wave in the n^{th} cell of the periodic mufflers
k	Wave number
L	Muffler length
L_c	Cavity length of the Helmholtz resonator
L_n	Neck length of the Helmholtz resonator
L_B	Equivalent length of the spiral duct
L_I	Length of straight duct I of the spiral neck
L_{II}	Length measured at the midline of the spiral duct
L_{III}	Length of straight duct III of the spiral neck

m	Area ratio of the expansion chamber and the duct
M	Mach number
M_{HR}	Inertance of the Helmholtz resonator
p_1	Sound pressure upstream at the junction of the side branch
p_2	Sound pressure downstream at the junction of the side branch
p_b	Sound pressure of the side branch at the junction
p_i	Sound pressure of incident plane wave
p_{iec}	Sound pressure of the incident plane wave in the expansion chamber
p_{in}	Sound pressure at the inlet of an acoustical element
p_r	Sound pressure of reflected plane wave
p_{rec}	Sound pressure of the reflected plane wave in the expansion chamber
p_{out}	Sound pressure at the outlet of an acoustical element
p_t	Sound pressure of the transmitted plane wave of the expansion chamber
R	The distance from the point to the curvature center
R_0	Curvature radius of the midline of the spiral duct
R_f	Resistance of the Helmholtz resonator introduced by flow
R_n	Amplitude of the reflected plane wave in the n^{th} cell of the periodic mufflers
R_{HR}	Resistance of the Helmholtz resonator
r_0	Radius of the cross sectional area of the spiral duct
r_n	Neck radius of the Helmholtz resonator
r_c	Cavity radius of the Helmholtz resonator

S	Cross sectional area of the duct
S_1	Cross sectional area of the main duct
S_2	Cross sectional area of the expansion chamber
S_c	Circular cross-sectional area of the cavity of the Helmholtz resonator
S_d	Cross sectional area of a rectangular duct
S_n	Circular cross-sectional area of the neck of the Helmholtz resonator
S_B	Equivalent cross-sectional area of the spiral duct
$\mathbf{T}$	Transfer matrix of an acoustical element
t	Thickness of the micro-perforation
TL	Transmission Loss
u^*	Friction velocity at the boundary surface
u_i	Particle velocity of the incident plane wave
u_{iec}	Particle velocity of the incident plane wave in the expansion chamber
u_{in}	Particle velocity at the inlet of an acoustical element
u_{out}	Particle velocity at the outlet of an acoustical element
u_r	Particle velocity of the reflected plane wave
u_{rec}	Particle velocity of the reflected plane wave in the expansion chamber
u_t	Particle velocity of the transmitted plane wave of the expansion chamber
V	Cavity volume of the Helmholtz resonator
$\mathbf{v}$	Eigenvector of the transfer matrix of the periodic mufflers
Z_{HR}	Impedance of the Helmholtz resonator
z	Non-dimensional acoustic impedance of the micro-perforation

ΔL	Sum of the end correction at the inner and outer neck ends
η	Air viscosity
κ	Bend abruptness
ρ	Density
ρ_0	Ambient density of the medium
σ	Micro-perforation porosity (the ratio of the micro-perforated area to the area of the panel)
ϕ	Curvature angle

List of Figures

List of Tables

Chapter 1

Introduction

1.1 Duct noise control methods

In modern buildings, a ductwork system is an essential part of the Heating Ventilation and Air Conditioning (HVAC) system and the ductwork system is mainly used for air exchange and heat transfer. The ducts bring in fresh air and give out warm exhaust in order to provide a comfortable environment for building users and also the equipment. However, the air conditioning units such as fans produce air-borne sound and the sound propagates along the ducts and finally emits as noise into the indoor environment. Besides, the ducts itself also generate noise when air flow passes through especially when the flow speed is high.

As the widely application of air conditioning system in modern buildings, the noise problem is of great concern as it imposes a detrimental impact on the occupants and machines in the buildings. Therefore, various noise control methods have been developed to eliminate the noise throughout the sound propagation path. The control methods can be categorized into three types: passive noise control, active noise control and semi-active control.

1.1.1 Passive noise control

Passive noise control can be classified as dissipative noise control or reactive noise control based on whether the energy is dissipated into heat or the sound is reflected due to acoustic impedance mismatch. In practice, combination of the dissipative noise control and the reactive noise control is often used in the design of the mufflers.

A. Dissipative noise control

The dissipative noise control devices generally attenuate the noise with sound absorbing materials lined within the duct where the sound waves propagates. The friction between the sound waves and the porous absorptive materials degrades the energy by converting the sound energy into heat. The dissipative mufflers usually can effectively attenuate medium to high frequency noise[1].

The performance of the dissipative mufflers is governed by the cross dimensions of the duct, lining thickness and the physical properties of the absorptive materials such as porosity, flow resistivity and thermal characteristics. The theory of the lined duct was started by Morse[2] in 1939. He presented an exact solution for the transmission loss of sound inside a rectangular lined duct with no flow. Scott[3] analyzed the acoustic attenuation in infinite rectangular and circular lined ducts in terms of bulk-reacting model. Davis et al.[4] conducted a systematic study on the evaluation of the mufflers with no flow to predict muffler characteristics. Later, a number of studies were conducted on the performance of the dissipative mufflers in flow ducts. Ko[5] investigated the sound transmission loss in acoustically lined flow ducts separated by porous splitters. Nilsson and brander[6] presented a theoretical model of wave propagation in cylindrical ducts with mean flow and bulk-reacting lining and the effects of a perforate screen was examined. Cummings and Chang[7] investigated a finite-length dissipative muffler and studied the effect of the mean flow on the performance of the dissipative devices in circular ducts. Peat[8] obtained the transfer matrix for a dissipative muffler for evaluating the acoustical performance with a low frequency approximation method. Wang[9] developed a de-coupling method based on the plane wave propagation to study the performance of a resonator with absorbent material. Finite element method[10, 11] and boundary element method[12, 13] were also developed to evaluate the acoustic behavior of the dissipative noise control.

B. Reactive noise control

Reactive noise control, also called reflective noise control, suppresses the noise by reflecting sound waves as a result of the impedance mismatches. A reactive muffler is composed of the acoustical element with different impedance such as a side branch resonator or a duct with different transverse areas. The impedance mismatch at the discontinuity junction reflects the acoustic energy back to the source.

A simple expansion chamber muffler is the most basic reactive muffler. It consists of an expansion chamber of larger cross sectional area than that of the main duct. The sound attenuation performance of the expansion chamber muffler can be described in terms of expansion ratio (the ration of the across sectional area of the expansion chamber to that of the duct) and the length of the muffler. The transmission loss is a periodic function with frequency. When the length of the muffler is an odd multiple of quarter-wavelengths, the transmission loss of the muffler reaches maximum[14].

Another type of the reactive muffler is the side branch resonator muffler. The resonator is placed as a side branch of the main duct. It functions by providing a very low impedance in parallel with the impedance of the main duct at the point where the resonator is placed. The side branch resonator can attenuate sound effectively around its resonance frequencies and this type of muffler usually works over very small frequency ranges which can be used to control tonal noise in practice. The side branch resonator may take the form of a short length of pipe[15] or a Helmholtz resonator (HR)[16]. At resonance frequencies, the input impedance of the side branch tends to be minimal which makes the branch element act as a short circuit to the sound wave at the junction and the sound energy is reflected back to upstream.

Stewart investigated the transmission loss of a duct with a branch line in 1925[17]. He presented a theory of acoustic transmission in a duct with a side branch. Next year he extended the theory to the case of Helmholtz resonator as a side branch[18] and concluded that the Helmholtz resonator could provide large acoustic transmission loss when the frequency of the noise source is near its resonance frequency. A typical

Helmholtz resonator is composed of a connecting neck and a backing volume cavity. The Helmholtz resonator is widely used in the control of duct noise due to its high sound absorption property at resonance frequency. Due to the radiation reactance at the end of resonator, an effective length of the resonator neck is taken into account when calculating the resonance frequency instead of the original physical length. Ingard[19] derived the interior end correction for different orifices. Alster[20] extended the classical formulation for calculating the resonance frequencies and increased the accuracy of the classical model. He took the effects of motion of mass in the resonator and found resonance frequencies also depended on the shape of the resonator. However, his theory was only applicable for the known resonator shape function. The classical analysis of resonator was made by lumped parameter method under the assumption that the wavelength is much bigger than the dimension. Tang and Sirignano[21] did not regard the resonator as lumped parameter and built up a model based on the one-dimensional wave propagation inside both the neck and the cavity. They did not consider the end correction and the result indicated that the theory worked well for resonators with a deep cavity or a long neck. Panton and Miller[22] presented a simple method to analysis cylindrical resonator for length much larger than classical model. They demonstrated that the classical model was valid only when length of resonator was less than 1/16 of the wave length. A different formula was proposed to calculate the resonant frequency based on one dimension propagation in the cavity. Chanaud[23] developed new equations for interior and external end corrections for calculation of the resonance frequency. He applied the formula to a rectangular parallelepiped cavity with a symmetrically placed orifice which was circular, rectangular or cross-shaped and. His model gave good predictions for the resonators with extreme cavity dimensions. Later, Chanaud[24] derived another formula for end corrections of resonator with cylindrical cavity. Experiments for both kinds of cavity were performed in the reference and agreed well with the simulation results.

1.1.2 Active noise control

It is known that the passive noise control method does not usually perform well at low frequencies and it is bulky and costly for low frequency noise control. In recent years, much work has been conducted on developing the active noise control (ANC) system since it has advantages over the traditional passive noise system. Active noise control uses a secondary source generating an anti-noise sound field to cancel noise from the primary source. Active noise control systems are more effective at low frequency and usually smaller than passive control system .With the use of adaptive algorithm the ANC system could follow up with the changes of the sources.

The principal of active cancellation of sound was first proposed by Lueg[25] in a 1936 US patent. He proposed to cancel sound by destructive interference and the system consisted of an upstream microphone detecting the plane wave propagating in the duct, a downstream loudspeaker producing an inverted wave to cancel the primary noise and a control system to generate proper drive signal for the loudspeaker. In 1953, Olson and May[26] introduced a different system which did not need the prior knowledge of the primary field and called feedback control. Conover[27] originally introduced harmonic control in 1956. He proposed to achieve best performance by adjusting the amplitude and phase of the individual harmonic manually. However, there was a long time before the widely application of ANC. The control system needs fast real time processing to follow up with the changes of the noise sources and the implementation of the technique came to a reality until 1980s with the development of low-cost fast digital signal processors (DSP).

In Lueg system, it is obvious that the secondary loudspeaker propagates both upwards and downwards and consequently the detect sensor would inevitably sense the sound from secondary loudspeaker which called acoustical feedback. The acoustical feedback badly contaminates the reference signal and deteriorates the system performance seriously. Many researchers tried to eliminate the influence of acoustical feedback. Based on Chelsea's work, Eghtesadi and Leventhall[28] developed a system which employed two secondary loudspeakers powered in antiphase. The microphone was located centrally between the two secondary source and isolated from the upwards of the secondary source by subtracting contributes of the standing wave between the two sources. Swinbanks[29] proposed to generate a directional secondary source with the use of a pair of monopole sources. He showed that if the delay between the two sources was set properly there will be no radiation downwards. However, this method is only applied to limited bandwidth and the frequency response match of two speakers is also difficult in practice. Jessel, Mangiante and Canevet[30, 31] developed the JMC method to produce zero upstream radiation at all frequency. The method used a combination of monopole and dipole sources to generate unidirectional secondary source and hence there was no upstream sound from the secondary source.

Adaptive filter are used in ANC system to make the system response quickly to the changes of the system. The noise source is usually time-varying and non-stationary. Changes of environment such as wind, temperature also influence the property of the source. A little change of the noise source will lead to significant system performance deterioration. Therefore, the controller needs to be adaptive to deal with the variations. Adaptive filter was first used in digital signal processing to cancel the electric noise component and Widrow et.al.[32] presented the concept of adaptive noise cancelling based on previous work in 1975. Later, Burgess[33] applied the adaptive digital filters to active noise control. His simulation implied that the use of adaptive algorithm could significantly improve the performance of the system. Chaplin and Smith[34] developed a control strategy called "waveform synthesis" to adapt to the variations of the system. His method only applied to the periodic noise. Roure[35] described an adaptive active noise control system for an air-conditioning duct with help of the programmable digital filter. Eriksson[36] proposed to solve with the acoustical feedback taken account into the FLMS algorithm. He used an IIR adaptive filter to cancel the unwanted noise and meantime to cancel the influence of the feedback.

1.1.3 Semi-active noise control

Although active noise control is efficient at low frequency and small, it is more costly and requires external power supply such as amplifiers and loudspeakers systems. The electronic equipment usually has a limit lifetime and is less stable than the passive noise control system. Furthermore, the complex control system also implies the potential instability.

An emerging solution is semi-active control. Semi-active noise control method combines both passive and active elements for noise control. The method takes use of the active control to adapt parameters of the passive control system in order to follow the changes of the operating conditions. Less power is needed in the strategy and therefore less instability than the fully active control. Adaptive algorithms can be used to tune the resonant frequency of some adjustable passive resonators for the suppression of transmission noise.

The study on semi active control has been increasing in the past years. Resonators such as quarter-wavelength resonator and Helmholtz resonator are the most common element used in semi active control. It is well known that the resonance frequency of resonator is mainly determined by physical parameters of the resonators. The natural frequency of a Helmholtz resonator can be changed by adjusting the cavity volume and the opening area. Therefore, the resonators could be tuned to reduce noise of different frequency. In a semi-active control system, the resonators are adjusted by control schemes in order to control the time varying noise.

Neise and Koopmann[37] used a quarter-wavelength resonator to reduce the dynamic noise produced by a centrifugal blower. They tuned the resonator by changing the length via a movable end plug in order to achieve better reduction. Lamancusa[38] proposed the use of tuned Helmholtz resonators instead of expansion chamber mufflers in automobiles. He changed the resonator volume by a movable piston and closable partitions in the cavity. He suggested tuning the resonator according to the engine speed and his manually adjust showed good reduction performance. Izumi[39] also presented a tunable resonator by changing the volume of the resonator. The adjustable volume usually was bulky. In order to reduce the volume variable resonator, Izumi[40] later investigated a compacted adjustable Helmholtz resonator. Unlike constructing a volume adjustable resonator he tuned the resonator by varying the opening area. However, the resonator was only applicable to sinusoidal source and the effective bandwidth was narrow.

These resonators were usually controlled manually and no control algorithms were given to achieve optimal tuning. Matsuhisa et al.[41, 42] introduced an automatically control strategy. They investigated noise reduction by a tunable resonator as a side branch in a duct. The experiment showed significantly reduction with the auto adjusting resonator. deBedout et al.[43] developed an adaptive algorithm based on feedback control. The resonator was tuned by the signal detected in duct downstream of the resonator. Optimal tuning was achieved with a gradient descent approach. In order to reducing high frequency noise, Nagaya et al.[44] suggested a new silencer consisting of a two stage Helmholtz resonator: one for low frequency noise attenuation and another for high frequency. Esteve et al.[45] used adaptive Helmholtz resonator to control broadband noise into a rocket payload fairing.

In these studies of active tuning the resonator, the adjustable functional frequency is still mainly around the natural frequency and the effective bandwidth is still narrow. Hence, it is hard to achieve satisfied performance for a wide bandwidth noise. Besides, the tunable mechanical structure is significantly complex and bulky for practical use. Okamoto et al.[46] investigated active noise control via a side branch resonator. The secondary source was mounted at the end of the side branch resonator and less power was required than mounted directly on the duct wall. Radcliffe and Birdsong[47] suggested changing the response of the resonator through the active control rather than tuning the structure. A secondary source was mounted at the end of the resonator to tuning the resonator resonance with a feedback approach. Utsumi[48] theoretically studied the possibility of broad band noise control through modifying the terminator impedance of the resonator. He derived the controller transfer function and demonstrated the efficiency of the method by computer simulation. Yuan[49] proposed an electrically tuned Helmholtz resonator with positive real impedance. The control strategy made the system more reliable and robust. Multiple resonators were used by

Zhao[50] to control multiple noise modes simultaneously. He developed algorithms for identifying the characteristics of all modes and tuning the neck areas of the Helmholtz resonators.

These adaptive algorithm usually tuned resonators by sensing pressure in the downstream duct and the detected signals were often contaminated by the exhaust and other noise. Singh[51] developed a control transfer function based on the phase relationship between the pressure at the top of the closed end of the cavity and the pressure at the neck wall. This method did not detect pressure in ducts and hence eliminated the influence of contamination by exhaust and other unrelated noise. Kook[52] used active control to suppress the associated unwanted noise. He also used a feedback control to adapt to varying flow conditions.

1.2 Periodic structure

Multiple mufflers are often used to enhance the sound attenuation performance. When the mufflers are distributed periodically in a duct, the periodic structure can produce peculiar dispersion characteristics in the overall transmission loss. Acoustic wave propagation in periodic waveguides involves two types of periodic waveguides[53]: waveguides with periodically nonuniform boundaries and uniform waveguides which including periodically scattering inclusions. The solutions of wave propagation in these two types of periodic waveguides were Bloch wave functions.

Many studies have investigated sound propagation in a spatial periodic structure. When the mufflers are distributed periodically in a duct, the periodic structure can produce peculiar dispersion characteristics in the overall transmission loss. At certain frequencies the Bloch wave cannot transmit through the structure which is called stopbands and at certain frequencies the Bloch wave can propagate freely through the periodic structure which is called passbands.

Bradley[53, 54] investigated the time-harmonic acoustic wave propagation in periodic waveguides both theoretically and experimentally. His work showed that the Bloch wave functions were solutions to a broad class of periodic acoustic waveguide. Sugimoto and Horioka[55] examined the dispersion characteristics of waves propagation in a tunnel with an array of Helmholtz resonators and the band structures exhibited as a result of the side branch resonance and the Bragg reflections. Wang and Mak[56, 57] investigated the attenuation performance of the periodic Helmholtz resonators array in a duct system. Owing to the coupling of the periodic structure and the resonator, it was found that the periodic Helmholtz resonators can provide a much broader sound attenuation than a single resonator.

The periodic structure may contain defects sometimes. The defects includes the disorder in the periodic distance and the characteristics of the periodic scattering inclusions. Mead[58] investigated wave propagation through a mono-coupled periodic system with a single disorder. He introduced three types of disorder and found that the introduced disorder resulted in reduced transmission when the frequency is in the passbands of the periodic system. Munday et al.[59] examined a simple one-dimensional acoustic band gap system which is made of a diameter-modulated periodic waveguide theoretically and experimentally. Their results showed that the defects leaded to narrow frequency transmission bands within the stopbands of the periodic waveguide. Wang and Mak[60] discussed the effect of disorder in a periodic Helmholtz resonators array. It was found that the periodic system was sensitive to defects in the periodic distance and might bring significant gaps to the perfect periodic system. However, disorder in geometries of Helmholtz resonators with the periodic distance unchanged did not influence the main attenuation band of the original periodic structure.

1.3 Objective and Scope of Research

This thesis aims to study the effect of the periodic arrangement on the transmission loss of the mufflers. When the mufflers are periodically mounted on the duct, the sound attenuation of the periodic mufflers is determined by the characteristics of both the muffler itself and the periodic structure. This thesis therefore provides a systematic investigation of the effect of the periodic arrangement on the transmission loss of the mufflers including the simple expansion chamber muffler and the micro-perforated muffler.

The first objective of this thesis is to examine the theory of various mufflers including the side branch resonator, the expansion chamber muffler and the micro-perforated muffler. To improve the performance of the side branch Helmholtz resonator, a Helmholtz resonator with a spiral neck is proposed to lower the resonance frequency within a limited space. Besides, in order to adapt to the changes, a semi-active resonator via the control of the termination impedance of the resonator is used. A theoretical study is conducted to investigate the effect of flow on the semi active Helmholtz resonator in a low Mach number flow duct.

The second objective of this thesis is to investigate the wave propagation in a periodic array of expansion chamber mufflers. Although multiple expansion chamber mufflers have been used to improve the sound attenuation performance, there is little works on the transmission loss of the periodic expansion chamber mufflers. The specific objectives are list below:

1) To understand the wave propagation in the periodic expansion chamber mufflers based on transfer matrix method and the Bloch wave theory
2) To evaluate the effect of the periodic structure on the transmission loss of the periodic expansion chamber mufflers

The third objective of this thesis is to investigate the micro-perforated muffler and the transmission loss of an array of periodic micro-perforated mufflers. The development of the acoustic Bloch wave motivates us to combine it with the micro-perforated tube muffler. The specific objectives are list below:

1) To understand the underlying physics related to the micro-perforation and its impact on the muffler performance;
2) To study the wave propagation in the periodic micro-perforated mufflers and obtain the transfer matrix of the micro-perforated muffler in the periodic structure;
3) To investigate the dispersion relation of the periodic micro-perforated mufflers and evaluate the effect of the periodic structure on the transmission loss of the micro-perforated mufflers

1.4 Outline

The thesis is divided into six chapters. Chapter 1 introduces the background of the present work. Literature of related previous work is reviewed and the motivations as well as the objectives of this study are presented.

In Chapter 2, the transmission loss of the side Helmholtz resonator was investigated theoretically and numerically. In order to adapt to the environmental changes, a semi-active resonator via the control of the termination impedance of the resonator is used. A theoretical study is conducted to investigate the effect of flow on the semi active Helmholtz resonator in a low Mach number flow duct.

In Chapter 3, the Helmholtz resonator with a spiral neck is proposed in order to improve the attenuation performance of the Helmholtz resonator at lower frequencies. The transmission loss of the proposed Helmholtz resonator is studied theoretically based on the equivalent of the curved duct. The performance derived from the theoretical prediction are compared with finite element method for validation.

In Chapter 4, a theoretical study of the acoustic attenuation of periodic expansion chamber mufflers is conducted. The transfer matrix of the periodic structure is derived to determine the Bloch wave in periodic expansion chamber mufflers. The dispersion characteristics of periodic mufflers is examined. Periodic expansion chamber mufflers have different transmission loss than a single expansion chamber muffler, which may have potential applications in muffler design.

In Chapter 5, the wave propagation in a periodic array of micro-perforated tube mufflers is investigated theoretically, numerically and experimentally. Because of the high acoustic resistance and low mass reactance due to the sub-millimeter perforation, the micro-perforated muffler can provide considerable sound attenuation of duct noise. The Bloch wave theory and the transfer matrix method are used to study the wave propagation in periodic micro-perforated tube mufflers and the dispersion characteristics of periodic micro-perforated mufflers are examined. The results predicted by the theory are compared with finite element method simulation and the experimental results.

Chapter 6 summarizes the investigation of the present study and together provides suggestions of improving the work for further investigations.

Chapter 2

The Side Branch Resonator Muffler

Side branch elements attached to ducts are very useful devices for suppressing tonal noise in a ductwork system. At the junction, the sound energy is distributed among the duct and the side branch depending on the relative impedances of the junctions. The side branch resonator functions at the frequencies where the impedance of the side branch is relatively low and the side branch is equivalent to a short circuit which suppresses the sound power transmitted to the downstream duct.

2.1 The Side Branch Helmholtz Resonator

2.1.1 Transmission Loss of the side branch

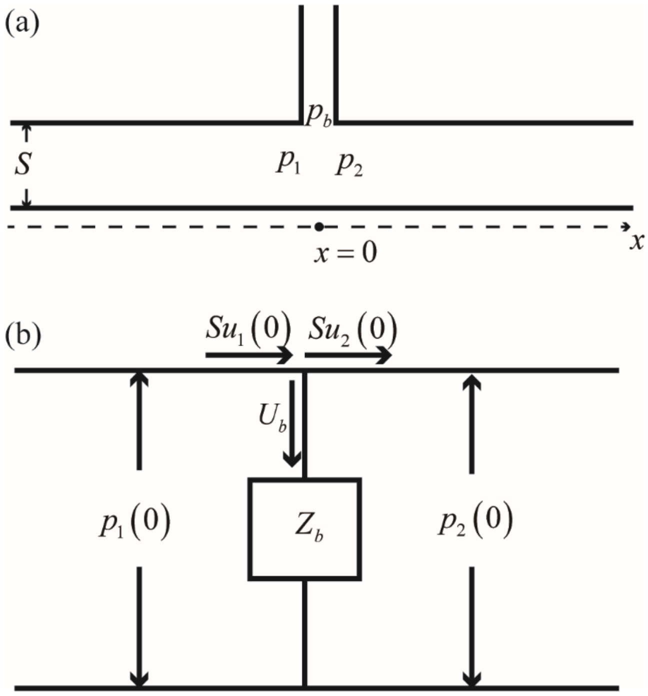

Figure 2-1 A duct with a side branch: (a) acoustical system; (b) equivalent analogous circuit

The configuration of a duct with a side branch is shown in Figure 2-1 and the duct ends in an anechoic termination. Assuming only plane waves propagate in the duct. The cross-sectional area of the duct is *S*. The junction where the side branch joins the duct is set as $x = 0$. The acoustic pressure upstream of the junction is p_1 and the acoustic pressure downstream of the junction is p_2. The acoustic pressures and the particle velocities can be expressed as follows:

$$p_1(x) = A_I e^{j(\omega t - kx)} + A_R e^{j(\omega t + kx)} \tag{2.1}$$

$$p_2(x) = A_T e^{j(\omega t - kx)} \tag{2.2}$$

$$u_1(x) = \frac{1}{\rho_0 c_0}\left[A_I e^{j(\omega t - kx)} - A_R e^{j(\omega t + kx)}\right] \tag{2.3}$$

$$u_2(x) = \frac{1}{\rho_0 c_0} A_T e^{j(\omega t - kx)} \tag{2.4}$$

where ρ_0, c_0 are the density and the sound speed in air, ω is the angular frequency and k is the wave number.

The acoustic pressure of the side branch at the junction is $p_b = A_b e^{j\omega t}$. As indicated in Figure 2-1, the acoustic pressure p_b is the same as the acoustic pressure in the duct at the junction (x = 0) and the volume velocity is continuous.

$$p_1(0) = p_2(0) = p_b \tag{2.5}$$

$$Su_1(0) = Su_2(0) + U_b \tag{2.6}$$

$$U_b = \frac{p_b}{Z_b} \tag{2.7}$$

where Z_b is the acoustic impedance of the side branch at the junction and U_b is the volume velocity of the side branch at the junction. Substituting Eq. (2.1) to (2.4) into Eq. (2.5) and Eq. (2.6), yields

$$A_I + A_R = A_T = A_b \tag{2.8}$$

$$\frac{S}{\rho_0 c_0}(A_I - A_R) = \frac{S}{\rho_0 c_0} A_T + \frac{A_b}{Z_b} \tag{2.9}$$

By eliminating B_1, the relation between A_I and A_T can be expressed as

$$A_I = \left(1 + \frac{\rho_0 c_0}{2SZ_b}\right) A_T \tag{2.10}$$

The transmission loss is defined as the ratio of the incident acoustic power and the transmitted acoustic power. The transmission loss of the side branch can be obtained

$$TL = 20\log_{10}\left|\frac{p_1(x)}{p_2(x)}\right| = 20\log_{10}\left|\frac{A_I}{A_T}\right| = 20\log_{10}\left|1 + \frac{\rho_0 c_0}{2SZ_b}\right| \tag{2.11}$$

For a side branch resonator muffler, the transmission loss is determined by the acoustic impedance of the side branch,

2.1.2 Impedance of the Helmholtz resonator

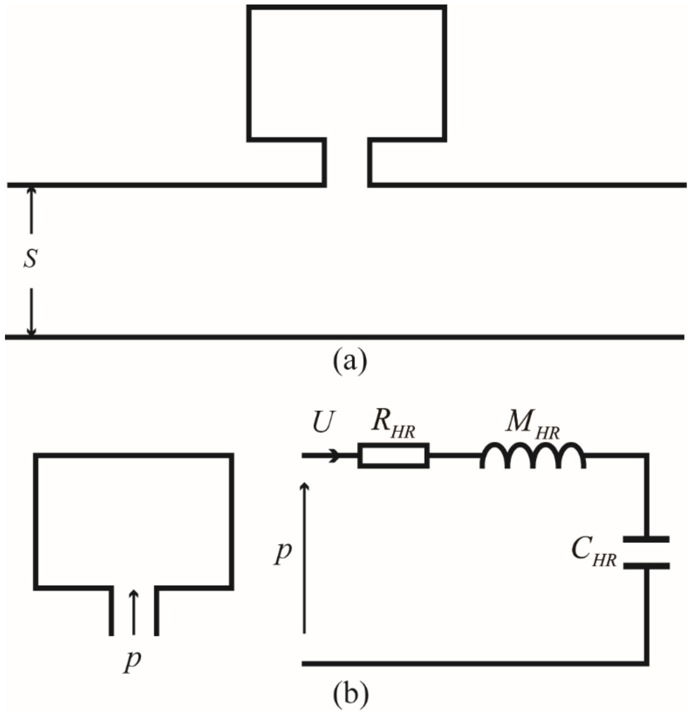

Figure 2-2 (a) The side branch Helmholtz resonator, (b) equivalent analogous circuit of the HR

The Helmholtz resonator consists of a narrow neck and a cavity volume. As shown in Figure 2-2, the side branch is a circular concentric Helmholtz resonator with neck/radius r_n/r_c, circular cross sectional area S_n/S_c, and length L_n/L_c respectively. The Helmholtz resonator is mounted on a rectangular duct with cross sectional area S. When the wave length is much greater than the dimensions of the Helmholtz resonator, the modeling of a Helmholtz resonator can be simplified as a lumped model. The Helmholtz resonator is analogous to a mass-spring system. The air in the neck of the resonator is modeled as a lumped mass element and the air compacted in the cavity volume is modeled as an acoustic compliance. The thermos-viscous losses at the neck walls and the sound radiation at the neck can be modeled as an acoustic resistance. Thus, the impedance of the Helmholtz resonator at the junction is made up of a resistance term, an inertance term and a compliance term:

$$Z_{HR} = R_{HR} + j\left(\omega M_{HR} - \frac{1}{\omega C_{HR}}\right) \tag{2.12}$$

The acoustic mass is given by

$$M_{HR} = \frac{\rho_0 \left(L_n + \Delta L\right)}{S_n} \tag{2.13}$$

where L_n is the length of the neck of the resonator and S_n is the cross sectional area of the resonator. ΔL is the sum of the end correction at the inner and outer neck ends. The end correction is given as[19]:

$$\Delta L = 0.85 r_n \left(1 - 1.25 \frac{r_n}{r_c}\right) + 0.85 r_n \tag{2.14}$$

where r_n and r_c are the radius of the neck and the cavity.

The acoustic compliance is derived based on assuming a uniform pressure throughout the whole cavity and an isentropic compression process.

$$C_{HR} = \frac{V}{\rho_0 c_0^2} \tag{2.15}$$

where $V = S_c L_c$ is the cavity volume and S_c and L_c are the cross sectional area and the length of the cavity.

At low frequencies, the resistance of the Helmholtz resonator can be represented as below[19]

$$R_{HR} = \frac{\rho_0 c_0 k^2}{2\pi} \tag{2.16}$$

where $k = \omega/c_0$ is the wave number. ρ_0, c_0 are the density and the sound speed in the air. The acoustic impedance of the Helmholtz resonator can be expressed as

$$Z_{HR} = R_{HR} + j\left(\omega M_{HR} - \frac{1}{\omega C_{HR}}\right) = \frac{\rho_0 c_0 k^2}{2\pi} + j\left(\frac{\omega\rho_0\left(L_n + \Delta L\right)}{S_n} - \frac{\rho_0 c_0^2}{\omega V}\right) \tag{2.17}$$

2.1.3 Transmission Loss of the side branch Helmholtz resonator

According to Eq. (2.11), the transmission loss of a side branch can be given if the impedance of the side branch at the junction is known. Therefore, with the impedance of the side branch Helmholtz resonator of Eq. (2.17), the transmission loss of a side branch Helmholtz resonator can be calculated.

$$TL = 20\log_{10}\left|1 + \frac{\rho_0 c_0}{2SZ_{HR}}\right| \tag{2.18}$$

The resonance frequency of the Helmholtz resonator is the frequency at which the reactance of the impedance is zero.

$$\frac{\omega\rho_0\left(L_n + \Delta L\right)}{S_n} = \frac{\rho_0 c_0^2}{\omega V} \tag{2.19}$$

The resonance frequency is f_0

$$f_0 = \frac{c_0}{2\pi}\sqrt{\frac{S_n}{\left(L_n + \Delta L\right)V}} \tag{2.20}$$

It can be seen from the Eq. (2.20), the resonance frequency is determined by the geometries of the Helmholtz resonator.

Let the geometries of the Helmholtz resonator be: r_n = 0.01 m, L_n = 0.02 m, r_c = 0.06 m, L_c = 0.1 m. The cross sectional area of the duct is set as 0.12 m*0.12 m. The transmission loss of the side branch Helmholtz resonator according to Eq. (2.18) is plotted in Figure 2-3. The resonance frequency is 153 Hz. It is seen that the side branch resonator can effectively attenuate noise over a narrow frequency range around its resonance frequency.

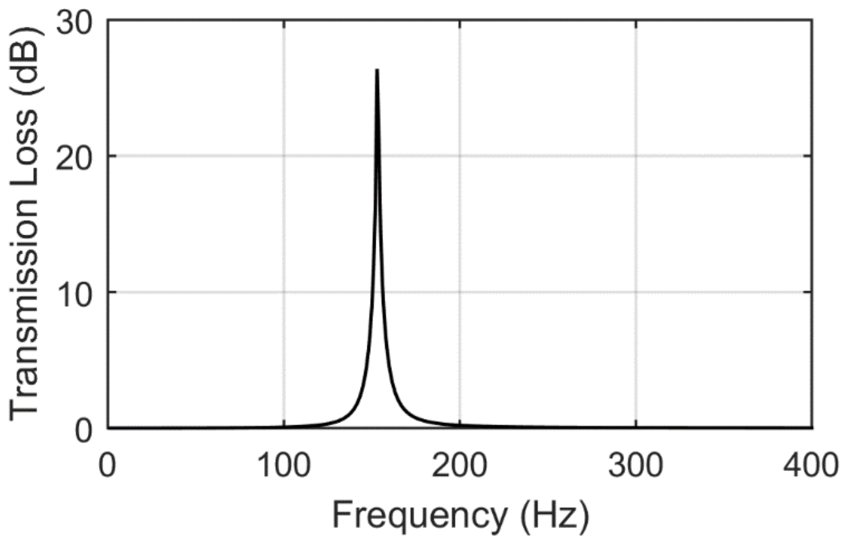

Figure 2-3 Transmission loss of the Helmholtz resonator by theoretical analysis

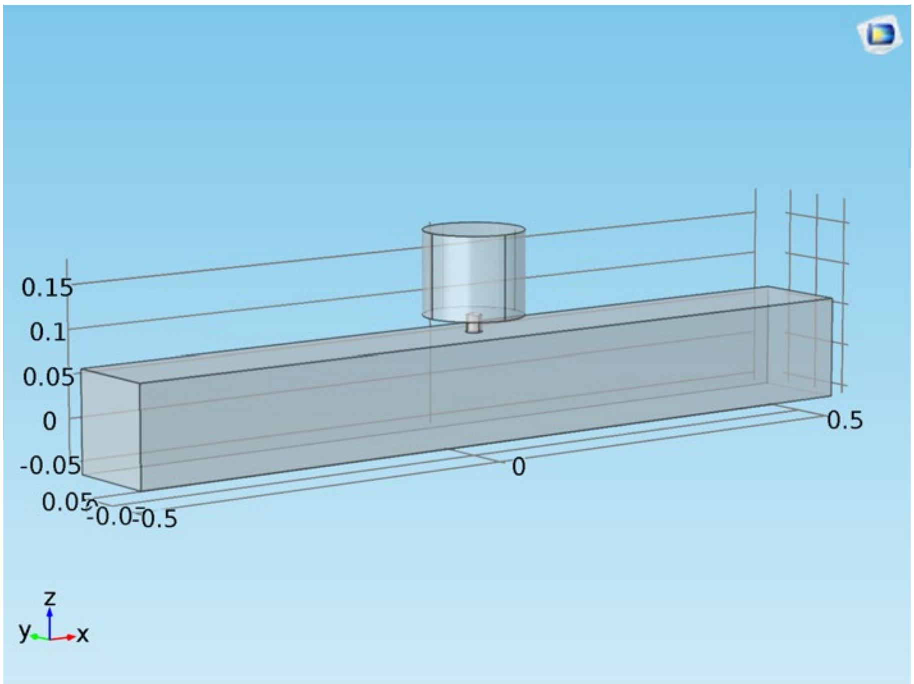

Figure 2-4 The side branch Helmholtz resonator in FEM simulation

To compare with the theoretical results, a three dimensional finite element method (FEM) is used to simulate the side branch Helmholtz resonator. The numerical model consists of a duct with a side branch Helmholtz resonator and an excitation from an oscillating sound pressure at fixed magnitude $P_0 = 1$ at the inlet of the duct. The end termination was set to be anechoic. The configuration of the FEM model is illustrated in Figure 2-4 and the geometries is the same as the theoretical model.

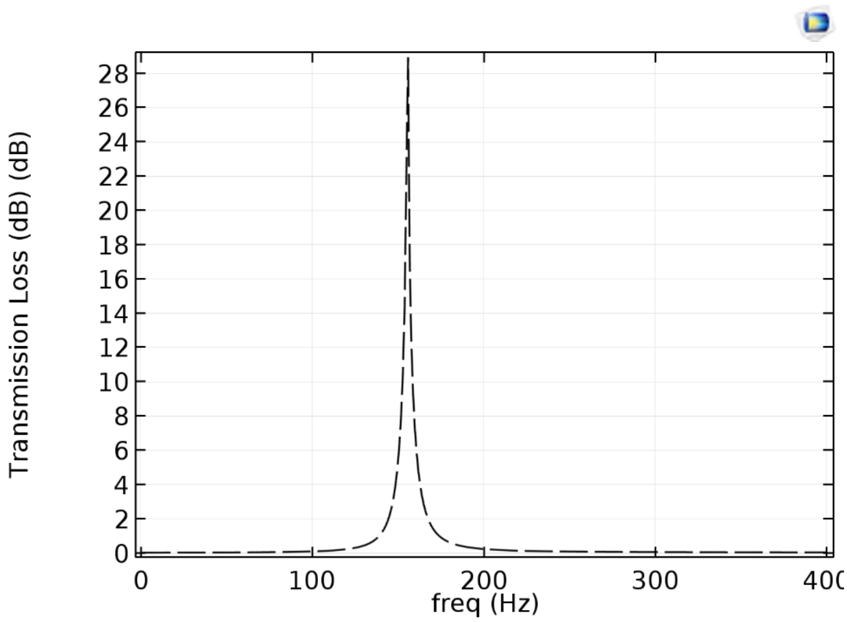

Figure 2-5 Transmission Loss calculated by FEM simulation

Figure 2-5 shows the transmission loss of the side branch Helmholtz resonator based on the FEM method. It is seen that the FEM results is identical with the theoretical results in Figure 2-3. In the FEM results, the resonance frequency is 156 Hz which is a little different from that of the theoretical results shown in Figure 2-3. The difference is due to the end corrections of the length of the Helmholtz resonator is different from the three dimensional FEM simulation.

2.2 Semi-Active Helmholtz Resonator

This study aims at studying the effect of flow on the semi active Helmholtz resonator for duct noise control. First the plane wave propagation in a flow duct is introduced and the discontinuity condition is analytically derived. Then, the control controller transfer function under flow condition is then proposed.

2.2.1 Wave propagates in a mean flow duct

When a plane wave propagates in a mean flow duct, the wave equation is [61]:

$$\left(1-M^2\right)\frac{\partial^2 p}{\partial x^2}+k^2 p-2jkM\frac{\partial p}{\partial x}=0 \tag{2.21}$$

M denotes the Mach number $M = u_0/c$. The solution to the wave equation is:

$$\begin{gathered} p(x)=p^+e^{-jk_+x}+p^-e^{-jk_-x} \\ k_+=\frac{k}{1+M},k_-=\frac{k}{1-M} \end{gathered} \tag{2.22}$$

Eq. (2.22) presents superposition of two progressive waves moving in opposite directions.

When there is a side branch Helmholtz resonator along the flow duct as shown in Figure 2-6. A side-branch Helmholtz resonator is mounted on the side wall of an infinitely duct and the plane wave propagates along the duct. The cross-sectional area of the duct is S. The mean flow in the duct is U_0. The dotted area indicates the pressure discontinuity due to the mean flow. At the connection, the upstream pressure is p_1 and the downstream pressure is p_2. The pressure at the neck of the Helmholtz resonator is p_3 and is assumed to be equal to the upstream pressure at the junction.

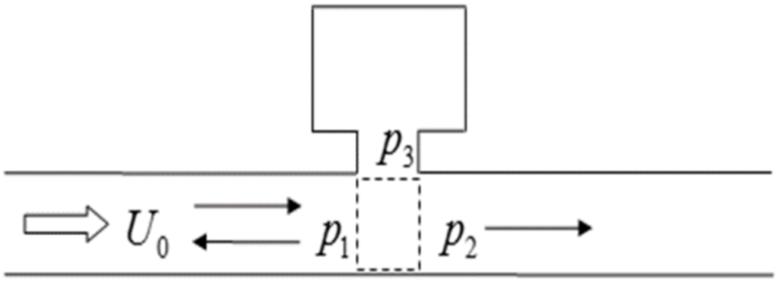

Figure 2-6 A side branch Helmholtz resonator in a grazing flow duct

At the junction, according to Eq. (2.22) the sound pressure can be expressed as follows:

$$p_1 = \left(Ie^{-ik_I x} + Re^{ik_R x} \right) e^{i\omega t} \tag{2.23}$$

$$p_2 = Te^{ik_T x} e^{i\omega t} \tag{2.24}$$

$$\begin{gathered} k_I = \frac{\omega / c_0}{1+M},\ k_R = \frac{\omega / c_0}{1-M}, \\ k_T = \frac{\omega / c_0}{1+M} \end{gathered} \tag{2.25}$$

The fluid particle velocities satisfy the following equation:

$$\frac{Du_1}{Dt} = -\frac{1}{\rho_0}\frac{\partial p_1}{\partial x},\ \frac{Du_2}{Dt} = -\frac{1}{\rho_0}\frac{\partial p_2}{\partial x} \tag{2.26}$$

The propagation of the wave can be characterized by the following equations [62]:

$$\begin{aligned} &\left(P_0 + p_1\right) S + \left(\rho_0 + \rho_1\right)\left(U_0 + u_1\right)^2 S \\ &= \left(P_0 + p_2\right) S + \left(\rho_0 + \rho_2\right)\left(U_0 + u_2\right)^2 S \end{aligned} \tag{2.27}$$

$$\begin{aligned} &\left(\rho_0 + \rho_1\right)\left(U + u_1\right) S \\ &= \left(\rho_0 + \rho_2\right)\left(U + u_2\right) S + \left(\rho_0 + \rho_3\right) S_n u_3 \end{aligned} \tag{2.28}$$

where P_0 is the equilibrium pressure, U_0 is the mean flow velocity and ρ_0 is the equilibrium density. Eq. (2.27) and Eq. (2.28) respectively indicates conservation of momentum and flow mass at the junction. Substituting Eqs. (2.21)-(2.25) into Eq. (2.27) and Eq. (2.28)

$$(1+M)^2 I + (1-M)^2 R = \left(1+M^2\right)T \tag{2.29}$$

$$\begin{aligned} &(1+M-C)I-(1+M+C)R=(1+M)T \\ &C=\rho_0 c_0 / S Z_{HR} \end{aligned} \tag{2.30}$$

R is eliminated from the Eq. (2.29) and Eq. (2.30). Thus, T is indicated with I as follows:

$$\frac{T}{I}=\frac{2\left[(1+M)\left(1+M^2\right)+2CM\right]}{2\left(1+M^3\right)+C\left(1+M^2\right)} \tag{2.31}$$

Eq. (2.31) shows the relationship between transmission wave and incident wave in a grazing flow duct.

2.2.2 Flow effect on acoustic impedance of Helmholtz resonator

As shown in Eq. (2.31), the transmission loss performance of the Helmholtz resonator is mainly determined by the acoustic impedance and the Mach number. The acoustic impedance of Helmholtz resonator can be expressed as below:

$$\begin{aligned} Z_{HR} &= R_{HR} + jX_{HR} \\ &= R_{HR} + j\left(\omega M_{HR} - \frac{1}{\omega C_{HR}}\right) \end{aligned} \tag{2.32}$$

R_{HR} and X_{HR} are respectively the acoustic resistance and the acoustic reactance of the Helmholtz resonator. The resonance frequency $f_0 = 1/\sqrt{M_{HR}C_{HR}} = \sqrt{S/l_{eff}V}$ (l_{eff} is the effective length of the neck) of Helmholtz resonator is determined by the reactance. The acoustic reactance reaches minimum when resonance occurs.

A lot of studies have been conducted on the acoustics impedance of a HR in a grazing flow duct. Although there is no unified model to indicate the flow effect on acoustic impedance of the HR, it is agreed that the flow mainly influence the resistance and the effective length of Helmholtz resonator. Many experimental work shows that acoustic resistance increases linearly and the effective length of the neck decrease as the flow velocity increased. Cummings [63] proposed an empirical impedance model:

$$\frac{R_f c_0}{fd} = \left(12.52\left(\frac{t}{d}\right)^{-0.32} - 2.44\right)\left(\frac{u_*}{fd}\right) - 3.2 \tag{2.33}$$

$$\begin{aligned} \frac{\delta}{\delta_0} &= 1 && \left(\frac{u_*}{ft} \le 0.12\frac{d}{t}\right) \\ \frac{\delta}{\delta_0} &= \left(1+0.6\frac{t}{d}\right)\exp\left[-\frac{\dfrac{u_*}{ft} - 0.12\dfrac{d}{t}}{0.25+\dfrac{t}{d}}\right] - 0.6\frac{t}{d} && \left(\frac{u_*}{ft} > 0.12\frac{d}{t}\right) \end{aligned} \tag{2.34}$$

d and *t* are respectively diameter and the length of the neck of the Helmholtz resonator. R_f denotes resistance introduced by flow. δ is the end correction of the neck with grazing mean flow, δ_0 is the end correction without flow, c_0 is the sound speed in air. u_* is friction velocity at the boundary surface. With Cummings' model, the effect of various flow speeds on a Helmholtz resonator is show in Figure 2-7.

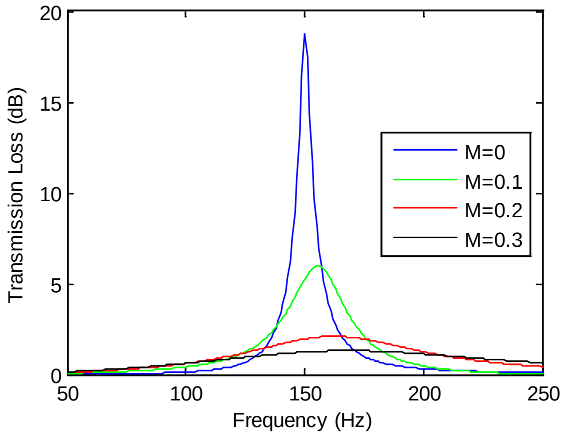

Figure 2-7 Transmission loss of a Helmholtz resonator under different flow condition.

In Figure 2-7, the geometries of the Helmholtz resonator are: cross sectional area of duct $S_d = 0.0144\ \mathrm{m}^2$, resonator orifice area $S_n = 0.0004\ \mathrm{m}^2$, length of the resonator neck is $L_n = 0.03$ m, the cavity of the resonator $V = 0.0014\ \mathrm{m}^3$. From the result shown in Figure 2-7, the transmission loss is influenced in the items of the resonant frequency and the transmission loss amplitude at resonant frequency. As the mean flow speed increased, the resonance occurs at a higher frequency and the transmission loss performance decreased at the higher frequency.

In a practical exhaust ductwork system, the Mach number is normally less than 0.3. In that case, the convective flow effects in the duct can be neglected[64]. The mainly important effect of mean flow is on the acoustic impedance of Helmholtz resonator. The transmission loss is below:

$$TL = 10\log\left[\frac{\left(\rho_0 c_0/2S + R_{HR}\right)^2 + X_{HR}^2}{R_{HR}^2 + X_{HR}^2}\right] \tag{2.35}$$

This equation indicates that the transmission loss reach a peak when the reactance approaching to zero and the resistance significantly influence the sound reduction performance at the resonance frequency. At resonance frequency, the acoustic reactance is close to zero, therefore the transmission loss will be:

$$TL = 10\log\left[\frac{\left(\rho_0 c_0/2S + R_{HR}\right)^2}{{R_{HR}}^2}\right] \tag{2.36}$$

Transmission loss will decrease as the resistance increases. It is known that acoustic resistance increases linearly and the effective length of the neck decrease as the flow velocity increased. Therefore, the flow influences the attenuation performance of Helmholtz resonator in two ways: the resistance at the orifice and the effective length of the neck. The decrease in length end correction results in resonance frequency shifts to a higher frequency and the increased resistance leads to lower transmission loss amplitude at resonance frequency.

2.2.3 Termination impedance control

This formula (2.31) indicates the discontinuity condition due to the mean flow and the flow will reduce the transmission loss performance of Helmholtz resonator. An emerging solution aims to adapt to the changes of the environment is semi active control system. Semi active control method using active noise control strategy adaptively changes the passive resonator to follow the environmental variation.

However, controlling low frequency makes the system bulky and costly. The concept of semi-active control is to control noise by changing the acoustic impedance of Helmholtz resonator. Here we control the acoustic impedance of Helmholtz through controlling end termination impedance instead of physical geometries.

After the discontinuity condition where the main duct joins the side branch Helmholtz resonator is formulated, it is possible to consider reducing the noise via termination impedance control of the side branch Helmholtz resonator.

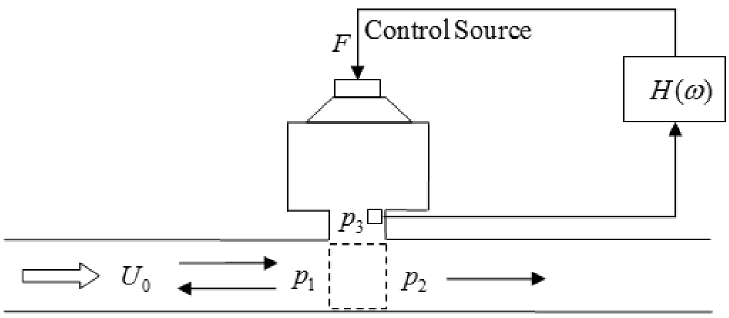

Figure 2-8 Control system model

The system configuration is shown in Figure 2-8. The side Helmholtz resonator is ended by a control source. The termination impedance is controlled by detecting the sound pressure near the resonator neck and the controller function is defined as $H(\omega)$. The acoustic circuit of the semi active Helmholtz resonator is shown in Figure 2-9. The R_{HR}, M_{HR}, and C_{HR} are the acoustic resistance, acoustic inertance, and acoustic compliance of the Helmholtz resonator under flow condition.

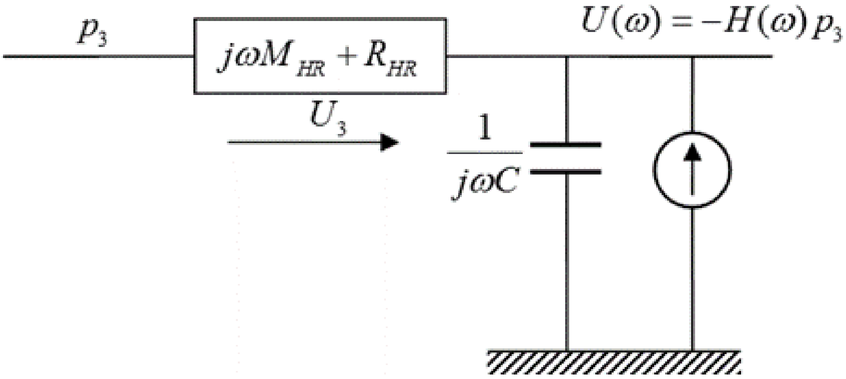

Figure 2-9 Acoustic circuit of the semi active Helmholtz resonator

According to the acoustic circuit, the pressure p_3 can be readily expressed as:

$$p_3 = U_3\left(j\omega M_{HR} + R_{HR}\right) + \frac{U_3 - H(\omega)\,p_3}{j\omega C_{HR}} \tag{2.37}$$

Thus, the impedance of the semi active Helmholtz resonator is:

$$Z_3 = \frac{p_3}{U_3} = \frac{j\omega M_{HR} + R_{HR} + 1/j\omega C_{HR}}{1 + H(\omega)/j\omega C_{HR}} \tag{2.38}$$

Substituting Eq. (2.38) to Eq. (2.31) we can obtain the transmission coefficient with the termination impedance control:

$$\frac{T}{I} = \frac{2\left[\left(1+M\right)\left(1+M^2\right) + 2\frac{\rho_0 c_0}{SZ_3}M\right]}{2\left(1+M^3\right) + \frac{\rho_0 c_0}{SZ_3}\left(1+M^2\right)} \tag{2.39}$$

To suppress the transmitted wave means to let transmission coefficient approach to minimum. Thus, the controller function should be determined such that the Eq. (2.39) equal to zero. Thus, we obtain

$$H(\omega) = j\omega C_{HR}\left[1 + \frac{S}{2\rho_0 c_0 M}\left(1+M\right)\left(1+M^2\right)\left(j\omega M_{HR} + R_{HR} + 1/j\omega C_{HR}\right)\right] \tag{2.40}$$

The controller function is related to impedance of the Helmholtz resonator and the mean flow velocity. Adjusting the controller function could reach maximum transmission loss over a wider frequency range. The mean flow significantly influences the acoustic impedance of the Helmholtz resonator and there is no a unify model to predict the effect of flow on the acoustic impedance of the Helmholtz resonator and it will be determined by investigating the lumped parameters under different air flow velocities experimentally.

2.3 Summary

The side branch resonator muffler is investigated. For a side branch Helmholtz resonator, the resonance frequency is mainly determined by the physical parameters of the resonator. The side branch resonator can effectively attenuate noise over a narrow frequency range around its resonance frequency. The transmission loss of the side Helmholtz resonator was investigated theoretically and numerically.

The performance of the Helmholtz resonator is fixed once the resonator is made. In order to adapt to the environmental changes, a semi-active resonator via the control of the termination impedance of the resonator is used. A theoretical study is conducted to investigate the effect of flow on the semi active Helmholtz resonator in a low Mach number flow duct.

Chapter 3

Helmholtz Resonator with a spiral neck

To improve the sound attenuation performance of a HR at low frequencies, much work has been conducted on making them as small as possible while keeping the effective resonance frequency low enough. Selamet and Lee[65] extended the neck into the cavity and find that this shifted the resonance frequency down within it. Later, Selamet et al.[66] presented another approach to lowering the resonance frequency of a HR by lining it with fibrous material. This was found to lower the resonance frequency and peak transmission loss without changing the cavity dimensions.

Apart from improving the passive control system, researchers have also used active control methods to shift the efficient frequency range of the HR. Radcliffe and Birdsong[47] proposed a means to control the acoustic impedance of the HR by mounting a loudspeaker at the end. The control source was stimulated by a closed-loop adaptive control strategy to change the resonance frequency. Utsumi[48] also investigated a side branch HR with dynamic termination impedance and explored the possibility of broad band noise control through varying the termination impedance.

This chapter focuses on improving the noise reduction performance of HR at low frequency within a limited space. In order to make the neck as long as possible, a spiral duct takes the place of the traditional short neck of the HR. The curved structure lengthens the neck without requiring a large space. The wave propagation in the spiral duct neck is analyzed and the acoustic impedance formulated based on the transfer matrix method. The results show that the resonance frequency of the HR can be reduced by using the spiral neck, which has potential applications in tonal noise control in a limited space.

3.1 Wave propagation in the spiral neck

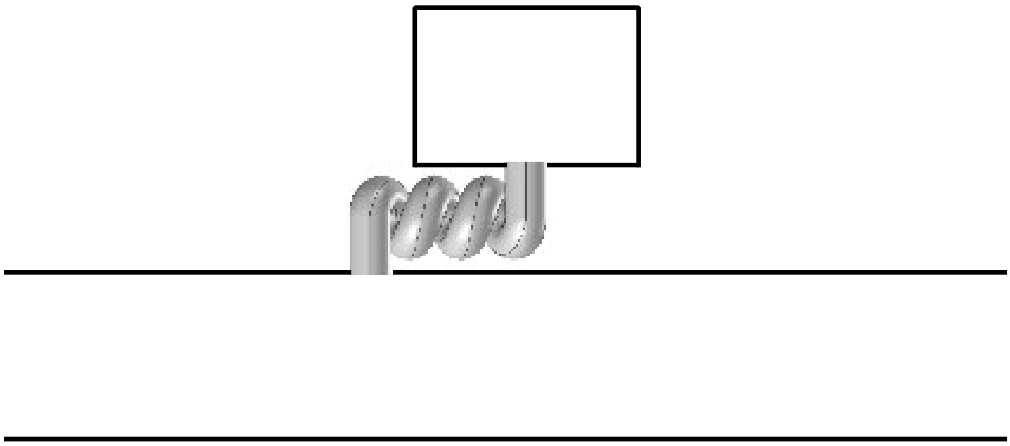

Figure 3-1 The Helmholtz resonator with a spiral neck

Figure 3-1 illustrates a Helmholtz resonator mounted on a rectangular duct with cross-sectional area S_d. Unlike the traditional straight duct neck, the neck considered in this study is a spiral duct of circular cross-sectional area S_n. The cavity of the Helmholtz resonator is a circular duct of cross-sectional area S_c and length L_c.

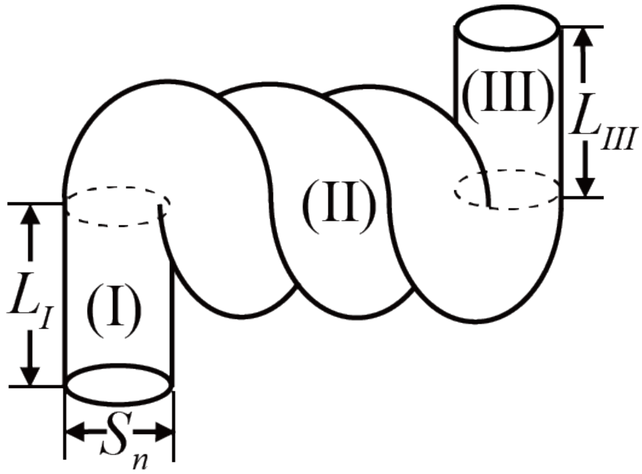

Figure 3-2 The spiral neck with three turns

As shown in Figure 3-2, the spiral neck can be divided into three parts: straight duct I of length L_I, spiral duct II of length L_{II} measured at the midline, and straight duct III of length L_{III}. The spiral neck has three turns and compacts the long neck within a smaller space. The spiral duct has a circular cross section of radius r_0 and its midline has a curvature radius R_0 as shown in Figure 3-3.

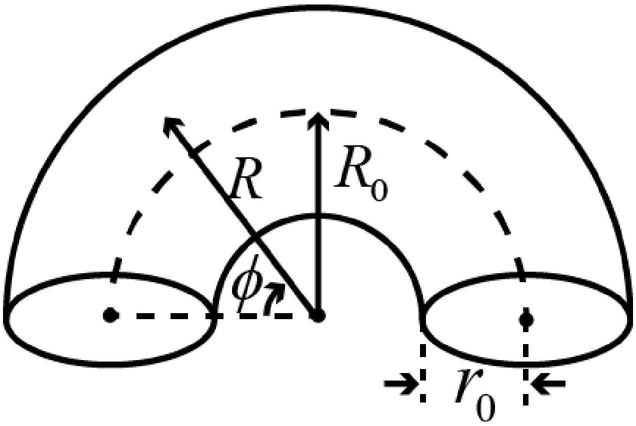

Figure 3-3 A section of the curved duct

The spiral duct takes N turns and the length L_{II} is N*2π*R_0. From Newton's Second Law, the particle velocity along the toroidal axis is:

$$v(R,\phi) = \frac{-1}{j\omega\rho_0}\left[\frac{1}{R}\frac{\partial p}{\partial \phi} + \frac{\partial p}{\partial R}\right] \tag{3.1}$$

where p is the pressure, ω is the angular frequency, ρ_0 is the medium density, ϕ is the curvature angle, and R is the distance from the point to the curvature center. Nederveen[67] assumed the radial dependence of the pressure is small at low frequency which meant the pressure is the same over the cross section; this is valid for the frequency range discussed in this study. Therefore, the particle velocity is:

$$v(R,\phi) = \frac{-1}{j\omega\rho_0}\frac{1}{R}\frac{\partial p}{\partial \phi} \tag{3.2}$$

The volume velocity in the duct in terms of the axial pressure gradient at the midline and the volume velocity in the bent duct is expressed:

$$U = \pi r_0^2 \frac{-1}{j\omega\rho_0} \frac{1}{F} \frac{\partial p}{\partial (R_0\phi)}$$
$$F = \frac{0.5\kappa^2}{1-\sqrt{1-\kappa^2}} \qquad \kappa = \frac{r_0}{R_0} \tag{3.3}$$

The ratio $\kappa = r_0/R_0$ indicates the abruptness of the bend and the factor F represents the flow change as a result of the curvature in the duct. The effect of the curvature is described as a change in the input impedance of the duct. For a spiral duct of cross-sectional area S_n and length L_{II} measured at the midline, the input impedance of the spiral duct can be written as a straight circular duct with cross-sectional area S_B and length L_B:

$$S_B = S_n / \sqrt{F}$$
$$L_B = L_{II}\sqrt{F} \tag{3.4}$$

This means the spiral duct can be seen as an equivalent straight tube with cross area S_B and length L_B. According to Eq. (3.3), the factor F is always less than 1. The equivalent circular duct is wider and shorter than the original spiral duct. Therefore, the spiral neck can be equivalent to the combination of three connected straight ducts as shown in Figure 3-4 and it is obviously that the spiral neck is different from a straight duct neck with the same length as a result of the curvature effect of the bend duct.

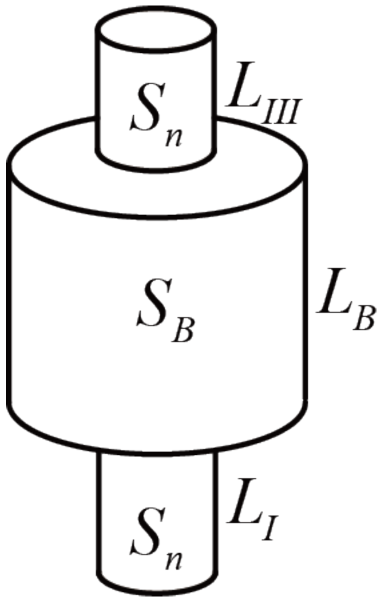

Figure 3-4 The equivalent of the spiral neck

3.2 Impedance of the spiral HR

The transfer matrix for a straight circular duct of area S and length L is given by Munjal[1]:

$$\begin{bmatrix} p_{in} \\ U_{in} \end{bmatrix} = \begin{bmatrix} \cos kL & -j\dfrac{\rho_0 c_0}{S}\sin kL \\ j\dfrac{S}{\rho_0 c_0}\sin kL & \cos kL \end{bmatrix} \begin{bmatrix} p_{out} \\ U_{out} \end{bmatrix} \tag{3.5}$$

p_{in}, U_{in} and p_{out}, U_{out} are the acoustic pressures and volume velocities at the input and output ends of the duct, respectively. L is the effective length of the duct which includes two end corrections at each side.

Figure 3-1 illustrates a duct system with a side branch Helmholtz resonator. The impedance of the HR can be calculated by the transfer matrix between the inlet of the neck and the end of the cavity. As shown in Figure 3-2, the neck section can be divided into three parts; straight duct I, equivalent straight duct II, and straight duct III. $\mathbf{T}_I$, $\mathbf{T}_{II}$, and $\mathbf{T}_{III}$ are respectively the transfer matrices of the three parts. $\mathbf{T}_c$ is the transfer matrix of the cavity. According to Eq. (3.5), theses transfer matrices can be expressed as follows

$$\mathbf{T}_I = \begin{bmatrix} \cos kL_{Ie} & -j\dfrac{\rho_0 c_0}{S_n}\sin kL_{Ie} \\ j\dfrac{S_n}{\rho_0 c_0}\sin kL_{Ie} & \cos kL_{Ie} \end{bmatrix} \tag{3.6}$$

$$\mathbf{T}_{II} = \begin{bmatrix} \cos kL_B & -j\dfrac{\rho_0 c_0}{S_B}\sin kL_B \\ j\dfrac{S_B}{\rho_0 c_0}\sin kL_B & \cos kL_B \end{bmatrix} \tag{3.7}$$

$$\mathbf{T}_{III} = \begin{bmatrix} \cos kL_{IIIe} & -j\dfrac{\rho_0 c_0}{S_n}\sin kL_{IIIe} \\ j\dfrac{S_n}{\rho_0 c_0}\sin kL_{IIIe} & \cos kL_{IIIe} \end{bmatrix} \tag{3.8}$$

$$\mathbf{T}_c = \begin{bmatrix} \cos kL_c & -j\dfrac{\rho_0 c_0}{S_c}\sin kL_c \\ j\dfrac{S_c}{\rho_0 c_0}\sin kL_c & \cos kL_c \end{bmatrix} \tag{3.9}$$

Therefore, the pressure and the volume velocity between the inlet of the neck and the end of the cavity can be written as

$$\begin{bmatrix} p_1 \\ U_1 \end{bmatrix} = \mathbf{T}_I \mathbf{T}_{II} \mathbf{T}_{III} \mathbf{T}_c \begin{bmatrix} p_2 \\ U_2 \end{bmatrix} = \begin{bmatrix} A & B \\ C & D \end{bmatrix} \begin{bmatrix} p_2 \\ U_2 \end{bmatrix} \tag{3.10}$$

where p_1, U_1 and p_2, U_2 are the acoustic pressures and volume velocities at the neck and the end of the cavity of the Helmholtz resonator, respectively. L_{Ie} and L_{IIIe} are the effective length of the straight duct I and straight duct III which including the end correction effects. Eq. (3.10) gives the overall transfer matrix of the Helmholtz resonator.

Assuming the wall of the cavity is rigid, which means that the volume velocity at the end of the cavity is zero $U_2 = 0$, the Eq. (3.10) will be

$$p_1 = Ap_2 \tag{3.11}$$

$$U_1 = Cp_2 \tag{3.12}$$

Therefore, the input impedance of the HR can be expressed as:

$$Z_{in} = \frac{p_1}{U_1} = \frac{A}{C} \tag{3.13}$$

Once the input impedance of the Helmholtz resonator determined, the transmission loss of a side HR can be described as[1]:

$$TL = 20\log_{10}\left|\frac{\rho_0 c_0 / 2S_d + Z_{in}}{Z_{in}}\right| \tag{3.14}$$

3.3 Results and discussion

3.3.1 Validation of the FEM model

The three-dimensional finite element method (FEM) is used to enable comparison with the theoretical analysis. Firstly, a duct with a bent portion is calculated. The model described in Figure 3-5 is the same as given in the literature[68] and consists of two straight circular and one bent duct. The geometries are illustrated in Figure 3-5. The sound source is located at the beginning of the duct and the output end is set as rigidly closed.

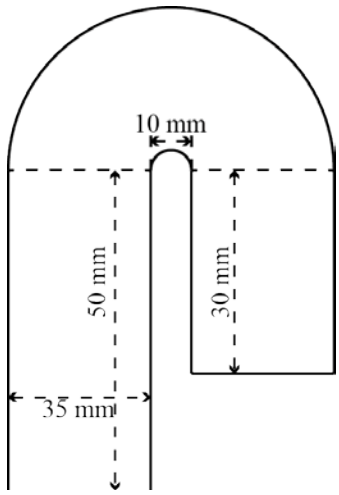

Figure 3-5 A curved duct with a close end

Figure 3-6 shows the model of the curved duct with a close end in FEM simulation. The geometries are set the same as shown in Figure 3-5. The boundaries of the duct are set as rigid. The duct at left side is the inlet and the duct at the right side is the outlet. The inlet of the curved duct is set as the plane wave radiation boundary condition and the outlet of the duct is set as a rigid wall.

A probe is located at the center of the inlet of the curved duct to measure the sound pressure and the particle velocity. Then the non-dimensional input impedance can be evaluated with the measured sound pressure and the particle velocity.

$$z_{in} = \frac{1}{\rho_0 c_0} \frac{p}{v} \tag{3.15}$$

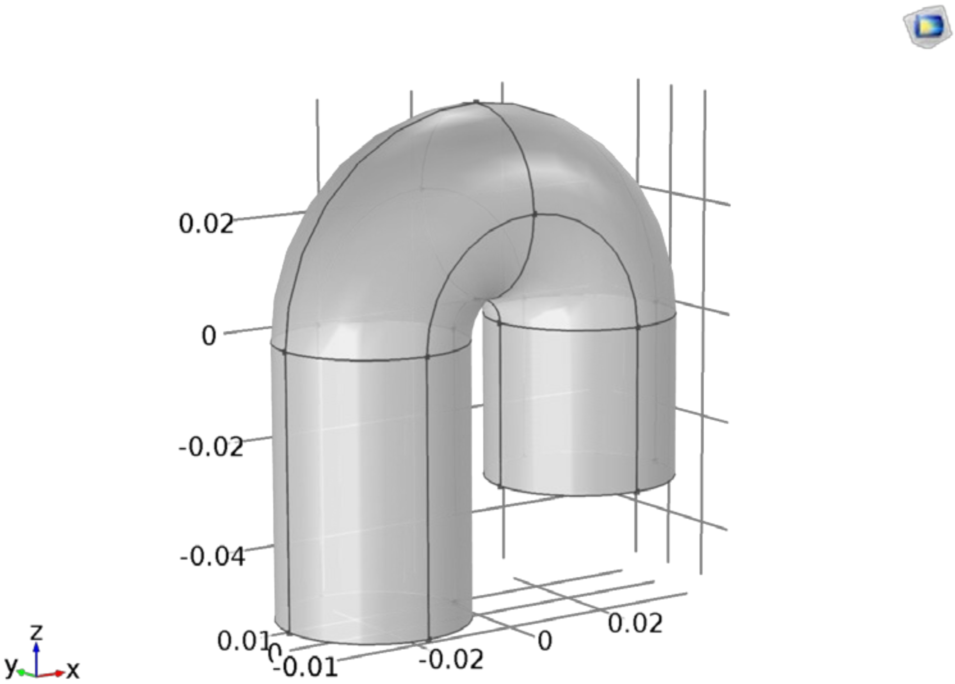

Figure 3-6 The curved duct in FEM simulation

The input impedance of the curved duct is calculated with FEM simulation and the result is shown in Figure 3-7. The modulus of the input impedance of the curved duct gives a result identical with the theoretical and experimental results in the reference[68]. It can be concluded that the FEM simulation is an effective approach to evaluate the effect of the curvature of the bend duct.

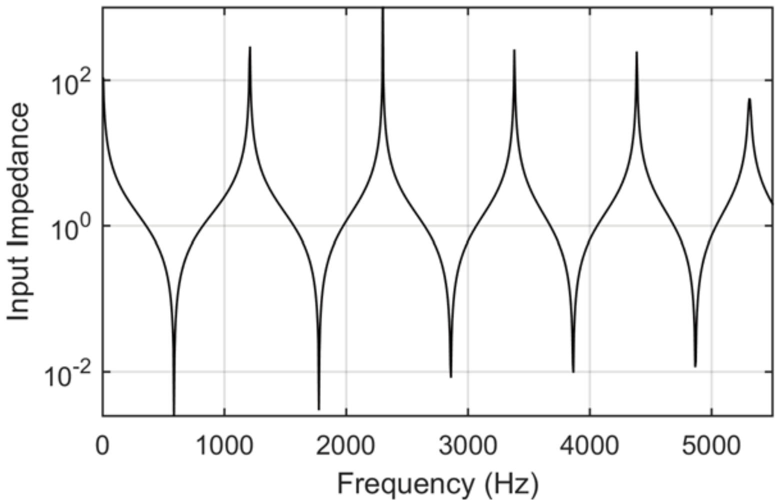

Figure 3-7 Input impedance (modulus) calculated by FEM.

3.3.2 FEM Simulation of the HR with a spiral neck

As the Finite Element Method has been proved an effective way to simulate the curved duct in last section, it is used here to simulate the Helmholtz resonator with a spiral neck.

As shown in Figure 3-8, the numerical model is composed of a rectangular duct with a side branch Helmholtz resonator. The geometries of the duct system are the same as defined in Figure 3-1 and are set as follows; $S_c = 36\pi\,\text{cm}^2$, $L_c = 10$ cm, $S_d = 144\,\text{cm}^2$, $L_d = 100$ cm, $S_n = \pi\,\text{cm}^2$, $L_I = 3$ cm, $L_{III} = 3$ cm, $R_0 = 1.2$ cm, and $r_0 = 1$ cm. The mesh divides the duct-HR system into more than 2200 triangular elements and the minimum element size is 1.8 cm.

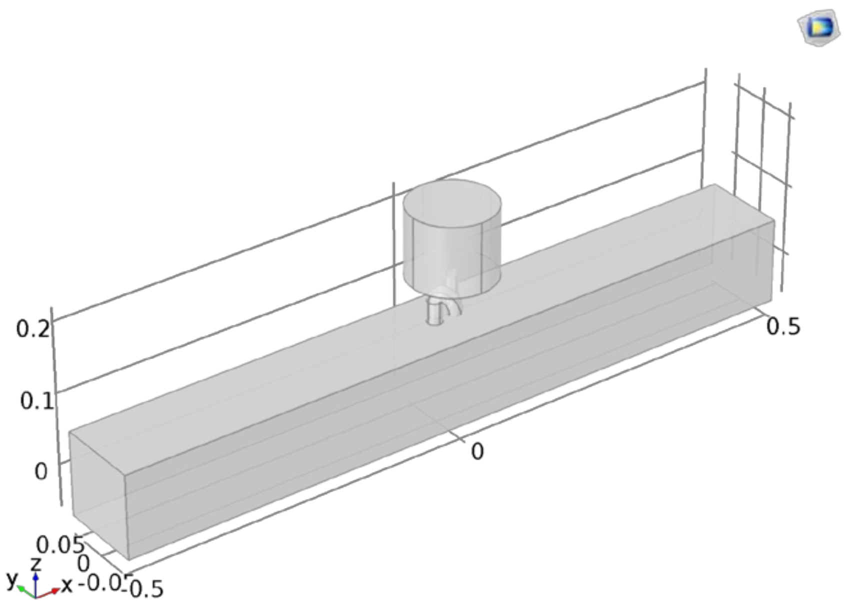

Figure 3-8 The Helmholtz resonator with a spiral neck in FEM simulation

The left end of the rectangular duct is the inlet and the right end of the duct is the outlet. The inlet boundary is set as a plane wave radiation boundary condition and the incident pressure is p_0 = 1 Pa. The outlet boundary is also set as a plane wave radiation boundary condition with no incident pressure which means the outlet boundary of the duct is set to be anechoic. A probe is set at the center of the outlet of the duct to measure the transmitted sound pressure and then to be used to calculate the transmission loss of the Helmholtz resonator.

The FEM simulation of the transmission loss of the duct-HR system is compared with the theoretical prediction described in Section 3.2. The number of turns N of the spiral neck is set from 1 to 4. Figure 3.9 shows the transmission loss of a side branch HR with a spiral neck. In Figure 3-9 the solid lines represent the theoretical results of the transmission loss and the dashed lines represent the FEM simulation results. Comparing the solid lines to the dashed lines, the theoretical prediction agrees well with the FEM calculations.

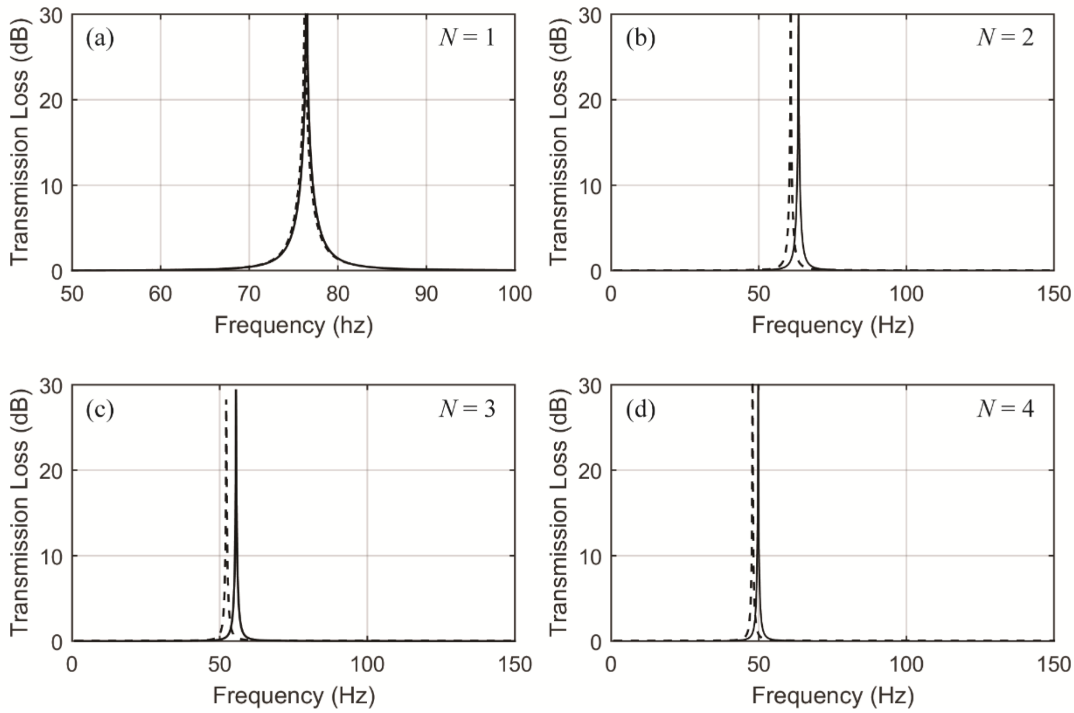

Figure 3-9 Transmission loss of the HR with a spiral neck (solid lines represent the results of theoretical prediction and dashed lines those of the FEM simulation).

For a traditional Helmholtz resonator, the maximum length of the neck as considered in Figure 3-1 will be the sum of the length of straight ducts I and III, which is 6 cm in the FEM simulation. The resonance frequency of the traditional HR will be f_0 = 105 Hz. For the HR with a spiral neck, the resonance occurs at 76 Hz, 61 Hz, 54 Hz, and 48 Hz for the turns of the spiral duct N = 1, 2, 3, and 4 as shown in Figure 3-9(a)-(d).

It is apparent that the spiral neck substantially downshifts the resonance frequency without requiring a lot of space compared to the traditional Helmholtz resonator, and that giving the spiral neck more turns results in a much lower resonance frequency of the proposed Helmholtz resonator.

3.3.3 High frequency modes of the HR

The Helmholtz resonator with a spiral neck is different to the traditional Helmholtz resonator. When there are large turns, the dimension of the neck may be comparable with the sound wavelength being considered. It is therefore necessary to investigate the effect of the spiral neck on the transmission loss at high frequencies.

Figure 3-10 illustrates the transmission loss of the Helmholtz resonator when the number of turns of the spiral neck is set to be 3.

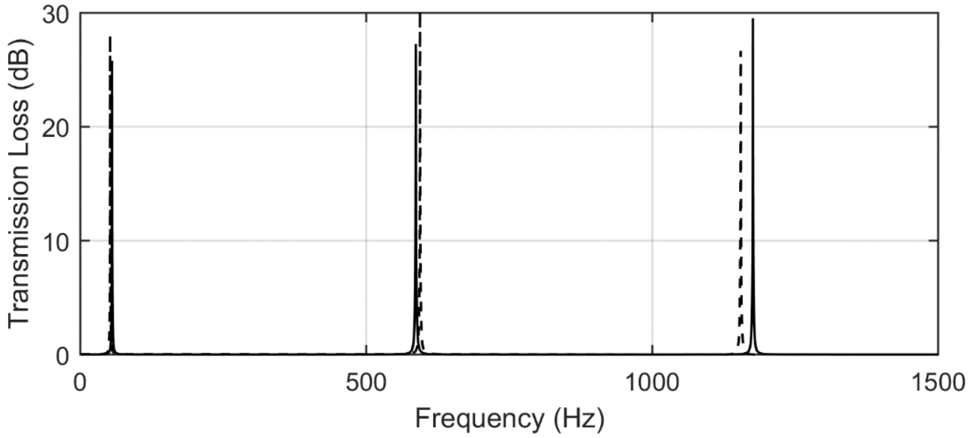

Figure 3-10 Transmission loss of the HR with a spiral neck at higher frequencies (solid lines represent the results of theoretical prediction and dashed lines those of the FEM simulation).

As shown in Figure 3-10, resonance occurs at more than one frequency. These higher modes are generated by the long neck of the Helmholtz resonator. When the frequency is high, the side branch HR can be modelled as a long tube, similar to the quarter wave resonator, which has more resonance frequencies. Therefore, the spiral neck not only lowers the resonance of the HR but also gives more resonance at higher frequencies. This is very useful in practice, especially when the noise source contains more than one frequency to be controlled. Fan noise is a good example, where the frequency is determined by the speed of the fan rotation. Traditional HR only work at one frequency and so cannot respond to changes in fan speed. With the help of the spiral neck, the HR can be designed to control the different tonal noise.

3.4 Summary

To improve the attenuation of the Helmholtz resonator at lower frequencies, a Helmholtz resonator with a spiral neck is proposed. The transmission loss of the proposed Helmholtz resonator is studied theoretically based on the equivalent of the curved duct.

The Finite element method is used to simulate the Helmholtz resonator with a spiral neck and the turns of the spiral neck is set as different to investigate its effect. The theoretical results agree well with the FEM simulation results. The results show that the resonance frequency of the Helmholtz resonator can be effectively lowered by incorporating the spiral neck and larger number of the turns of the spiral neck results in lower resonance frequency of the Helmholtz resonator, which have potential application of tonal noise control within a limited space.

Additionally, the effect of the higher modes of the Helmholtz resonator is investigated and the results show that the spiral neck not only lowers the resonance of the HR but also gives more resonance at higher frequencies. This is very useful in practice, especially when the noise source contains more than one frequency to be controlled.

Chapter 4

Periodic Expansion Chamber Mufflers

The expansion chamber muffler is an effective noise reduction device for duct systems. The transmission loss of a single expansion muffler has a periodic character that is often used for the control of periodic noise. Combining several mufflers is a way to improve performance.[69, 70]

When mufflers are periodically loaded along a duct, this periodic structure can produce peculiar dispersion characteristics in overall transmission loss. Bloch waves were introduced to explain the wave propagation in periodic waveguides. Bradley[53, 54] investigated acoustic Bloch waves in periodic waveguides theoretically and experimentally and proved that Bloch waves were the solution to infinite, semi-infinite, and finite periodic waveguides. Sugimoto and Horioka[55] examined the dispersion characteristics of wave propagation in a tunnel with an array of Helmholtz resonators. Wang and Mak[56, 57] found that periodic Helmholtz resonators can provide a much broader sound attenuation than a single resonator.

This Chapter aims to investigate wave propagation in periodic expansion chamber mufflers. The transfer matrix of the periodic structure is derived to determine the Bloch wave in periodic expansion chamber mufflers. The dispersion characteristics of periodic mufflers is examined. Periodic expansion chamber mufflers have different transmission loss than a single expansion chamber muffler, which may have potential applications in muffler design.

4.1 Single Expansion Chamber Muffler

4.1.1 Transmission Loss of the single expansion chamber

The single expansion chamber is a common device for attenuating noise in ductwork systems. The single expansion chamber is composed of one expansion chamber to provide an acoustic impedance mismatch. The acoustic energy is reflected by the expansion chamber at effective frequencies and the expansion chamber muffler is a reactive noise control device.

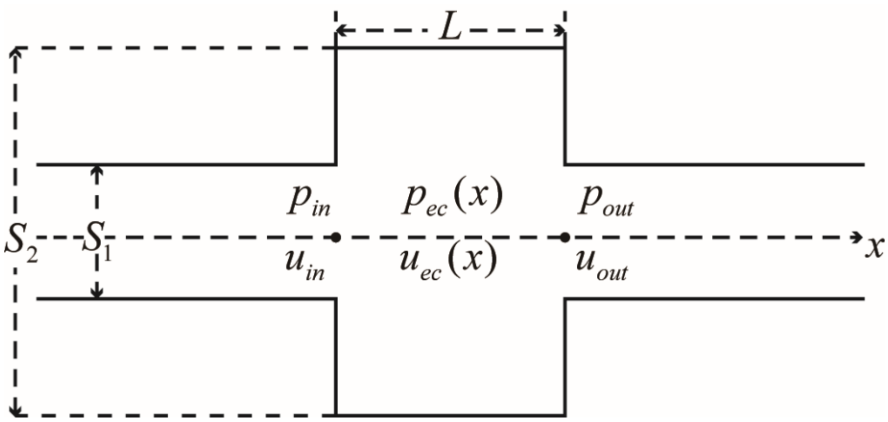

Figure 4-1 The configuration of the single expansion chamber muffler

As shown in Figure 4-1, the diameter of the circular duct is d_1 and the diameter of the single expansion chamber is d_2. The length of the muffler is L. Assuming that only plane waves propagate in the duct and the expansion chamber muffler. The incident wave and the reflected wave in the inlet duct can be represented as:

$$p_i = A_i e^{j(\omega t - kx)} \quad u_i = \frac{A_i}{\rho_0 c_0} e^{j(\omega t - kx)} \tag{4.1}$$

$$p_r = A_r e^{j(\omega t + kx)} \quad u_r = -\frac{A_r}{\rho_0 c_0} e^{j(\omega t + kx)} \tag{4.2}$$

where ρ_0 and c_0 are the density and the speed of sound in air. Similarly, the sound pressure in the expansion chamber can also be represented by the combination of the incident plane wave p_{iec} and the reflected plane wave p_{rec}.

$$p_{iec} = A_{iec} e^{j(\omega t - kx)} \quad u_{iec} = \frac{A_{iec}}{\rho_0 c_0} e^{j(\omega t - kx)} \tag{4.3}$$

$$p_{rec} = A_{rec} e^{j(\omega t + kx)} \quad u_{rec} = -\frac{A_{rec}}{\rho_0 c_0} e^{j(\omega t + kx)} \tag{4.4}$$

Assuming the outlet duct is end with anechoic termination, the sound pressure and the particle velocity at the outlet duct can be expressed as:

$$p_t = A_t e^{j(\omega t - kx)} \quad u_t = \frac{A_t}{\rho_0 c_0} e^{j(\omega t - kx)} \tag{4.5}$$

At the junction of the duct and the expansion chamber muffler, the pressures and the volume velocities are continuous. At the inlet of the muffler, the instantaneous acoustic pressure in the inlet duct and in the expansion chamber are equal and at the outlet of the muffler, the instantaneous acoustic pressure in the expansion chamber equals to that in the outlet duct. The instantaneous volume velocities are equal on each side of the inlet and outlet junction of the expansion chamber.

At the junction of the inlet of the expansion chamber muffler (x = 0), the sound pressure and the volume velocity are continuous.

$$p_i(0) + p_r(0) = p_{iec}(0) + p_{rec}(0) \tag{4.6}$$

$$S_1 u_i(0) + S_1 u_r(0) = S_2 u_{iec}(0) + S_2 u_{rec}(0) \tag{4.7}$$

where S_1 and S_2 are the cross sectional area of the main duct and the expansion chamber.

Similarly, at the junction of the outlet of the expansion chamber muffler ($x = L$), he sound pressure and the volume velocity are continuous.

$$p_{iec}(L) + p_{rec}(L) = p_t(L) \tag{4.8}$$

$$S_2 u_{iec}(L) + S_2 u_{rec}(L) = S_1 u_t(L) \tag{4.9}$$

Substituting Eqs. (4.1) to (4.5) into Eqs. (4.6) to (4.9)

$$A_i + A_r = A_{iec} + A_{rec} \tag{4.10}$$

$$S_1(A_i - A_r) = S_2(A_{iec} - A_{rec}) \tag{4.11}$$

$$A_{iec}e^{-jkL} + A_{rec}e^{jkL} = A_t e^{-jkL} \tag{4.12}$$

$$S_2\left(A_{iec}e^{-jkL} - A_{rec}e^{jkL}\right) = S_1 A_t e^{-jkL} \tag{4.13}$$

Eliminating A_r , the Eq (4.10) and Eq. (4.11) yield

$$2S_1 A_i = (S_1 + S_2)A_{iec} + (S_1 - S_2)A_{rec} \tag{4.14}$$

According to Eq. (4.12) and Eq. (4.13), the incident wave and the reflected wave in the expansion chamber can be expressed as

$$A_{iec} = \frac{(S_1 + S_2)}{2S_2} A_t \tag{4.15}$$

$$A_{rec} = \frac{(S_2 - S_1)}{2S_2} A_t e^{-j2kL} \tag{4.16}$$

Substituting Eq. (4.15) and Eq. (4.16) into Eq. (4.14)

$$A_i = \frac{(S_1 + S_2)^2}{4S_1 S_2} A_t - \frac{(S_2 - S_1)^2}{4S_1 S_2} A_t e^{-j2kL} \tag{4.17}$$

Let $m = S_2/S_1$ be the area ratio of the expansion chamber and the duct.

$$\begin{aligned} A_i &= \frac{(S_1 + S_2)^2}{4S_1 S_2} A_t - \frac{(S_2 - S_1)^2}{4S_1 S_2} A_t e^{-j2kL} \\ &= e^{-jkL} \left[\frac{(S_1 + S_2)^2}{4S_1 S_2} e^{jkL} - \frac{(S_2 - S_1)^2}{4S_1 S_2} e^{-jkL} \right] A_t \\ &= e^{-jkL} \left[\cos kL + \frac{j}{2} \left(m + \frac{1}{m} \right) \sin kL \right] A_t \end{aligned} \tag{4.18}$$

The transmission loss of the single expansion chamber is

$$\begin{aligned} TL &= 10 \log_{10} \left(\left| \frac{A_i}{A_t} \right|^2 \right) = 10 \log_{10} \left(\cos^2 kL + \frac{1}{4} \left(m + \frac{1}{m} \right)^2 \sin^2 kL \right) \\ &= 10 \log_{10} \left(1 + \frac{1}{4} \left(m - \frac{1}{m} \right)^2 \sin^2 kL \right) \end{aligned} \tag{4.19}$$

4.1.2 Transfer matrix of the single expansion chamber

The transfer matrix method has been used for evaluating the performance of the muffler for a long time. Transfer matrix is usually suitable for one-dimensional systems such as the mufflers. The performance of the muffler can be evaluated in terms of the transfer matrix of the system. The transfer matrix relates the variables on the two side of the element as shown in Figure 4-2.

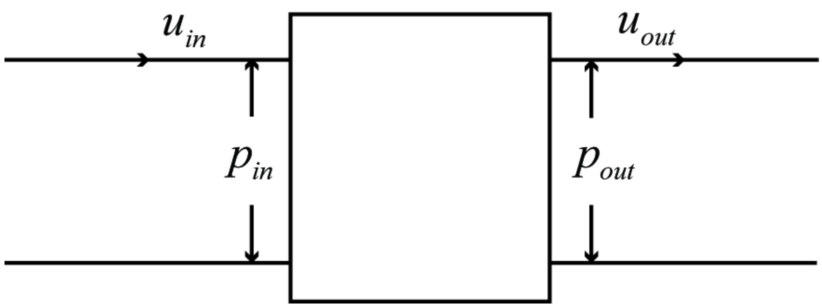

Figure 4-2 General representation of an element for transfer matrix

The variables on the two sides of the element can be related by its transfer matrix as follows:

$$\begin{bmatrix} p_{in} \\ \rho c u_{in} \end{bmatrix} = \mathbf{T} \begin{bmatrix} p_{out} \\ \rho c u_{out} \end{bmatrix} = \begin{bmatrix} T_{11} & T_{12} \\ T_{21} & T_{22} \end{bmatrix} \begin{bmatrix} p_{out} \\ \rho c u_{out} \end{bmatrix} \tag{4.20}$$

where p_{in} u_{in} are sound pressure and particle velocity at the inlet of the element and p_{out} u_{out} are sound pressure and particle velocity at the inlet of the element. The transfer matrix of the element is denoted as **T**.

In order to evaluate the transmission loss of the element in terms of the transfer matrix, the outlet of the element is assumed to be anechoic. The pressures and the particle velocities at the inlet junction and the outlet junction of the element is expressed as follows

$$\begin{aligned} p_{in} &= A_i + A_r \\ \rho_0 c_0 u_{in} &= A_i - A_r \\ p_{out} &= A_t \\ \rho_0 c_0 u_{out} &= A_t \end{aligned} \tag{4.21}$$

where A_i, A_r are the amplitudes of the incident wave and the reflected wave at the inlet junction, A_t is the amplitude of the incident wave at the outlet junction.

$$\begin{bmatrix} A_i + A_r \\ A_i - A_r \end{bmatrix} = \begin{bmatrix} T_{11} & T_{12} \\ T_{21} & T_{22} \end{bmatrix} \begin{bmatrix} A_t \\ A_t \end{bmatrix} \tag{4.22}$$

Eliminating A_r, the relation between A_i and A_t can be expressed as:

$$A_i = \frac{1}{2}\left[T_{11} + T_{12} + T_{21} + T_{22}\right] A_t \tag{4.23}$$

Therefore, the transmission loss of the element is expressed in terms of the transfer matrix.

$$TL = 10\log_{10}\left|\frac{S_{in}A_i^2/2\rho_0 c_0}{S_{out}A_t^2/2\rho_0 c_0}\right| = 20\log_{10}\left|\frac{1}{2}\left[T_{11} + T_{12} + T_{21} + T_{22}\right]\right| + 10\log_{10}\left|\frac{S_{in}}{S_{out}}\right|$$

(4.24)

where S_{in} and S_{out} are the cross-sectional area of the inlet and the outlet.

For a straight duct with length L shown in Figure 4-3, the wave in the straight duct can be expressed as the combination of the incident wave and the reflected wave.

$$p(x) = Ie^{j(\omega t - kx)} + Re^{j(\omega t + kx)} \tag{4.25}$$

and the particle velocity is

$$u(x) = \frac{I}{\rho_0 c_0} e^{j(\omega t - kx)} - \frac{R}{\rho_0 c_0} e^{j(\omega t + kx)} \tag{4.26}$$

where S is the cross sectional area of the straight duct, ρ,c are the density and speed of sound in the air.

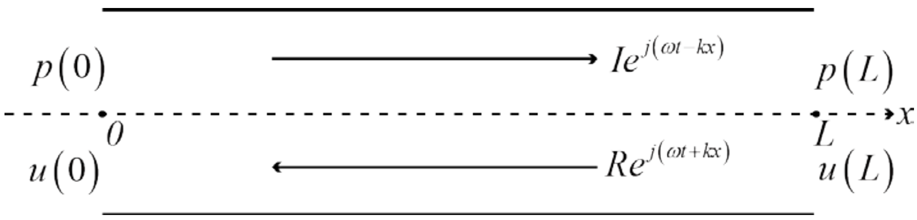

Figure 4-3 A straight duct with length *L*

$$p(0) = [I + R]e^{j\omega t} \tag{4.27}$$

$$u(0) = \frac{1}{\rho_0 c_0}[I - R]e^{j\omega t} \tag{4.28}$$

$$\begin{aligned} p(L) &= \left[Ie^{-jkL} + Re^{jkL}\right]e^{j\omega t} \\ &= \cos kL[I + R]e^{j\omega t} - j\sin kL[I - R]e^{j\omega t} \end{aligned} \tag{4.29}$$

$$\begin{aligned} u(L) &= \frac{1}{\rho_0 c_0}\left[Ie^{-jkL} - Re^{jkL}\right]e^{j\omega t} \\ &= \frac{\cos kL}{\rho_0 c_0}[I - R]e^{j\omega t} - \frac{j\sin kL}{\rho_0 c_0}[I + R]e^{j\omega t} \end{aligned} \tag{4.30}$$

Eq. (4.29) and (4.30) can be rewritten in the matrix form

$$\begin{bmatrix} p(L) \\ \rho_0 c_0 u(L) \end{bmatrix} = \begin{bmatrix} \cos kL & -j\sin kL \\ -j\sin kL & \cos kL \end{bmatrix} \begin{bmatrix} p(0) \\ \rho_0 c_0 u(0) \end{bmatrix} \tag{4.31}$$

and the transfer matrix can be obtained by inverting the Eq. (4.31)

$$\begin{bmatrix} p(0) \\ \rho_0 c_0 u(0) \end{bmatrix} = \begin{bmatrix} \cos kL & j\sin kL \\ j\sin kL & \cos kL \end{bmatrix} \begin{bmatrix} p(L) \\ \rho_0 c_0 u(L) \end{bmatrix} \tag{4.32}$$

Therefore, the transfer matrix **T** of a straight duct with cross sectional area *S* and length *L* can be expressed as:

$$\mathbf{T} = \begin{bmatrix} \cos kL & j\sin kL \\ j\sin kL & \cos kL \end{bmatrix} \tag{4.33}$$

For the expansion chamber as shown in Figure 4-1, the sound pressure and the particle velocity in the inlet straight duct, the expansion chamber and the outlet straight duct are p_{in}/u_{in}, p_{ec}/u_{ec}, p_{out}/u_{out} respectively. At the inlet junction of the muffler, the sound pressures and the particle velocities in the inlet duct and the expansion chamber can be related as:

$$\begin{bmatrix} p_{in} \\ \rho_0 c_0 u_{in} \end{bmatrix} = \begin{bmatrix} 1 & 0 \\ 0 & \dfrac{S_2}{S_1} \end{bmatrix} \begin{bmatrix} p_{ec}(0) \\ \rho_0 c_0 u_{ec}(0) \end{bmatrix} \tag{4.34}$$

Similarly, at the outlet junction of the muffler, the sound pressures and the particle velocities in the expansion chamber and the outlet duct can be related as follows:

$$\begin{bmatrix} p_{ec}(L) \\ \rho_0 c_0 u_{ec}(L) \end{bmatrix} = \begin{bmatrix} 1 & 0 \\ 0 & \dfrac{S_1}{S_2} \end{bmatrix} \begin{bmatrix} p_{out} \\ \rho_0 c_0 u_{out} \end{bmatrix} \tag{4.35}$$

Now the transfer matrix of the expansion chamber can be obtained with Eq. (4.34) and Eq. (4.35)

$$\begin{aligned} \begin{bmatrix} p_{in} \\ \rho_0 c_0 u_{in} \end{bmatrix} &= \begin{bmatrix} 1 & 0 \\ 0 & \dfrac{S_2}{S_1} \end{bmatrix} \begin{bmatrix} \cos kL & j\sin kL \\ j\sin kL & \cos kL \end{bmatrix} \begin{bmatrix} 1 & 0 \\ 0 & \dfrac{S_1}{S_2} \end{bmatrix} \begin{bmatrix} p_{out} \\ \rho_0 c_0 u_{out} \end{bmatrix} \\ &= \begin{bmatrix} \cos kL & j\dfrac{\sin kL}{m} \\ jm\sin kL & \cos kL \end{bmatrix} \begin{bmatrix} p_{out} \\ \rho_0 c_0 u_{out} \end{bmatrix} \end{aligned} \tag{4.36}$$

where m is the area ratio of the expansion chamber and the duct defined as in section 3.1.1. Therefore, the transfer matrix of the single expansion chamber can be expressed as:

$$\mathbf{T}_{ec} = \begin{bmatrix} \cos kL & j\dfrac{\sin kL}{m} \\ jm\sin kL & \cos kL \end{bmatrix} \tag{4.37}$$

According to Eq. (4.24), the transmission loss of the single expansion chamber muffler can be expressed as:

$$
\begin{aligned}
TL &= 20\log_{10}\left|\cos kL + \frac{j\sin kL}{2}\left(m+\frac{1}{m}\right)\right| \\
&= 10\log_{10}\left(\cos^2 kL + \frac{1}{4}\left(m+\frac{1}{m}\right)^2 \sin^2 kL\right) \\
&= 10\log_{10}\left(1+\frac{1}{4}\left(m-\frac{1}{m}\right)^2 \sin^2 kL\right)
\end{aligned}
\tag{4.38}
$$

which is the same as Eq. (4.19)

4.1.3 Simulation

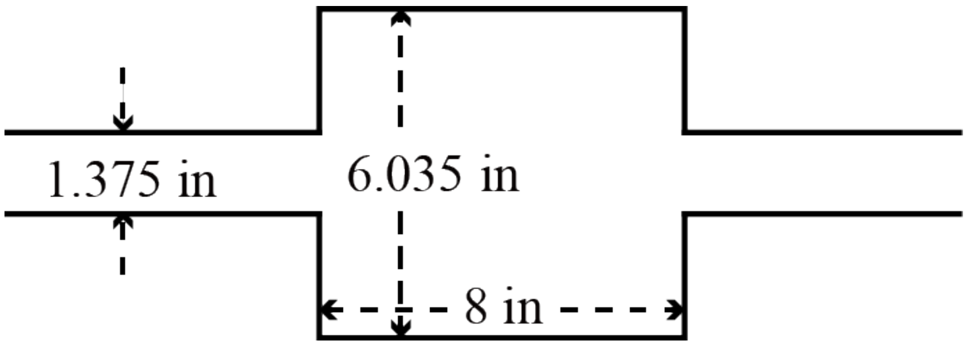

Figure 4-4 The geometries of the model

As shown in Figure 4-4, let the geometries of the expansion chamber be: the diameter of the circular duct d_1 = 1.375 in, the diameter of the expansion chamber d_2 = 6.035 in, and the length of the expansion chamber L = 8 inch (the geometry is the same as the model used by Tao[71]).

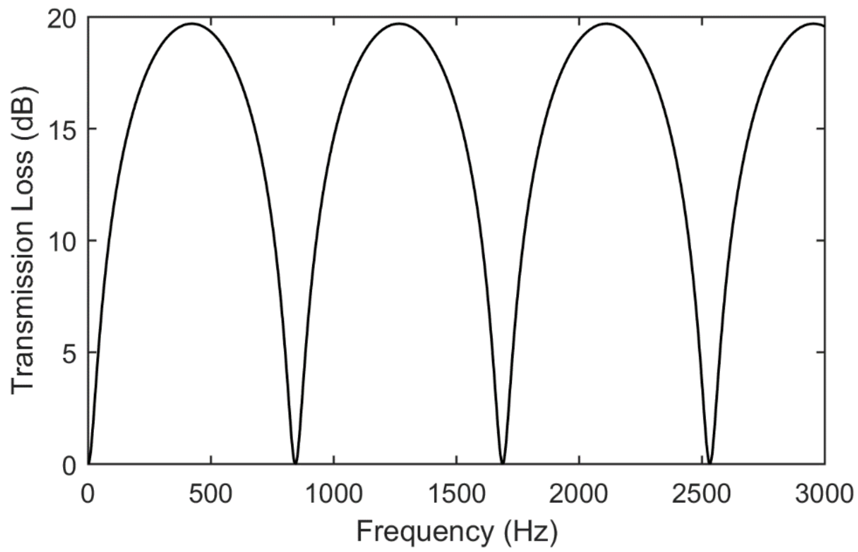

Figure 4-5 Transmission Loss of a single expansion chamber of 1D theoretical analysis

The transmission loss of the expansion chamber muffler according to Eq. (4.38) is plotted in Figure 4-5. The 1D theoretical results are based on the plane wave assumption. It is seen that the transmission loss of the single expansion chamber muffler is a periodic function. As indicated in Eq. (4.38), the transmission loss is a periodic function of kL. When $\sin kL = 0$, the transmission loss is zero which means the element has no sound attenuation at these frequencies. When $\sin kL = 1$, the transmission loss reaches maximum. The sound attenuation performance of the expansion chamber is determined by the area ratio and the length of the expansion chamber. The larger of the area ration, the larger of the transmission at frequencies when $\sin kL = 1$.

To compare with the theoretical results, a 2D axisymmetric finite element method (FEM) is used to simulate the expansion chamber muffler. The numerical model is composed of a circular duct with expansion chamber and an excitation from an oscillating sound pressure at fixed magnitude $P_0 = 1$ at the inlet of the duct. The end termination is set to be anechoic. The configuration of the FEM model is illustrated in Figure 4-6. The geometries is the same as the theoretical model.

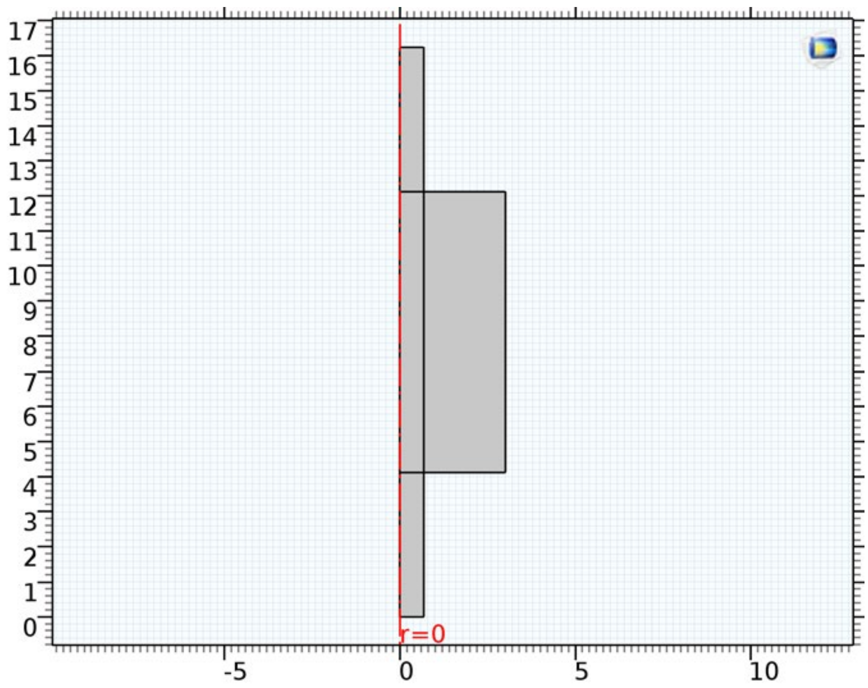

Figure 4-6 The FEM model of the expansion chamber

As shown in Figure 4-6, the beginning and the end of the main duct are set as a plane wave radiation boundary condition. The plane wave radiation boundary condition means the boundary allow an outgoing wave to leave the domain with minimal reflections. At the beginning of the duct, the plane wave radiation boundary, the incident pressure is set as 1 Pa which is the incident wave of the expansion chamber. At the end of the main duct the plane wave boundary is associate with no incident pressure and thus the boundary is identical to anechoic termination. A probe is set at the center of the end boundary of the termination to measure the transmitted sound wave. Therefore, the transmission loss in FEM model can be calculated with the incident wave and the transmitted wave.

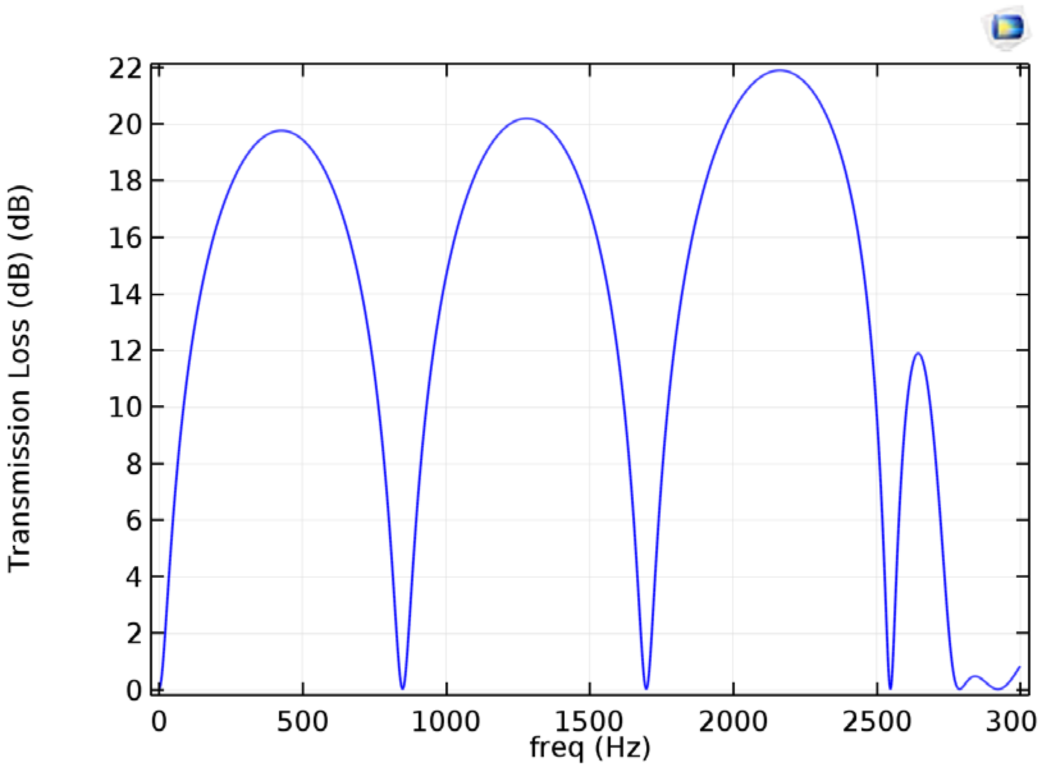

Figure 4-7 Transmission loss of the single expansion chamber by FEM

Figure 4-7 gives the transmission loss of the single expansion chamber muffler calculated with FEM model. The result agrees well with the experiment data measured by Tao and Seybert[71]. However, the FEM result is different from the predicted by 1D plane wave theory shown in Figure 4-5. The difference occurs at higher frequencies where the plane wave assumption is no longer suitable for the model and the higher modes exists in the expansion chamber and the main duct.

4.2 Periodic Expansion Chamber Mufflers

4.2.1 Transfer matrix of the periodic expansion chamber

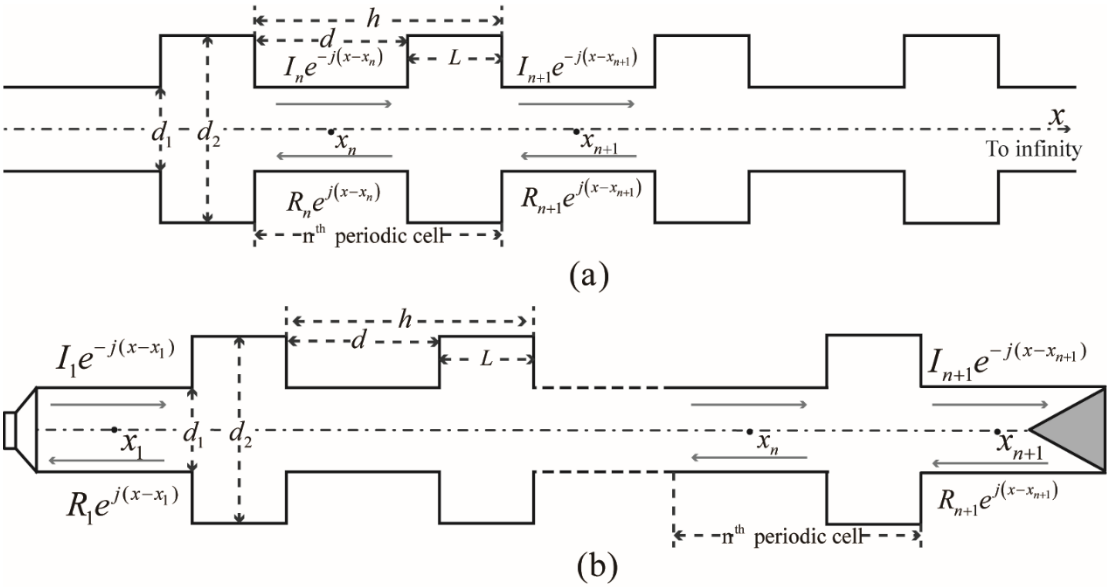

Figure 4-8 (a) Infinite periodic expansion chamber mufflers; (b) Finite periodic expansion chamber mufflers with anechoic termination.

Figure 4-8(a) shows an infinite array of periodic expansion chamber mufflers loaded periodically along a circular duct and Figure 4-8(b) shows a finite array of periodic expansion chamber mufflers. The diameters of the duct and the expansion chamber are d_1 and d_2 respectively. A typical periodic cell consists of a uniform duct of length d and an expansion chamber of length L. The length of a periodic cell is: $h = L+d$.

Assume that only planar waves propagate both in the duct and the mufflers and that the time-harmonic disturbance takes the form $e^{-j\omega t}$. The sound wave propagation in a spatially periodic structure has been examined by Bradley,[53, 54] who found that Bloch wave functions are the solution for a periodic waveguide. For the Bloch waves, the relation between waves in two adjacent periodic cells is:

$$\begin{bmatrix} I_{n+1} \\ R_{n+1} \end{bmatrix} = \mathbf{T} \begin{bmatrix} I_n \\ R_n \end{bmatrix} = e^{-jqh} \begin{bmatrix} I_n \\ R_n \end{bmatrix} \quad \mathbf{T} = \begin{bmatrix} T_{11} & T_{12} \\ T_{21} & T_{22} \end{bmatrix} \tag{4.39}$$

where the transfer matrix **T** relates to the sound fields at the center of the uniform duct in the n^{th} periodic cell and that in the $n+1^{\text{th}}$ periodic cell, h is the length of a periodic cell and q is called the Bloch wave number. In the n^{th} periodic cell shown in Figure 4-8(a), the Bloch wave in the uniform duct is composed of two conventional plane waves traveling in opposite directions, associated with the amplitudes I_n and R_n. In a periodic waveguide, the Bloch waves in the $n+1^{\text{th}}$ cell are related to ones in the n^{th} cell with e^{-jqh}. Finding the solution of the Bloch waves requires determining the transfer matrix **T** of the periodic structure and its eigenvalue problem:

$$\begin{bmatrix} T_{11} & T_{12} \\ T_{21} & T_{22} \end{bmatrix} \begin{bmatrix} v_I \\ v_R \end{bmatrix} = e^{-jqh} \begin{bmatrix} v_I \\ v_R \end{bmatrix} \tag{4.40}$$

where e^{-jqh} and **v** are, respectively, the eigenvalue and the corresponding eigenvector of the transfer matrix **T** of the periodic expansion chamber mufflers.

In the n^{th} periodic cell, the sound pressure can be expressed as:

$$p_n(x) = I_n e^{-jk(x-x_n)} + R_n e^{jk(x-x_n)} \tag{4.41}$$

Let the sound pressures and the particle velocities at the inlet and outlet of the expansion chamber muffler in the n^{th} cell be p_{in}, u_{in} and p_{out}, u_{out} respectively:

$$p_{in} = I_n e^{-jkd/2} + R_n e^{jkd/2} \qquad p_{out} = I_{n+1} e^{jkd/2} + R_{n+1} e^{-jkd/2}$$
$$\rho_0 c_0 u_{in} = I_n e^{-jkd/2} - R_n e^{jkd/2} \qquad \rho_0 c_0 u_{out} = I_{n+1} e^{jkd/2} - R_{n+1} e^{-jkd/2} \tag{4.42}$$

Eq. (4.42) can be rewritten in the form of matrices:

$$\begin{bmatrix} p_{in} \\ \rho_0 c_0 u_{in} \end{bmatrix} = \begin{bmatrix} e^{-jkd/2} & e^{jkd/2} \\ e^{-jkd/2} & -e^{jkd/2} \end{bmatrix} \begin{bmatrix} I_n \\ R_n \end{bmatrix} \tag{4.43}$$

$$\begin{bmatrix} I_{n+1} \\ R_{n+1} \end{bmatrix} = \begin{bmatrix} 0.5e^{-jkd/2} & 0.5e^{-jkd/2} \\ 0.5e^{jkd/2} & -0.5e^{jkd/2} \end{bmatrix} \begin{bmatrix} p_{out} \\ \rho_0 c_0 u_{out} \end{bmatrix} \tag{4.44}$$

$p_{\mathrm{out}}, u_{\mathrm{out}}$ and $p_{\mathrm{in}}, u_{\mathrm{in}}$ can be related by transfer matrix method:[72]

$$\begin{aligned} \begin{bmatrix} p_{out} \\ \rho_0 c_0 u_{out} \end{bmatrix} &= \begin{bmatrix} 1 & 0 \\ 0 & S_1/S_2 \end{bmatrix} \begin{bmatrix} \cos kL & -j\sin kL \\ -j\sin kL & \cos kL \end{bmatrix} \begin{bmatrix} 1 & 0 \\ 0 & S_2/S_1 \end{bmatrix} \begin{bmatrix} p_{in} \\ \rho_0 c_0 u_{in} \end{bmatrix} \\ &= \begin{bmatrix} \cos kL & -jm\sin kL \\ -j\sin kL/m & \cos kL \end{bmatrix} \begin{bmatrix} p_{in} \\ \rho_0 c_0 u_{in} \end{bmatrix} \end{aligned} \tag{4.45}$$

where $m = S_2/S_1$. S_1 and S_2 are the cross-sectional areas of the duct and the expansion chamber respectively. Combining Eqs. (4.43), (4.44), and (4.45) yields:

$$\begin{bmatrix} I_{n+1} \\ R_{n+1} \end{bmatrix} = \begin{bmatrix} \dfrac{e^{-jkd/2}}{2} & \dfrac{e^{-jkd/2}}{2} \\ \dfrac{e^{jkd/2}}{2} & -\dfrac{e^{jkd/2}}{2} \end{bmatrix} \begin{bmatrix} \cos kL & -jm\sin kL \\ -j\dfrac{\sin kL}{m} & \cos kL \end{bmatrix} \begin{bmatrix} e^{-jkd/2} & e^{jkd/2} \\ e^{-jkd/2} & -e^{jkd/2} \end{bmatrix} \begin{bmatrix} I_n \\ R_n \end{bmatrix}$$

(4.46)

Therefore, the transfer matrix **T** is:

$$\mathbf{T} = \begin{bmatrix} \dfrac{e^{-jkd}}{2}\left(2\cos kL - j\left(m + \dfrac{1}{m}\right)\sin kL\right) & \dfrac{j}{2}\left(m - \dfrac{1}{m}\right)\sin kL \\ \dfrac{j}{2}\left(\dfrac{1}{m} - m\right)\sin kL & \dfrac{e^{jkd}}{2}\left(2\cos kL + j\left(m + \dfrac{1}{m}\right)\sin kL\right) \end{bmatrix}$$

(4.47)

4.2.2 Eigen problem of the periodic transfer matrix

The Bloch wave number q determine the transmission character of the Bloch waves and this can be solved by solving the characteristic Equation of the eigenvalues of transfer matrix **T**:

$$\begin{vmatrix} T_{11}-e^{-jqh} & T_{12} \\ T_{21} & T_{22}-e^{-jqh} \end{vmatrix} = e^{-(qh)^2} - \left(T_{11}+T_{22}\right)e^{-jqh} + \left|\mathbf{T}\right| = 0 \qquad (4.48)$$

According to the principle of reciprocity, the determinant of the matrix **T** is unity[53]. The two solutions of Eq. (4.48) are q_1 and q_2 respectively. The solutions must satisfy the relations as follows:

$$e^{-jq_1h}e^{-jq_2h} = 1 \qquad (4.49)$$

$$e^{-jq_1h} + e^{-jq_2h} = T_{11} + T_{22} \qquad (4.50)$$

According to Eqs. (4.40) and (4.47), the dispersion relation of the periodic structure can be expressed as:[53]

$$\cos\left(q_1h\right) = \frac{1}{2}\left(T_{11}+T_{22}\right) = \cos kL \cos kd - \frac{1}{2}\left(m+\frac{1}{m}\right)\sin kL \sin kd \qquad (4.51)$$

The solution of q is multivalued due to the inverse cosine function. When the absolute value of the term on the right side of Eq. (4.51) is no more than unity, the solution of q is real and the waves traveling through each periodic cell are only changed with a phase delay of e^{-jqh}. These spectral regions under this condition are known as passbands, where waves propagate through the structure with no amplitude attenuation. When the solution of q is complex, the coefficient e^{-jqh} can be expressed as:

$$e^{-jqh} = e^{-j(q_r + jq_i)h} = e^{q_i h} e^{-jq_r h} \tag{4.52}$$

where q_i and q_r are the real part and the imaginary part of q, respectively. In these spectral regions, the amplitudes of the waves propagating through each periodic cell are attenuated by $e^{q_i h}$. When the number of periodic cells is large enough, the waves are eliminated and cannot transmit through the whole periodic structure; such frequency regions are referred as stopbands of the periodic structure.

Eq. (4.40) can be rewritten by eliminating e^{-jqh}:

$$T_{21}\left(\frac{v_I}{v_R}\right)^2 + \left(T_{22} - T_{11}\right)\frac{v_I}{v_R} - T_{12} = 0 \tag{4.53}$$

where $[v_I, v_R]^{\mathrm{T}}$ is the solution of the Bloch waves and represents the linear combination of the conventional plane waves and has two solutions. When $v_I / v_R > 1$, the magnitude of the incident wave is larger than that of the reflected wave in the periodic cell, which indicates that the total energy is transported in the direction of the propagation (+x direction) and this type of Bloch wave is categorized as a forward-traveling Bloch wave. When $v_I / v_R < 1$, the reflected wave dominates in each periodic cell and the total energy of the Bloch wave is transported in the opposite direction to the propagation; this is called a backward-traveling Bloch wave.

4.2.3 Finite periodic expansion chamber mufflers

In the case of a finite periodic structure, Bradley[54] has proven that forward- and backward-traveling Bloch wave functions are also solutions to the finite periodic waveguide and the combination of two types of Bloch wave functions are able to produce an arbitrary termination impedance. Figure 4-8(b) shows a duct loaded periodically with *n* expansion chambers mufflers at an identical distance. A loudspeaker is mounted at the beginning of the duct and the termination is assumed to be anechoic. The waves in the first periodic cell can be described as a combination of forward- and backward-traveling Bloch waves:

$$\begin{bmatrix} I_1 \\ R_1 \end{bmatrix} = a \begin{bmatrix} v_{1I} \\ v_{1R} \end{bmatrix} + b \begin{bmatrix} v_{2I} \\ v_{2R} \end{bmatrix} \tag{4.54}$$

where $[v_{1I}, v_{1R}]^{\mathbf{T}}$ and $[v_{2I}, v_{2R}]^{\mathbf{T}}$ are forward- and backward-traveling Bloch waves associated with Bloch numbers q_1 and q_2 respectively. *a* and *b* are arbitrary constants determined by the boundary conditions. Therefore, the waves after the n^{th} cell are:

$$\begin{bmatrix} I_{n+1} \\ R_{n+1} \end{bmatrix} = \mathbf{T}^n a \begin{bmatrix} v_{1I} \\ v_{1R} \end{bmatrix} + \mathbf{T}^n b \begin{bmatrix} v_{2I} \\ v_{2R} \end{bmatrix} = e^{-jq_1 hn} a \begin{bmatrix} v_{1I} \\ v_{1R} \end{bmatrix} + e^{-jq_2 hn} b \begin{bmatrix} v_{2I} \\ v_{2R} \end{bmatrix} \tag{4.55}$$

When the duct ends with anechoic termination, there is no reflection in the last cell, which means that R_{n+1} is equal to zero.

$$R_{n+1} = e^{-jq_1 hn} a v_{1R} + e^{-jq_2 hn} b v_{2R} = 0 \tag{4.56}$$

Then the ratio of the forward- and backward-traveling Bloch waves can be expressed as:

$$b/a = -\frac{e^{-jq_1 hn}}{e^{-jq_2 hn}} \frac{v_{1R}}{v_{2R}} \tag{4.57}$$

The incident wave and the transmitted wave of the *n* periodic expansion chamber mufflers are I_1 and I_{n+1} respectively. The transmission loss of the finite periodic structure can be calculated by:

$$TL = 20\log_{10}\left|\frac{I_1}{I_{n+1}}\right| = 20\log_{10}\left|\frac{v_{1I} + b/a\, v_{2I}}{e^{-jq_1hn}v_{1I} + b/a\, e^{-jq_2hn}v_{2I}}\right| \tag{4.58}$$

In an infinite periodic waveguide, the transmission loss of n mufflers can be easily calculated as $TL_{\inf} = 20\log_{10}\left|av_{1I}/\left(e^{-jqhn}av_{1I}\right)\right|$. When the number of finite periodic mufflers is large enough, the ratio b/a reaches zero and the transmission loss will be similar to that in an infinite periodic waveguide. Figure 4-9 and Figure 4-10 show the comparison of averaged transmission loss (TL/n) of n expansion chamber mufflers in a finite and an infinite periodic waveguide.

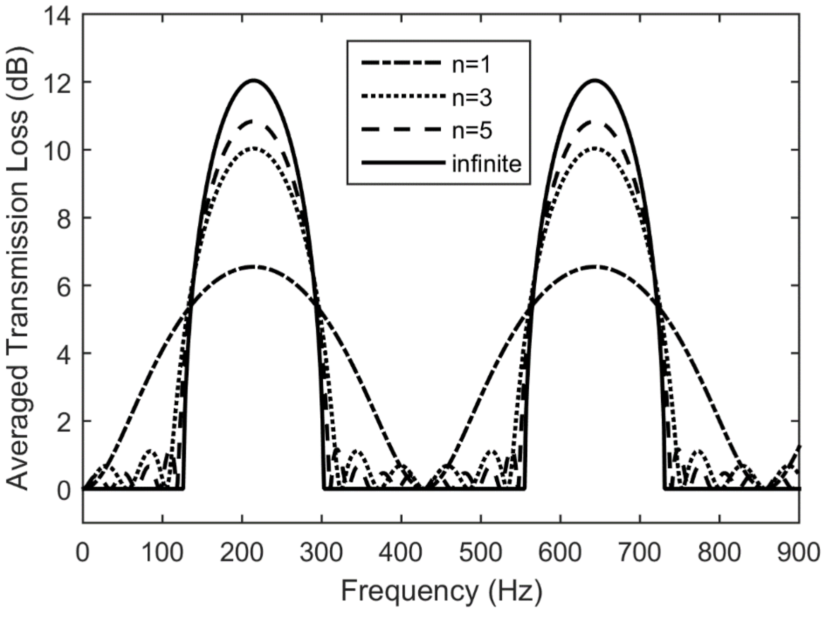

Figure 4-9 The averaged transmission loss (TL/n) of n expansion chamber mufflers in a finite waveguide (dashed-dotted lines: n = 1; dotted lines: n = 3; dashed lines: n = 5) and in an infinite periodic waveguide (solid lines). L = 0.4m, d = 0.4m

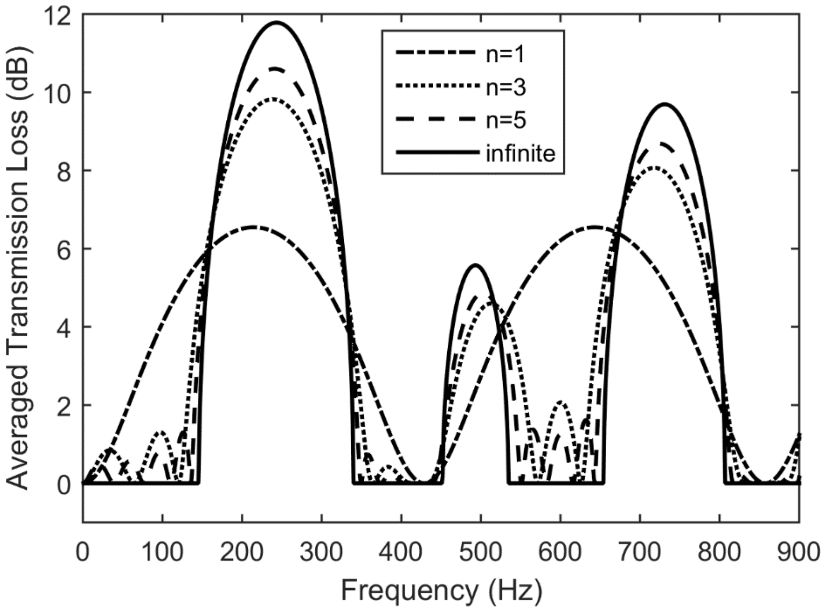

Figure 4-10 The averaged transmission loss (TL/n) of n expansion chamber mufflers in a finite waveguide (dashed-dotted lines: n = 1; dotted lines: n = 3; dashed lines: n = 5) and in an infinite periodic waveguide (solid lines). L = 0.4m, d = 0.3m.

In Figure 4-9 the length of the muffler equals to the distance between the mufflers (L = 0.4 m, d = 0.4 m) and in Figure 4-10 the length of the muffler is different from the distance between mufflers (L = 0.4 m, d = 0.3 m). It is seen from Figure 4-9 and Figure 4-10 that as the number of finite periodic mufflers increases, the averaged transmission loss of n finite expansion chamber mufflers approaches that in the infinite periodic waveguide no matter the length of the muffler equals to the distance between mufflers or not. The stopbands and passbands of the finite expansion mufflers are similar to those in a perfect infinite system. Therefore, the dispersion characteristics determined by Eq. (4.51) can be used with the finite periodic expansion chamber mufflers to predict their stopbands.

4.3 Theoretical Results and discussion

The finite element method (FEM) is used to verify the theoretical analysis of periodic expansion chamber mufflers. The wave propagation is governed by the Helmholtz equation in the inner duct and the expansion chamber.

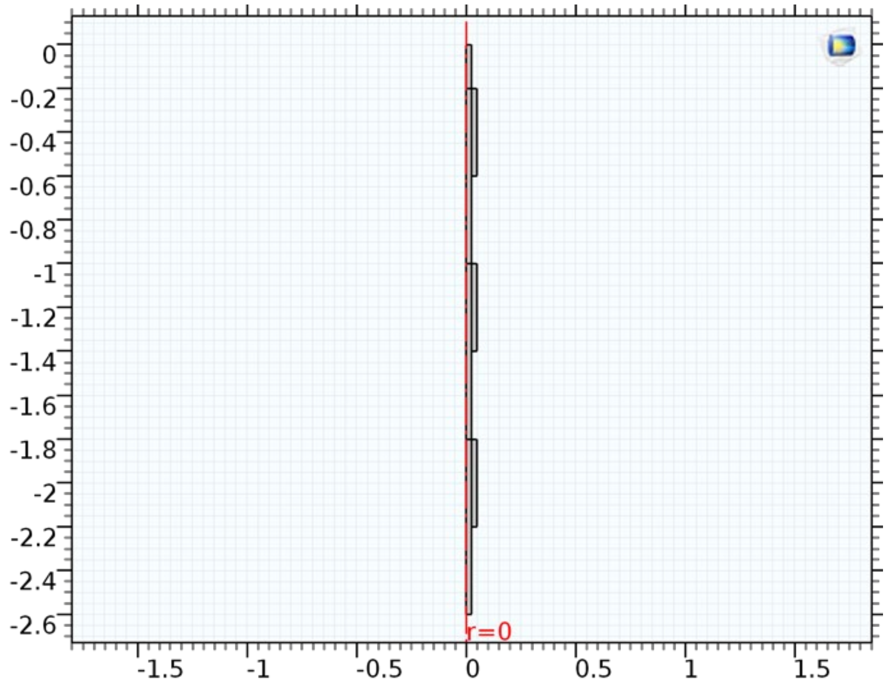

Figure 4-11 The periodic expansion chamber mufflers in FEM simulation

Figure 4-11 shows the periodic expansion chamber muffler in FEM simulation. As the structure considered here is structurally symmetric, a 2D axisymmetric model is selected to simulate the periodic expansion chamber. The numerical model consists of a circular duct with three periodic expansion chamber mufflers. The beginning of the duct is modeled with a plane wave radiation boundary condition with amplitude p_0 = 1 and the end is modeled with a no-reflection boundary. In the simulation, the temperature and the air pressure are 20 degrees Celsius and 1 atmosphere respectively. The geometries of the periodic structure in the analysis below are set as: the diameter of the duct d_1 is 0.05m and the diameter of the expansion chamber d_2 is 0.1m.

When the length of the expansion chamber L is equal to the distance d between two mufflers, Eq. (4.51) will be

$$\begin{aligned} \cos(qh) &= \cos^2 kL - \frac{1}{2}\left(m + \frac{1}{m}\right)\sin^2 kL \\ &= 1 - \left[\frac{1}{2}\left(m + \frac{1}{m}\right) + 1\right]\sin^2 kL \end{aligned} \tag{4.59}$$

The term on the right side of Eq. (4.59) is a periodic function and consequently the solution of Bloch number q is also a periodic function in kL. This is identical to the character of the transmission loss of a single expansion chamber muffler.

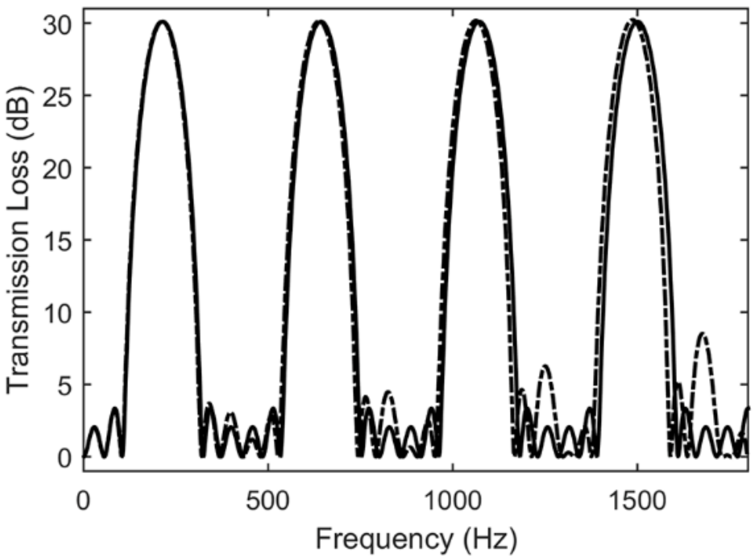

Figure 4-12 The transmission loss of three finite periodic expansion chamber mufflers with *L* = 0.4m, *d* = 0.4m (the solid line represents the results of theoretical prediction and the dashed-dotted lines those of the FEM simulation).

Figure 4-12 shows the transmission loss of three finite periodic expansion chamber mufflers. *L* and *d* are set as 0.4 m. The solid line and dashed-dotted line respectively represent the theoretical result and the FEM simulation result. It is seen that the FEM simulation fits well with the theoretical results. When frequencies are relatively high, there are some discrepancies between the theoretical and FEM results. This is mainly due to the differences between the one-dimensional theoretical model and the three-dimensional FEM simulation. The plane wave assumption is not valid at higher frequencies. Figure 4-12 demonstrates that when the length of the expansion chamber *L* is equal to the distance *d* between two mufflers, the transmission loss of the finite expansion chamber mufflers is periodic with the same period of transmission loss as a single expansion chamber. The periodic expansion chamber mufflers can offer significant improvement in transmission loss within a narrowed frequency range compared to the single expansion chamber muffler.

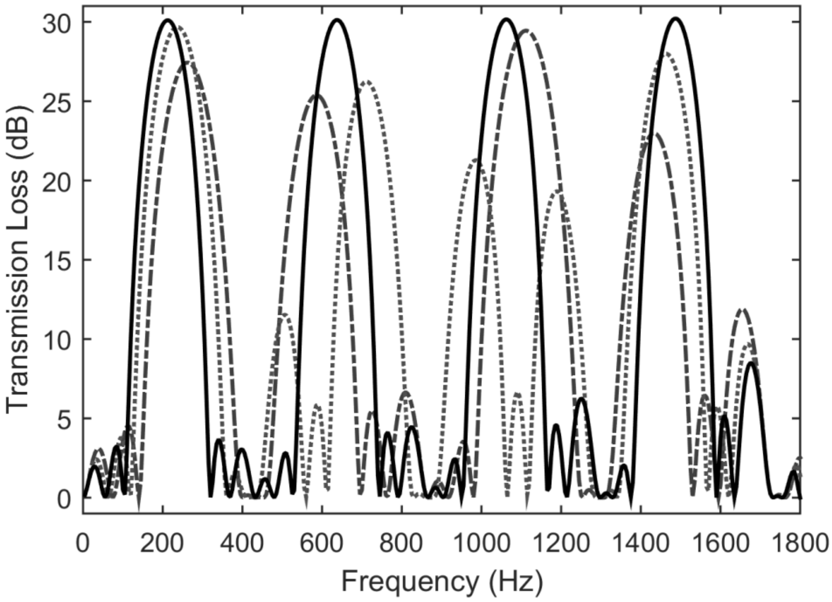

Figure 4-13 The transmission loss of three finite periodic expansion chamber mufflers with *L* = 0.4m and *d* = 0.2m (dashed-dotted line), 0.3m (dotted line), 0.4m (solid line) respectively.

Figure 4-13 shows the comparison of the transmission loss of three finite periodic expansion chamber mufflers with different distances *d* between two mufflers. The transmission loss is obtained from the FEM simulation. The length of the expansion chamber *L* is set as 0.4m and the distance *d* is set as 0.4m (solid line), 0.3m (dotted line), and 0.2m (dotted-dashed line). As shown in Figure 4-13, when the length of the expansion chamber muffler *L* is not equal to the distance *d* between mufflers, the periodic character of the transmission loss changes. The peak of the periodic mufflers' transmission loss is no longer identical to that of the single expansion chamber muffler and shifts in different ways with different distances between periodic mufflers. The stopbands of the periodic expansion chamber mufflers can be predicted by Eq. (4.51), which has a potential application in changing the effective control frequency ranges. This should be avoided in the design of periodic expansion chamber mufflers when the controlled noise is periodic.

4.4 Summary

This Chapter presents a theoretical study of the acoustic attenuation of periodic expansion chamber mufflers. The theoretical results fit well with the FEM simulation. The stopbands and passbands of finite expansion mufflers are similar to those in a perfect infinite system.

Investigation of the influence of the distance between periodic mufflers has revealed that when the distance between mufflers is the same as the length of the expansion chamber ($d = L$), the transmission loss of periodic expansion chamber mufflers has the same period in frequencies and is largely enhanced within a narrowed frequency range. For other cases ($d \neq L$), the transmission loss of periodic expansion chamber mufflers is no longer a periodic function in kL and the frequencies of peak transmission loss change with different d. In general, unlike with a single expansion chamber muffler, the stopbands of the periodic structure are mainly due to the dispersion characteristics of the Bloch waves. A different configuration can enhance the transmission loss within a narrow frequency range or shift the stopbands.

Chapter 5

Periodic Micro-perforated Mufflers

A micro-perforated panel (MPP) is composed of a thin plate across whose surface are distributed holes of sub-millimetric size. Maa[73] initially proposed an approximate theory to predict the impedance of an MPP, which revealed that the panel itself can provide high acoustic resistance and low mass reactance, making the structure an efficient sound absorber. The MPP was introduced as an alternative to conventional porous absorbers avoiding the problems of bacterial contamination and small particle discharge. Many studies have since been conducted on the application of MPPs in fields such as room acoustics[74-78] and environmental noise control[79].

In addition to its application in the field of room acoustics, the MPP has also been used to attenuate noise in duct systems[80, 81]. The micro-perforated tube muffler consists of micro-perforated tubes backed by air cavities. This kind of muffler is similar to conventional silencers except for its sub-millimeter perforation and the absence of porous material in the cavities. Because there is no fibrous material, the muffler can be used in situations where there are concerns about hygiene and health problems, such as hospitals and food industries. Although many studies have been done on the performance of perforated mufflers[82-84], the perforated screen is usually used to retain fibrous material and the perforation diameter of such mufflers is usually greater than a millimeter, unlike the micro-perforated tube mufflers. Wu[80] first presented a preliminary study evaluating the sound attenuation of MPP silencers and discussed the effect of geometric parameters on silencer performance. Allam and Åbom[85] found that the micro-perforated muffler had minima at higher frequencies. These minima occurred due to the resonances in the outer chamber and were reduced by introducing an uneven split to the outer chamber. Wang et al.[86] introduced micro perforation to a light plate silencer to broaden the effective frequency range of noise control. The vibration of the light micro-perforated plate was taken into account and the proposed hybrid silencer provided wider stopbands. Multiple MPP absorbers were used to achieve a broader frequency range of noise control and attenuate duct noise[87]. These devices comprised an MPP back with different cavities and the proposed silencer can offer wider stopbands than the single-plate silencer.

Because of the high acoustic resistance and low mass reactance due to the sub-millimeter perforation, the micro-perforated muffler can provide considerable sound attenuation of duct noise. Multiple mufflers are often used to enhance attenuation performance. When mufflers are distributed periodically in a duct, the periodic structure produces peculiar dispersion characteristics in the overall sound transmission loss. The Bloch wave theory and the transfer matrix method are used to study the wave propagation in periodic micro-perforated tube mufflers and the dispersion characteristics of periodic micro-perforated mufflers are examined. The results predicted by the theory are validated against finite element method simulation and the experimental results. The results indicate that periodic structure can influence the performance of micro-perforated mufflers. With different periodic distances, the combination of periodic structure and the micro-perforated tube muffler can contribute to the control of lower frequency noise with a broader frequency range or improvement of the peak transmission loss around the resonant frequency.

5.1 Theory

5.1.1 Bloch waves in the periodic structure

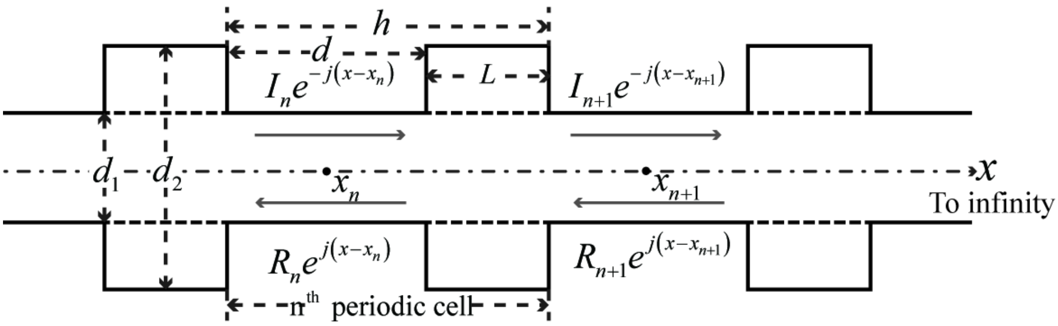

Figure 5-1 A periodic array of micro-perforated mufflers.

As shown in Figure 5-1, an array of micro-perforated mufflers are distributed periodically along a circular duct. Each periodic cell here consists of a uniform duct and a micro-perforated muffler. The diameter of the inner duct of the muffler is identical with the uniform duct. The length of the micro-perforated muffler is L and the distance between two adjacent mufflers is d. The length of a periodic cell is: $h = L+d$.

Assume that only planar waves propagate in the duct and the mufflers the time-harmonic disturbance takes the form $\exp(-j\omega t)$. The sound wave propagating in a spatially periodic structure has been examined by Bradley [53, 54] and the solution wave functions of the periodic waveguide are Bloch wave functions which can be expressed as:

$$\begin{bmatrix} I_{n+1} \\ R_{n+1} \end{bmatrix} = \mathbf{T} \begin{bmatrix} I_n \\ R_n \end{bmatrix} = e^{-jqh} \begin{bmatrix} I_n \\ R_n \end{bmatrix} \quad \mathbf{T} = \begin{bmatrix} T_{11} & T_{12} \\ T_{21} & T_{22} \end{bmatrix} \tag{5.1}$$

where the transfer matrix **T** relates the sound fields at the center of the uniform duct in the nth periodic cell and that in the $(n+1)^{th}$ periodic cell, h is the length of a periodic cell and q is called the Bloch wave number. In the n^{th} periodic cell shown in Figure 5-1, the Bloch wave in the uniform duct is composed of two conventional plane waves traveling in opposite directions associated with the amplitudes I_n and R_n. In a periodic waveguide, the waves in the $(n+1)^{th}$ cell are related to ones in the n^{th} cell with e^{-jqh}. Finding the solution of the Bloch waves falls into determining the transfer matrix **T** and its eigenvalue problem:

$$\begin{bmatrix} T_{11} & T_{12} \\ T_{21} & T_{22} \end{bmatrix} \mathbf{v} = e^{-jqh} \mathbf{v} \tag{5.2}$$

where e^{-jqh} and $\mathbf{v}$ are the eigenvalue and the corresponding eigenvector of the transfer matrix **T** of the periodic mufflers.

5.1.2 The transfer matrix T of the periodic structure

The sound pressure p_n and the velocities u_n in the nth periodic cell can be expressed as:

$$\begin{aligned} p_n(x) &= I_n e^{-jk(x-x_n)} + R_n e^{jk(x-x_n)} \\ \rho_0 c_0 u_n(x) &= I_n e^{-jk(x-x_n)} - R_n e^{jk(x-x_n)} \end{aligned} \tag{5.3}$$

where x_n is at the center of the uniform duct in the nth periodic cell, ρ_0 and c_0 are the density and the sound speed in the air.

In the nth periodic cell of Figure 5-1, let the sound pressures and the particle velocities at the inlet ($x = x_n+d/2$) and the outlet ($x = x_{n+1}-d/2$) of the micro-perforated muffler be p_{in}, u_{in} and p_{out}, u_{out} which can be expressed with (5.3):

$$\begin{aligned} p_{in} &= p_n(x_n + d/2) & p_{out} &= p_{n+1}(x_{n+1} - d/2) \\ &= I_n e^{-jkd/2} + R_n e^{jkd/2} & &= I_{n+1} e^{jkd/2} + R_{n+1} e^{-jkd/2} \\ \rho_0 c_0 u_{in} &= \rho_0 c_0 u_n(x_n + d/2) & \rho_0 c_0 u_{out} &= \rho_0 c_0 u_{n+1}(x_{n+1} - d/2) \\ &= I_n e^{-jkd/2} - R_n e^{jkd/2} & &= I_{n+1} e^{jkd/2} - R_{n+1} e^{-jkd/2} \end{aligned} \tag{5.4}$$

Define the transfer matrix **C** of sound pressures and particle velocities between the inlet and outlet of the inner duct of the micro-perforated muffler, the sound pressure and particle velocity at the outlet of the micro-perforated muffler in the nth periodic cell can be expressed as:

$$\begin{bmatrix} p_{out} \\ u_{out} \end{bmatrix} = \mathbf{C} \begin{bmatrix} p_{in} \\ u_{in} \end{bmatrix} \tag{5.5}$$

Eq. (5.4) can be rewritten in the form of matrices:

$$\begin{bmatrix} p_{in} \\ \rho_0 c_0 u_{in} \end{bmatrix} = \begin{bmatrix} e^{-jkd/2} & e^{jkd/2} \\ e^{-jkd/2} & -e^{jkd/2} \end{bmatrix} \begin{bmatrix} I_n \\ R_n \end{bmatrix} \tag{5.6}$$

$$\begin{bmatrix} I_{n+1} \\ R_{n+1} \end{bmatrix} = \begin{bmatrix} 0.5e^{-jkd/2} & 0.5e^{-jkd/2} \\ 0.5e^{jkd/2} & -0.5e^{jkd/2} \end{bmatrix} \begin{bmatrix} p_{out} \\ \rho_0 c_0 u_{out} \end{bmatrix} \tag{5.7}$$

Combing Eqs. (5.5), (5.6) and (5.7) yields:

$$\begin{bmatrix} I_{n+1} \\ R_{n+1} \end{bmatrix} = \begin{bmatrix} 0.5e^{-jkd/2} & 0.5e^{-jkd/2} \\ 0.5e^{jkd/2} & -0.5e^{jkd/2} \end{bmatrix} \mathbf{C} \begin{bmatrix} e^{-jkd/2} & e^{jkd/2} \\ e^{-jkd/2} & -e^{jkd/2} \end{bmatrix} \begin{bmatrix} I_n \\ R_n \end{bmatrix} \tag{5.8}$$

According to the Eq. (5.1), the periodic transfer matrix **T** can be expressed as:

$$\mathbf{T} = \begin{bmatrix} T_{11} & T_{12} \\ T_{21} & T_{22} \end{bmatrix} = \begin{bmatrix} 0.5e^{-jkd/2} & 0.5e^{-jkd/2} \\ 0.5e^{jkd/2} & -0.5e^{jkd/2} \end{bmatrix} \mathbf{C} \begin{bmatrix} e^{-jkd/2} & e^{jkd/2} \\ e^{-jkd/2} & -e^{jkd/2} \end{bmatrix} \tag{5.9}$$

The transfer matrix **T** can be determined when the transfer matrix **C** of the micro-perforated muffler is known. In order to get the transfer matrix **C**, the n^{th} periodic cell is depicted in Figure 5-2. The micro-perforated muffler is composed of a micro-perforated inner duct of the diameter d_1 and an outer chamber of diameter d_2. The length of the muffler is L.

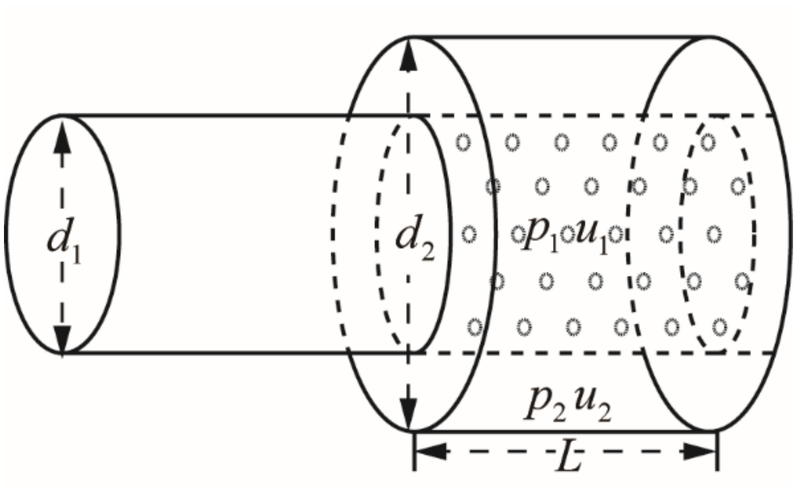

Figure 5-2 The n^{th} periodic cell of the periodic micro-perforated mufflers.

Assume that only harmonic planar waves propagate in both the micro-perforated inner duct and the outer chamber (Figure 5-2), and that the continuity and momentum Equations yield. In the absence of mean flow, the coupled wave Equations in the inner duct and the outer chamber are expressed as follows [13]:

$$\frac{d^2 p_1}{dx^2} + \left(k^2 - \frac{4}{d_1}\frac{ik}{z}\right)p_1 + \left(\frac{4}{d_1}\frac{ik}{z}\right)p_2 = 0 \tag{5.10}$$

$$\frac{d^2 p_2}{dx^2} + \left(\frac{4d_1}{d_2^2 - d_1^2}\frac{ik}{z}\right)p_1 + \left(k^2 - \frac{4d_1}{d_2^2 - d_1^2}\frac{ik}{z}\right)p_2 = 0 \tag{5.11}$$

where k is the wave number, p_1 and p_2 represent the sound pressures in the inner duct and outer chamber, respectively. z is the non-dimensional acoustic impedance of the micro perforation.

According to Maa's model [78], the non-dimensional acoustic impedance z can be expressed as:

$$z = \frac{32\eta}{\sigma\rho_0 c_0}\frac{t}{d_h^2}\left[\sqrt{1+\frac{K^2}{32}} + \frac{\sqrt{2}}{32}K\frac{d_h}{t}\right] + j\frac{\omega t}{\sigma c_0}\left[1 + 1\Big/\sqrt{3^2 + \frac{K^2}{2}} + 0.85\frac{d_h}{t}\right]$$

(5.12)

where η is the viscosity of air, σ, d_h and t are the porosity (the ratio of the micro-perforated area to the area of the panel), the hole diameter and the thickness of the micro perforation, $K = d_h\sqrt{\omega\rho_0/4\eta}$.

Eq. (5.10) and Eq. (5.11) can be rewritten in the form of matrix:

$$\begin{bmatrix} p_1' \\ \left(\dfrac{dp_1}{dx}\right)' \\ p_2' \\ \left(\dfrac{dp_2}{dx}\right)' \end{bmatrix} = \begin{bmatrix} 0 & 1 & 0 & 0 \\ -\left(k^2 - \dfrac{4}{d_1}\dfrac{ik}{z}\right) & 0 & -\dfrac{4}{d_1}\dfrac{ik}{z} & 0 \\ 0 & 0 & 0 & 1 \\ -\dfrac{4d_1}{d_2^2 - d_1^2}\dfrac{ik}{z} & 0 & -\left(k^2 - \dfrac{4d_1}{d_2^2 - d_1^2}\dfrac{ik}{z}\right) & 0 \end{bmatrix} \begin{bmatrix} p_1 \\ \dfrac{dp_1}{dx} \\ p_2 \\ \dfrac{dp_2}{dx} \end{bmatrix} \tag{5.13}$$

$(\ )'$ denotes the derivative with respect to x. The relation between the acoustic pressure and the particle velocity is:

$$\begin{aligned} \rho_0 c_0 u_1 &= -\frac{1}{jk}\frac{\partial p_1}{\partial x} \\ \rho_0 c_0 u_2 &= -\frac{1}{jk}\frac{\partial p_2}{\partial x} \end{aligned} \tag{5.14}$$

where u_1 and u_2 are the sound particle velocities in the inner duct and outer chamber, respectively. Substituting Eq. (5.14) into Eq. (5.13) gives:

$$\begin{aligned} \begin{bmatrix} p_1' \\ \rho_0 c_0 u_1' \\ p_2' \\ \rho_0 c_0 u_2' \end{bmatrix} &= \begin{bmatrix} 0 & -ik & 0 & 0 \\ -ik - \dfrac{4}{d_1 z} & 0 & -\dfrac{4}{d_1 z} & 0 \\ 0 & 0 & 0 & -i \\ \dfrac{4d_1}{d_2^2 - d_1^2}\dfrac{1}{z} & 0 & -i - \dfrac{4d_1}{d_2^2 - d_1^2}\dfrac{1}{z} & 0 \end{bmatrix} \begin{bmatrix} p_1 \\ \rho_0 c_0 u_1 \\ p_2 \\ \rho_0 c_0 u_2 \end{bmatrix} \\ &= \mathbf{A} \begin{bmatrix} p_1 \\ \rho_0 c_0 u_1 \\ p_2 \\ \rho_0 c_0 u_2 \end{bmatrix} \end{aligned} \tag{5.15}$$

The matrix **A** satisfies the equation below

$$\mathbf{A} * \mathbf{\Psi} = \mathbf{\Psi} * \mathbf{D} = \mathbf{\Psi} \begin{bmatrix} \lambda_1 & & & \\ & \lambda_2 & & \\ & & \lambda_3 & \\ & & & \lambda_4 \end{bmatrix} \tag{5.16}$$

where λ_n is the eigenvalue of the matrix **A** and $\mathbf{\Psi}$ is the modal matrix whose columns are the eigenvectors of the matrix **A**. Both sides of Eq. (5.16) multiplied by $\mathbf{\Psi}^{-1}$ yields:

$$\mathbf{A} = \mathbf{\Psi} * \mathbf{D} * \mathbf{\Psi}^{-1} \tag{5.17}$$

Eq. (5.15) becomes:

$$\begin{bmatrix} p_1' \\ \rho_0 c_0 u_1' \\ p_2' \\ \rho_0 c_0 u_2' \end{bmatrix} = \mathbf{A} \begin{bmatrix} p_1 \\ \rho_0 c_0 u_1 \\ p_2 \\ \rho_0 c_0 u_2 \end{bmatrix} = \mathbf{\Psi} * \mathbf{D} * \mathbf{\Psi}^{-1} \begin{bmatrix} p_1 \\ \rho_0 c_0 u_1 \\ p_2 \\ \rho_0 c_0 u_2 \end{bmatrix} \tag{5.18}$$

Both sides of Eq. (5.18) are multiplied by $\mathbf{\Psi}^{-1}$ from the left side:

$$\mathbf{\Psi}^{-1} \begin{bmatrix} p_1' \\ \rho_0 c_0 u_1' \\ p_2' \\ \rho_0 c_0 u_2' \end{bmatrix} = \mathbf{D} * \mathbf{\Psi}^{-1} \begin{bmatrix} p_1 \\ \rho_0 c_0 u_1 \\ p_2 \\ \rho_0 c_0 u_2 \end{bmatrix} \tag{5.19}$$

$\mathbf{\Psi}^{-1}$ is independent from x; Eq. (5.19) may be expressed as:

$$\left[\mathbf{\Psi}^{-1} \begin{bmatrix} p_1 \\ \rho_0 c_0 u_1 \\ p_2 \\ \rho_0 c_0 u_2 \end{bmatrix} \right]' = \begin{bmatrix} \lambda_1 & & & \\ & \lambda_2 & & \\ & & \lambda_3 & \\ & & & \lambda_4 \end{bmatrix} \left[\mathbf{\Psi}^{-1} \begin{bmatrix} p_1 \\ \rho_0 c_0 u_1 \\ p_2 \\ \rho_0 c_0 u_2 \end{bmatrix} \right] \tag{5.20}$$

Eq. (5.20) can be solved readily and the solution is:

$$\mathbf{\Psi}^{-1} \begin{bmatrix} p_1(x) \\ \rho_0 c_0 u_1(x) \\ p_2(x) \\ \rho_0 c_0 u_2(x) \end{bmatrix} = \begin{bmatrix} c_1 e^{\lambda_1 x} \\ c_2 e^{\lambda_2 x} \\ c_3 e^{\lambda_3 x} \\ c_4 e^{\lambda_4 x} \end{bmatrix} \tag{5.21}$$

where c_1, c_2, c_3 and c_4 are arbitrary constants. Then the sound pressure and particle velocity are obtained as follows:

$$\begin{bmatrix} p_1(x) \\ \rho_0 c_0 u_1(x) \\ p_2(x) \\ \rho_0 c_0 u_2(x) \end{bmatrix} = \mathbf{\Psi} \begin{bmatrix} e^{\lambda_1 x} & & & \\ & e^{\lambda_2 x} & & \\ & & e^{\lambda_3 x} & \\ & & & e^{\lambda_4 x} \end{bmatrix} \begin{bmatrix} c_1 \\ c_2 \\ c_3 \\ c_4 \end{bmatrix} = \mathbf{\Phi}(x) \begin{bmatrix} c_1 \\ c_2 \\ c_3 \\ c_4 \end{bmatrix} \tag{5.22}$$

where

$$\mathbf{\Phi}(x) = \mathbf{\Psi} \begin{bmatrix} e^{\lambda_1 x} & & & \\ & e^{\lambda_2 x} & & \\ & & e^{\lambda_3 x} & \\ & & & e^{\lambda_4 x} \end{bmatrix} \tag{5.23}$$

The acoustic pressures and particle velocities at the inlet and outlet of the muffler can be related by

$$\begin{bmatrix} p_1(L) \\ \rho_0 c_0 u_1(L) \\ p_2(L) \\ \rho_0 c_0 u_2(L) \end{bmatrix} = \left(\mathbf{\Phi}(0)\right)^{-1} \mathbf{\Phi}(L) \begin{bmatrix} p_1(0) \\ \rho_0 c_0 u_1(0) \\ p_2(0) \\ \rho_0 c_0 u_2(0) \end{bmatrix} = \mathbf{B} \begin{bmatrix} p_1(0) \\ \rho_0 c_0 u_1(0) \\ p_2(0) \\ \rho_0 c_0 u_2(0) \end{bmatrix} \tag{5.24}$$

$$\mathbf{B} = \left(\mathbf{\Phi}(0)\right)^{-1} \mathbf{\Phi}(L) \tag{5.25}$$

where **B** is the transfer matrix which relates the sound pressures and particle velocities of both the inner duct and the outer chamber at the inlet and outlet of the micro-perforated muffler.

Assuming that the wall of the outer chamber is rigid and the boundary condition of the outer chamber is that the velocities at the wall are zero.

$$\begin{aligned} u_2(0) &= 0 \\ u_2(L) &= 0 \end{aligned} \tag{5.26}$$

Then Eq. (5.24) will be:

$$\begin{bmatrix} p_1(L) \\ \rho_0 c_0 u_1(L) \end{bmatrix} = \mathbf{C} \begin{bmatrix} p_1(0) \\ \rho_0 c_0 u_1(0) \end{bmatrix} = \begin{bmatrix} C_{11} & C_{12} \\ C_{21} & C_{22} \end{bmatrix} \begin{bmatrix} p_1(0) \\ \rho_0 c_0 u_1(0) \end{bmatrix} \tag{5.27}$$

where

$$\begin{aligned} C_{11} &= B_{11} - \frac{B_{13}B_{41}}{B_{43}} \quad C_{12} = B_{12} - \frac{B_{13}B_{42}}{B_{43}} \\ C_{21} &= B_{21} - \frac{B_{23}B_{41}}{B_{43}} \quad C_{22} = TB_{22} - \frac{B_{23}B_{42}}{B_{43}} \end{aligned} \tag{5.28}$$

Equations (5.27) and (5.28) gives the transfer matrix **C** of sound pressures and particle velocities between the inlet and outlet of the inner duct of the micro-perforated muffler. The matrix relates the sound pressure and particle velocity at both ends of the muffler and now the periodic transfer matrix **T** is obtained according to Eq. (5.9).

5.1.3 Eigenvectors and eigenvalues of the periodic transfer matrix T

The transfer matrix **T** has two eigenvectors, $v_1 = \begin{bmatrix} v_{1I} & v_{1R} \end{bmatrix}^T$ and $v_2 = \begin{bmatrix} v_{2I} & v_{2R} \end{bmatrix}^T$, associated with the eigenvalues: exp($-q_1h$) and exp($-q_2h$). The eigenvectors indicate the conventional component makeup of the Bloch waves. Take the eigenvalue v_1, for example, when the plane waves $v_{1I}e^{-jk(x-x_n)} + v_{1R}e^{jk(x-x_n)}$ propagate in the n^{th} periodic cell, the plane wave in the next cell will be $e^{-jq_1h}\left[v_{1I}e^{-jk(x-x_{n+1})} + v_{1R}e^{jk(x-x_{n+1})}\right]$. The combining of the incident and reflected wave with the ratio v_{1I}/v_{1R} or v_{2I}/v_{2R} is called the Bloch wave. The Eq. (5.2) can be rewritten as below:

$$\begin{bmatrix} T_{11} - e^{-jqh} & T_{12} \\ T_{21} & T_{22} - e^{-jqh} \end{bmatrix} \begin{bmatrix} v_I \\ v_R \end{bmatrix} = \begin{bmatrix} 0 \\ 0 \end{bmatrix} \tag{5.29}$$

Eliminating e^{-jqh}, Eq. (5.29) can be rewritten as:

$$T_{21}\left(\frac{v_I}{v_R}\right)^2 + \left(T_{22} - T_{11}\right)\frac{v_I}{v_R} - T_{12} = 0 \tag{5.30}$$

The ratio v_I / v_R will be calculated from Eq.(5.30). When the ratio $\left|v_I / v_R\right| > 1$, that means the magnitude of the incident wave is larger than that of the reflected wave in the periodic cell, which indicates that the total energy is transported in the direction of the propagation (+*x* direction) and this Bloch wave is categorized as a forward-going Bloch wave. For the other case, when the ratio $\left|v_I / v_R\right| < 1$, the reflected wave dominates in each periodic cell and the total energy of the Bloch wave is transported in the opposite direction to the propagation (–*x* direction); this is called a backward-going Bloch wave.

As the definition of the Bloch wave in Eq. (5.1), the Bloch wave number *q* determine the transmission character of the Bloch waves and this can be solved by solving the characteristic Equation of the eigenvalues of transfer matrix **T**:

$$\begin{vmatrix} T_{11} - e^{-jqh} & T_{12} \\ T_{21} & T_{22} - e^{-jqh} \end{vmatrix} = e^{-(qh)^2} - \left(T_{11} + T_{22}\right)e^{-jqh} + \left|\mathbf{T}\right| = 0 \tag{5.31}$$

According to the principle of reciprocity, the determinant of the matrix **T** is unity[53]. The two solutions of Eq. (5.31) are q_1 and q_2 respectively. The solutions must satisfy the relations as follows:

$$e^{-jq_1h}e^{-jq_2h} = 1 \tag{5.32}$$

$$e^{-jq_1h} + e^{-jq_2h} = T_{11} + T_{22} \tag{5.33}$$

Substituting the Eq. (5.32) into Eq. (5.33) gives

$$\cos(q_1 h) = \frac{1}{2}(T_{11} + T_{22}) \tag{5.34}$$

This is the Bloch dispersion relation of the periodic structure. The solution of q is multivalued due to the inverse cosine function. q is real for the term on the right side of Eq. (5.34) is a real number and the absolute value is less than or equal to unity, or q is complex under other conditions. The waves in the $(n+1)^{th}$ cell are related to ones in the n^{th} with e^{-jqh}. When the solution of q is real, the waves traveling through a periodic cell are only changed with a phase delay. These spectral regions under this condition are known as pass bands, where waves propagate through the structure with no amplitude attenuation. In the other case when the solution of q is complex, the waves in the $(n+1)^{th}$ are that in n^{th} cell multiplied by $\exp(-j(q_r+jq_i)h) = \exp(-jq_r h)\exp(q_i h)$. The coefficient $\exp(q_i h)$ is necessarily less than or equal to unity according to the energy conservation theorem, otherwise the waves will become larger and larger through each periodic cell, which is not reasonable. In the spectral regions where $q_i h$ is less than zero, the Bloch waves are attenuated by $\exp(q_i h)$ through each periodic cell. When the number of periodic cells is large enough, the waves are eliminated and cannot transmit through the whole periodic structure; such frequency regions are called stopbands.

5.1.4 Finite periodic micro-perforated mufflers

In the preceding sections the periodic waveguide is infinite and the downstream boundary condition is different with that in finite periodic structure. Bradley [54] also investigated the wave propagation in a periodic waveguide of semi-infinite or finite. He proved that forward and backward traveling Bloch wave functions were also the solutions of the finite periodic waveguide.

For finite periodic micro-perforated mufflers with N cells, the waves in the n^{th} cell can be expressed as:

$$\begin{bmatrix} I_n \\ R_n \end{bmatrix} = \mathbf{T}\begin{bmatrix} I_{n-1} \\ R_{n-1} \end{bmatrix} = \mathbf{T}^2\begin{bmatrix} I_{n-2} \\ R_{n-2} \end{bmatrix} \cdots = \mathbf{T}^{n-1}\begin{bmatrix} I_1 \\ R_1 \end{bmatrix} \tag{5.35}$$

Waves in the finite periodic structure consist of both forward-going and backward-going Bloch waves. The makeup of the Bloch waves is determine by the boundary conditions at the beginning and end of the periodic duct.

For a finite periodic array of n micro-perforated mufflers, the waves in the first cell can be expressed as the linear superposition of the two types of Bloch wave:

$$\begin{bmatrix} I_1 \\ R_1 \end{bmatrix} = a\begin{bmatrix} v_{1I} \\ v_{1R} \end{bmatrix} + b\begin{bmatrix} v_{2I} \\ v_{2R} \end{bmatrix} \tag{5.36}$$

where a and b are arbitrary constants and can be solved with the boundary conditions.

The waves in the n^{th} cell of the periodic micro-perforated mufflers are:

$$\begin{aligned} \begin{bmatrix} I_n \\ R_n \end{bmatrix} &= \mathbf{T}^{n-1}a\begin{bmatrix} v_{1I} \\ v_{1R} \end{bmatrix} + \mathbf{T}^{n-1}b\begin{bmatrix} v_{2I} \\ v_{2R} \end{bmatrix} \\ &= e^{-jq_1h(n-1)}a\begin{bmatrix} v_{1I} \\ v_{1R} \end{bmatrix} + e^{-jq_2h(n-1)}b\begin{bmatrix} v_{2I} \\ v_{2R} \end{bmatrix} \end{aligned} \tag{5.37}$$

When the finite periodic micro-perforated mufflers end with anechoic termination, the incident wave in the first cell is I_1 and the transmitted wave in the last cell is I_n. The transmission loss of the n micro-perforated mufflers can be calculated as:

$$TL = 20\log_{10}\left|\frac{I_1}{I_n}\right| = 20\log_{10}\left|\frac{av_{1I} + bv_{2I}}{e^{-jq_1 d(n-1)}av_{1I} + e^{-jq_2 d(n-1)}bv_{2I}}\right| \tag{5.38}$$

Anechoic termination means that there is no reflection in the last cell. The reflected wave in the last cell is zero:

$$R_n = e^{-jq_1 h(n-1)}av_{1R} + e^{-jq_2 h(n-1)}bv_{2R} = 0 \tag{5.39}$$

and

$$\frac{b}{a} = -\frac{e^{-jq_1 h(n-1)}v_{1R}}{e^{-jq_2 h(n-1)}v_{2R}} \tag{5.40}$$

Substituting Eq. (5.40) for Eq. (5.38), the transmission loss of the finite periodic micro-perforated mufflers is then obtained.

$$TL = 20\log_{10}\left|\frac{I_1}{I_n}\right| = 20\log_{10}\left|\frac{v_{1I} - \dfrac{e^{-jq_1 h(n-1)}v_{1R}}{e^{-jq_2 h(n-1)}v_{2R}}v_{2I}}{e^{-jq_1 d(n-1)}v_{1I} - \dfrac{e^{-jq_1 h(n-1)}e^{-jq_2 d(n-1)}v_{1R}}{e^{-jq_2 h(n-1)}v_{2R}}v_{2I}}\right| \tag{5.41}$$

5.2 Experiment

5.2.1 Configuration of the experiment

In line with the theoretical analysis and FEM simulation, an experimental setup is established for comparison with the theoretical study. The configuration of the experimental setup is shown in Figure 5-4. The dimensions of the duct and the configuration of the micro-perforated muffler are shown in Table 5.1.

Table 5.1 The configuration of the micro-perforated muffler

Property	**Value**
The inner diameter	d_1 = 94 mm
The outer diameter	d_2 = 154 mm
The length of the micro-perforated tube	L = 100 mm
The hole diameter of the micro perforation	d_h = 1 mm
The thickness of the micro perforation	t = 3 mm
The porosity of the micro perforation	σ = 0.0085
Temperature	20 ℃
Pressure	1 atm
Viscosity in air	$1.8 \cdot 10^{-5}$ Pa·s

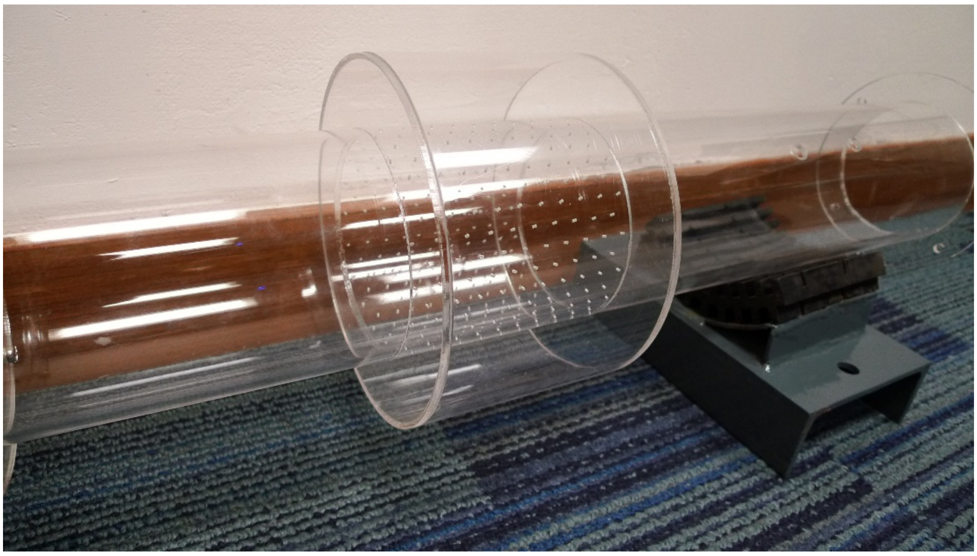

Figure 5-3 The micro-perforated muffler

Figure 5-3 shows the micro-perforated muffler used in the experiment. The walls of the inner duct and the expansion chamber are made of 3-mm-thick acrylic. Figure 5-4 and Figure 5-5 show the experimental setup for measuring the transmission loss of the periodic micro-perforated mufflers. The periodic mufflers consists of a duct with three micro-perforated mufflers. The distance between periodic micro-perforated mufflers is set to be 0.30 m and therefore the periodic distance h ($h = L+d$) is 0.40 m. The testing apparatus consists of a loudspeaker, four Brüel & Kjær microphones Type 4935 (Figure 5-6), Brüel & Kjær LAN-XI acquisition hardware Type 3160-B-042 (Figure 5-7), and Brüel & Kjær power amplifier Type 2706 (Figure 5-8).

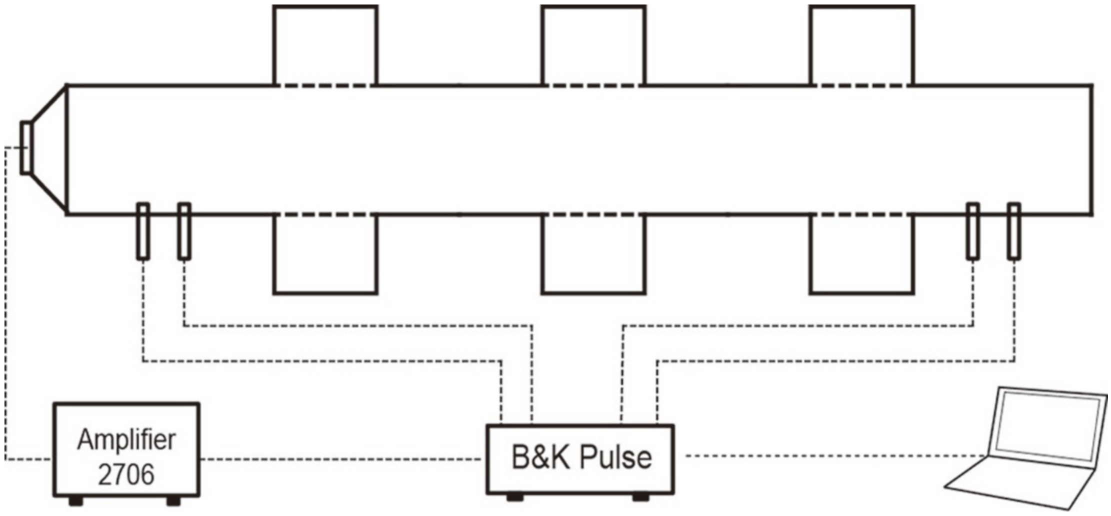

Figure 5-4 The schematic of the experimental setup

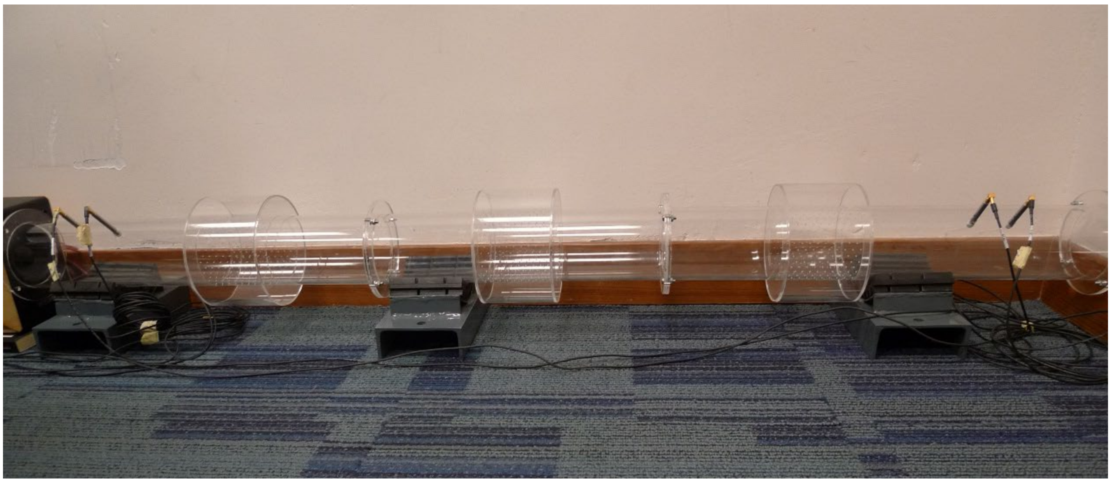

Figure 5-5 The experimental setup

Figure 5-6 Brüel & Kjær microphones Type 4935

Figure 5-7 Brüel & Kjær LAN-XI acquisition hardware Type 3160-B-042

Figure 5-8 Brüel & Kjær power amplifier Type 2706

5.2.2 Two-Load Method

In order to measure accurately the transmission loss of the periodic structure, the two-load method is applied in the experiment to measure the transfer matrix of the apparatus under test [88]. The two-load method means that the experiment is carried out with two different duct terminations and then the transfer matrix of the structure could be calculated by the measured sound pressure levels under the two different termination conditions. Once the matrix of the finite periodic micro-perforated muffler is measured, then the transmission loss of the muffler can be calculated based on the transfer matrix.

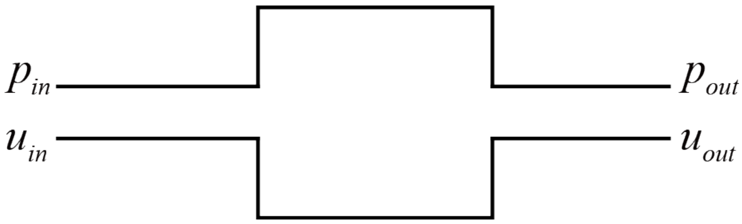

Figure 5-9 Transfer matrix representation of a system

The two-load method is based on the transfer matrix approach. As shown in Figure 5-9, an acoustical element can be represented by its transfer matrix (or called four-pole parameters).

$$\begin{bmatrix} p_{in} \\ u_{in} \end{bmatrix} = \begin{bmatrix} A & B \\ C & D \end{bmatrix} \begin{bmatrix} p_{out} \\ u_{out} \end{bmatrix} \tag{5.42}$$

where p_{in} and p_{out} are the sound pressure at the inlet and outlet of the element, respectively; u_{in} and u_{out} are particle velocity at the inlet and outlet of the element, respectively. *A*, *B*, *C* and *D* are the so-called four-pole parameters of the system.

In Eq. (5.42) there are four unknown variables but only two equations. In order to get two additional equations, changing the termination boundary condition is a way as shown in Figure 5-10. The measurement is carried out with two different end condition and four equations can be obtained for the four unknown variables. It should be noticed that the two load cannot be very similar which will result in unstable results.

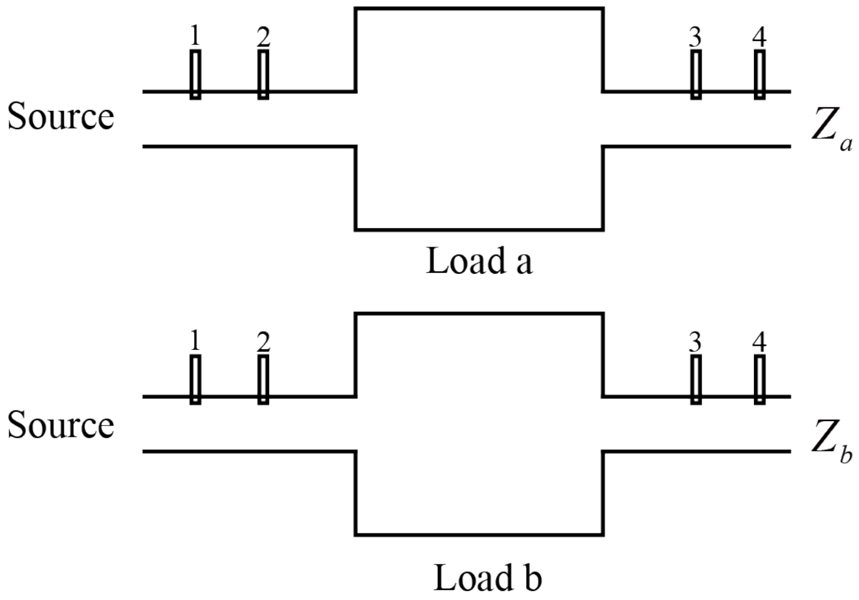

Figure 5-10 Setup of two-load method

In Eq. (5.42), p_{in}, u_{in} and p_{out}, u_{out} are measured in experiment. The sound pressure p_{in} and p_{out} can be measured directly with microphones while the particle velocities cannot be obtained with the microphones. The working frequency range of the two-load method is below the cut-off frequency[88] of the duct which means only plane waves are assumed propagate in the duct. Two microphones at both sides of the acoustic element are used to determine the particle velocity on both sides of the acoustic element.

For load a shown in Figure 5-10, the transfer matrix of the acoustic element is expressed below

$$\begin{bmatrix} p_{2a} \\ u_{2a} \end{bmatrix} = \begin{bmatrix} A & B \\ C & D \end{bmatrix} \begin{bmatrix} p_{3a} \\ u_{3a} \end{bmatrix} \tag{5.43}$$

where the sound pressures p_{2a} and p_{3a} are directly measured with the microphones at location 2 and location 3.

The sound pressures and the particle velocities at locations 1 and 2 can be related by the transfer matrix as below:

$$\begin{bmatrix} p_{1a} \\ u_{1a} \end{bmatrix} = \begin{bmatrix} A_{12} & B_{12} \\ C_{12} & D_{12} \end{bmatrix} \begin{bmatrix} p_{2a} \\ u_{2a} \end{bmatrix} \tag{5.44}$$

Therefore, the particle velocity u_{2a} at the location of the microphone 2 can be calculated as

$$u_{2a} = \frac{1}{B_{12}} \left(p_{1a} - A_{12} p_{2a} \right) \tag{5.45}$$

Similarly, the sound pressures and the particle velocities at locations 3 and 4 can be related by the transfer matrix as below:

$$\begin{bmatrix} p_{3a} \\ u_{3a} \end{bmatrix} = \begin{bmatrix} A_{34} & B_{34} \\ C_{34} & D_{34} \end{bmatrix} \begin{bmatrix} p_{4a} \\ u_{4a} \end{bmatrix} \tag{5.46}$$

and the particle velocity u_{3a} at the location 3 can be calculated as

$$u_{3a} = C_{34} p_{4a} + D_{34} \left(\frac{p_{3a} - A_{34} p_{4a}}{B_{34}} \right) \tag{5.47}$$

Substituting Eq. (5.45) and (5.47) into Eq. (5.43)

$$\begin{bmatrix} p_{2a} \\ \frac{1}{B_{12}} \left(p_{1a} - A_{12} p_{2a} \right) \end{bmatrix} = \begin{bmatrix} A & B \\ C & D \end{bmatrix} \begin{bmatrix} p_{3a} \\ C_{34} p_{4a} + D_{34} \left(\frac{p_{3a} - A_{34} p_{4a}}{B_{34}} \right) \end{bmatrix} \tag{5.48}$$

The transfer matrix between locations 1 and 2 is known as the transfer matrix of a straight duct with length l_{12}.

$$\begin{bmatrix} A_{12} & B_{12} \\ C_{12} & D_{12} \end{bmatrix} = \begin{bmatrix} \cos kl_{12} & j\rho c \sin kl_{12} \\ \dfrac{j \sin kl_{12}}{\rho c} & \cos kl_{12} \end{bmatrix} \tag{5.49}$$

Similarly, the transfer matrix between locations 3 and 4 is known as the transfer matrix of a straight duct with length l_{34}.

$$\begin{bmatrix} A_{34} & B_{34} \\ C_{34} & D_{34} \end{bmatrix} = \begin{bmatrix} \cos kl_{34} & j\rho c \sin kl_{34} \\ \dfrac{j \sin kl_{34}}{\rho c} & \cos kl_{34} \end{bmatrix} \tag{5.50}$$

For load b shown in Figure 5-10, the transfer matrix of the acoustic element is expressed below

$$\begin{bmatrix} p_{2b} \\ u_{2b} \end{bmatrix} = \begin{bmatrix} A & B \\ C & D \end{bmatrix} \begin{bmatrix} p_{3b} \\ u_{3b} \end{bmatrix} \tag{5.51}$$

where the sound pressures p_{2b} and p_{3b} can be directly measured with the microphones at location 2 and location 3.

The sound pressures and the particle velocities at locations 1 and 2 can be related by the transfer matrix as below:

$$\begin{bmatrix} p_{1b} \\ u_{b} \end{bmatrix} = \begin{bmatrix} A_{12} & B_{12} \\ C_{12} & D_{12} \end{bmatrix} \begin{bmatrix} p_{2b} \\ u_{2b} \end{bmatrix} \tag{5.52}$$

Therefore, the particle velocity u_{2b} at the location of the microphone 2 can be calculated as

$$u_{2b} = \frac{1}{B_{12}} \left(p_{1b} - A_{12} p_{2b} \right) \tag{5.53}$$

Similarly, the sound pressures and the particle velocities at locations 3 and 4 can be related by the transfer matrix as below:

$$\begin{bmatrix} p_{3b} \\ u_{3b} \end{bmatrix} = \begin{bmatrix} A_{34} & B_{34} \\ C_{34} & D_{34} \end{bmatrix} \begin{bmatrix} p_{4b} \\ u_{4b} \end{bmatrix} \tag{5.54}$$

and the particle velocity u_{3b} at the location 3 can be calculated as

$$u_{3b} = C_{34} p_{4b} + D_{34} \left(\frac{p_{3b} - A_{34} p_{4b}}{B_{34}} \right) \tag{5.55}$$

Substituting Eq. (5.53) and (5.55) into Eq. (5.52)

$$\begin{bmatrix} p_{2b} \\ \dfrac{1}{B_{12}} \left(p_{1b} - A_{12} p_{2b} \right) \end{bmatrix} = \begin{bmatrix} A & B \\ C & D \end{bmatrix} \begin{bmatrix} p_{3b} \\ C_{34} p_{4b} + D_{34} \left(\dfrac{p_{3b} - A_{34} p_{4b}}{B_{34}} \right) \end{bmatrix} \tag{5.56}$$

Now Eq. (5.48) and (5.56) contains four equations for the unknown pole parameters *A*, *B*, *C* and *D*. Thus, the four-pole parameters can be calculated as

$$A = \frac{\Delta_{34} \left(H_{32a} H_{34a} - H_{32b} H_{34a} \right) + D_{34} \left(H_{32b} - H_{32a} \right)}{\Delta_{34} \left(H_{34b} - H_{34a} \right)} \tag{5.57}$$

$$B = \frac{B_{34} \left(H_{32a} - H_{32b} \right)}{\Delta_{34} \left(H_{34b} - H_{34a} \right)} \tag{5.58}$$

$$C = \frac{\left(H_{31a} - A_{12} H_{32a} \right)\left(\Delta_{34} H_{34b} - D_{34} \right) - \left(H_{31b} - A_{12} H_{32b} \right)\left(\Delta_{34} H_{34a} - D_{34} \right)}{B_{12} \Delta_{34} \left(H_{34b} - H_{34a} \right)} \tag{5.59}$$

$$D = \frac{\left(H_{31a} - H_{31b} \right) + A_{12} \left(H_{32b} - H_{32a} \right)}{B_{12} \Delta_{34} \left(H_{34b} - H_{34a} \right)} B_{34} \tag{5.60}$$

where $\Delta_{12} = A_{12} D_{12} - B_{12} C_{12}$, $\Delta_{34} = A_{34} D_{34} - B_{34} C_{34}$ and $H_{ij} = p_i / p_j$ which can be measured readily with two-channel frequency analyzer.

Once the transfer matrix of the sound pressure and particle velocity between the inlet and outlet of the tested element is determined, the transmission loss can then be expressed in terms of the four-pole parameters.

$$TL = 20\log_{10}\left(\frac{1}{2}\left|A + \frac{B}{\rho_0 c_0} + \rho_0 c_0 C + D\right|\right) + 10\log_{10}\left(\frac{S_{in}}{S_{out}}\right) \tag{5.61}$$

where S_{in} and S_{out} are the cross-sectional area of the inlet and the outlet.

5.3 Results and discussion

5.3.1 FEM simulation

As the periodic structure in this study is structurally symmetric around the axis, a 2D axisymmetric finite element method (FEM) was used to verify the one dimensional theoretical analysis of the finite micro-perforated mufflers in the previous sections and then is also verified itself by experimental results in the next section.

The wave propagation is governed by the Helmholtz Equation in the inner duct and the outer chamber of the muffler. The numerical model is composed of a circular duct with three micro-perforated mufflers. The sound source is located at the beginning of the duct and modeled with the plane wave radiation boundary condition with amplitude $p_0 = 1$ which is the incident wave to the periodic micro-perforated mufflers. The main duct is ended with anechoic termination modeled with a non-reflective boundary condition and a probe at the termination boundary is used to measure the transmitted wave pressure. Therefore the transmission loss of the finite periodic micro-perforated muffler can be easily obtained with the transmitted pressure at the termination boundary and the incident wave pressure.

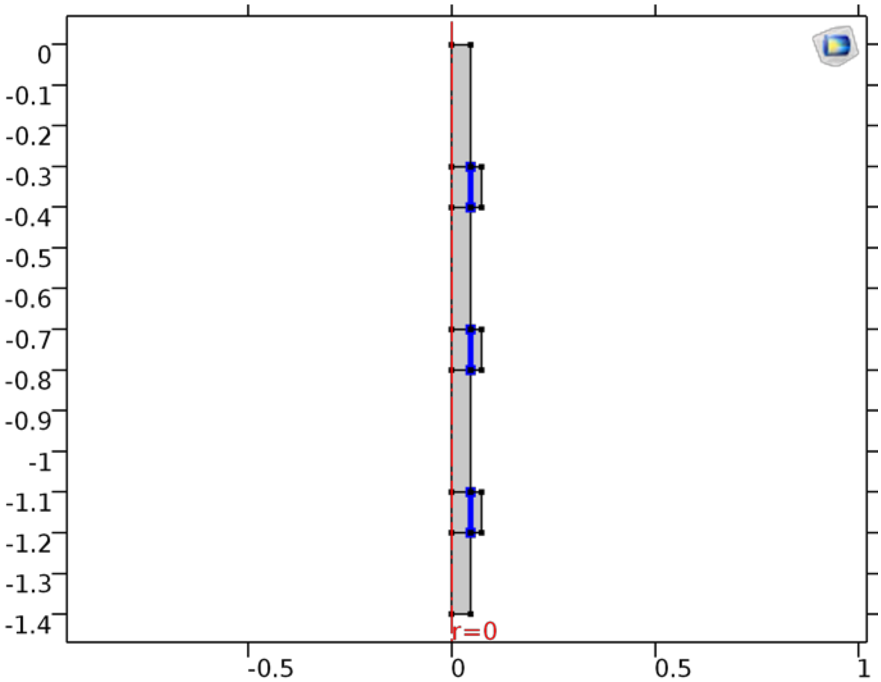

Figure 5-11 The periodic micro-perforated mufflers in FEM simulation

Figure 5-11 shows the periodic micro-perforated mufflers in FEM simulation. In the simulation, the temperature and the pressure in air are 20 degrees Celsius and 1 atmosphere respectively. The dimensions of the finite periodic micro-perforated muffler are the same as indicated in Table 1 of section 5.2.1.

As shown in Figure 5-11, the blue lines represents the micro-perforation boundaries which are modeled by the interior impedance boundary condition. The interior impedance relates the acoustic pressures in the inner duct and the muffler chamber through the boundary. Here the impedance of the micro-perforation is defined according to Maa's model as Eq.(5.12).

5.3.2 Results

The FEM model simulates a periodic array of three micro-perforated mufflers (the periodic distance h is set as 0.40 m). The simulation results are compared with the one dimensional theoretical analysis.

Figure 5-12 shows that the transmission loss predicted by the theoretical model agrees well with the simulation result obtained using the FEM method for the three periodic micro-perforated mufflers. Here the differences between the FEM and the theoretical model is very small, this is reasonable because both the FEM and the theoretical model use the Maa's impedance model to simulate the micro-perforation and assume only plane waves propagating in the ducts.

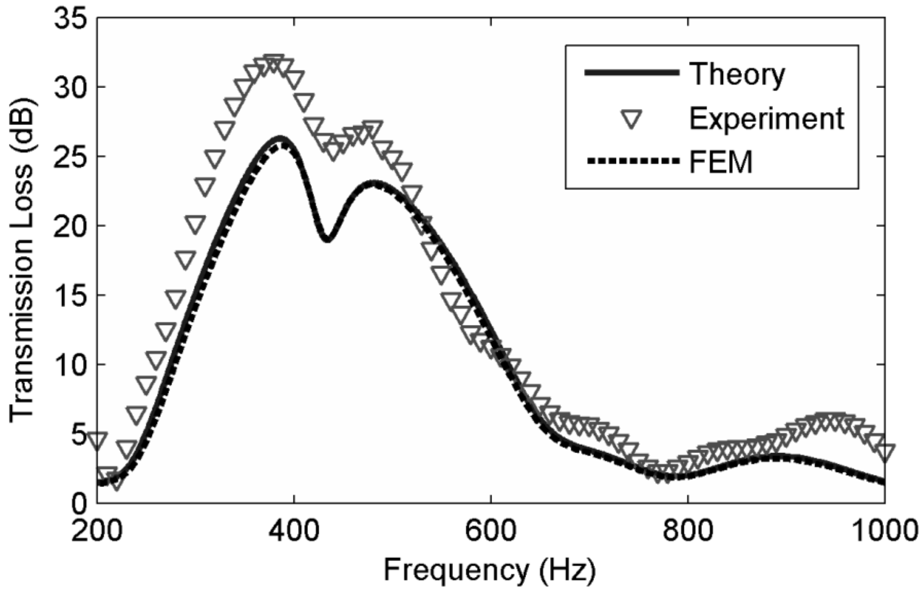

Figure 5-12 A comparison of transmission loss of the three periodic micro-perforated mufflers between theory, FEM simulation and experiment result (the distance between mufflers d = 0.30 m).

Figure 5-12 shows the comparison of the transmission loss between the theory, the FEM simulation and the experiments for a periodic array of three micro-perforated mufflers when the distance between periodic mufflers is set as 0.30 m. It can be seen that the experimental data agree well with the theoretical results and the FEM simulation. A periodic array of three micro-perforated mufflers can provide more than 15 dB noise attenuation from 300 Hz to 580 Hz. The results verify that, with appropriate periodic distance, micro-perforated mufflers can attenuate noise over a wider frequency range. It can also be noted from Figure 5-12 that there is a gap at around 430 Hz. This occurs due to the interaction between the Bragg reflection and the resonance of the micro-perforated tube. At the cost of such a gap, the effective noise control frequency range is extended and shifted to a lower frequency range.

The difference in magnitude between the experiment and the theoretical study is mainly due to the discrepancies between the one dimensional theoretical modal and the three dimensional experiment. It is assumed in the theoretical model and the FEM that only planar wave propagates in the inner duct and the outer chamber. However, the higher order modes below the cut-off frequencies are evanescent and cannot decay sufficiently if the muffler is not long enough. These higher order modes are different from the planar wave assumption of the theory and FEM. In addition, it is a fact that the acoustic impedance of the micro-perforation used in previous studies is a simplified model and does not consider the holes interactions that also contribute to the differences between the experiment and the theory.

Eq. (5.34) reveals the dispersion characteristic of the periodic micro-perforated muffler. The dispersion relation is determined by the characteristics of the micro-perforated muffler and the periodic structure. Here the effect of the periodic distance on the transmission loss is investigated.

Figure 5-13 shows a comparison of the transmission loss of three periodic micro-perforated mufflers with no space and 0.46 m between each other. The dimensions of the mufflers are the same as shown in Table 1. The distance between two mufflers *d* is set as 0 and 0.46 m respectively. The solid line indicates the three mufflers connected directly and the dotted line indicates the mufflers are distributed periodically at a distance of 0.46 m.

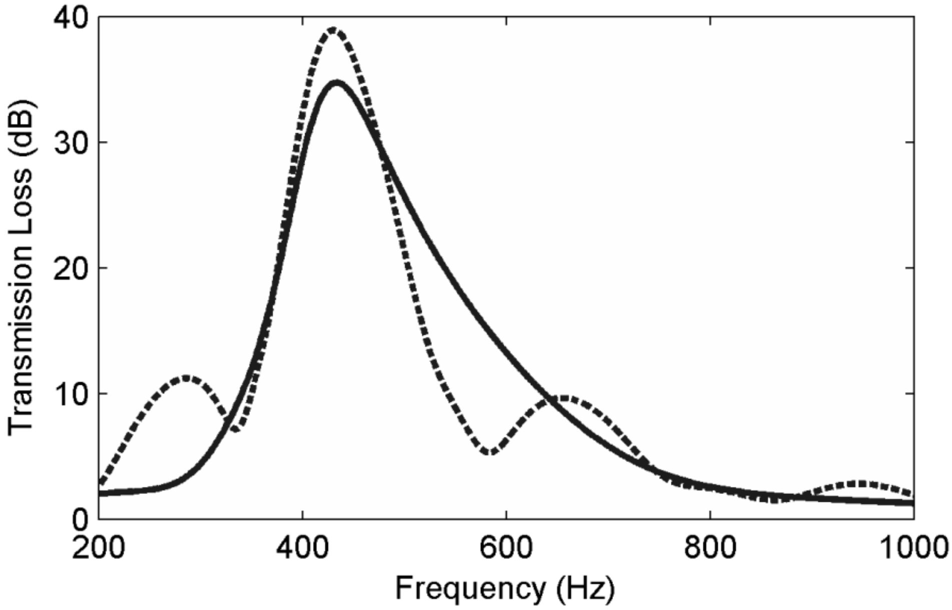

Figure 5-13 Transmission loss of a duct with three periodic micro-perforated mufflers. The distance between two mufflers is set at 0 (solid line) and 0.46 m (dotted line).

It can be seen from Figure 5-13 that the periodic placement of mufflers results in a different transmission loss from that of the mufflers connected directly. For d = 0.46 m (periodic distance h = 0.56 m), the maximum transmission loss is increased around resonant frequency but the effective attenuation frequency range is narrowed. In addition to the resonant frequency of the micro-perforated muffler, other stopbands occur at around 300 Hz and 640 Hz. These stopbands occur as a result of coupling between the resonance of the muffler itself and the Bragg reflection in the periodic structure [53]. For a periodic cell of length h, the Bragg stopbands occur around the Bragg frequency: $f_B = nc/2h \ \left(n = 1, 2, \cdots\right)$.

For the case in Figure 5-13, the periodic distance h = 0.56 m and the first Bragg frequency is 306 Hz. In order to investigate the coupling of the Bragg reflection and the resonance of the micro-perforated mufflers, Figure 5-14 shows the imaginary part of qh in this case. As analyzed in section 2, the frequencies in Figure 5-14, where an imaginary part of qh is less than zero, means that the Bloch waves are attenuated by exp(Im(qh)) and these spectral regions are referred as stopbands.

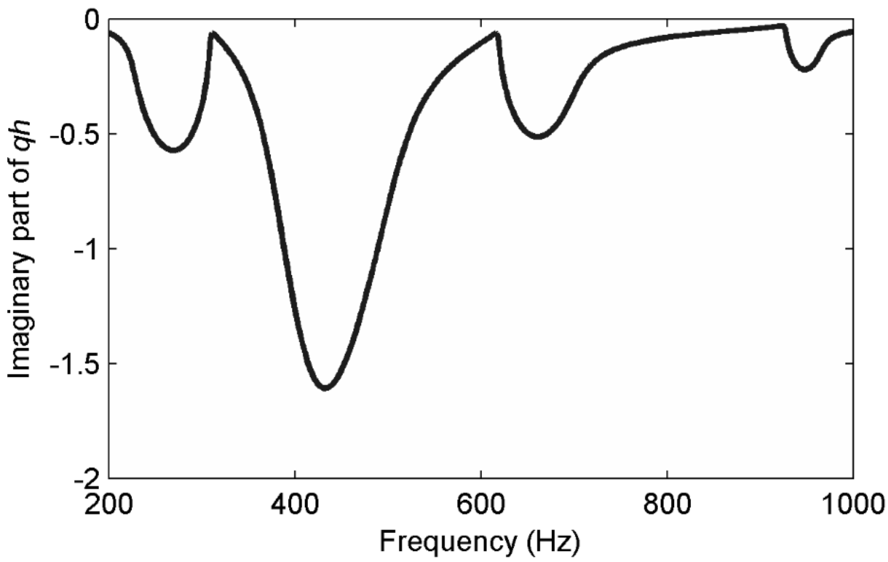

Figure 5-14 Imaginary part of qh.

As shown in Figure 5-14, the shape of the transmission loss of the periodic mufflers is more compressed than that of the directly connected mufflers. The control frequency range is narrowed but the maximum transmission loss is increased.

Since the Bragg resonance can narrow the frequency range, it may influence the performance of the muffler in another way, by adjusting the periodic distance. In Figure 5-15 the distance between two mufflers *d* is set as 0.30 m and the corresponding periodic distance *h* is 0.40 m. The first two Bragg frequencies are 429 Hz and 860 Hz. In this case, although the peak of the transmission loss is decreased compared to that of the directly connected mufflers, the transmission loss is increased at lower frequencies and the efficient frequency range is widened, which has potential implications for lower frequency noise control.

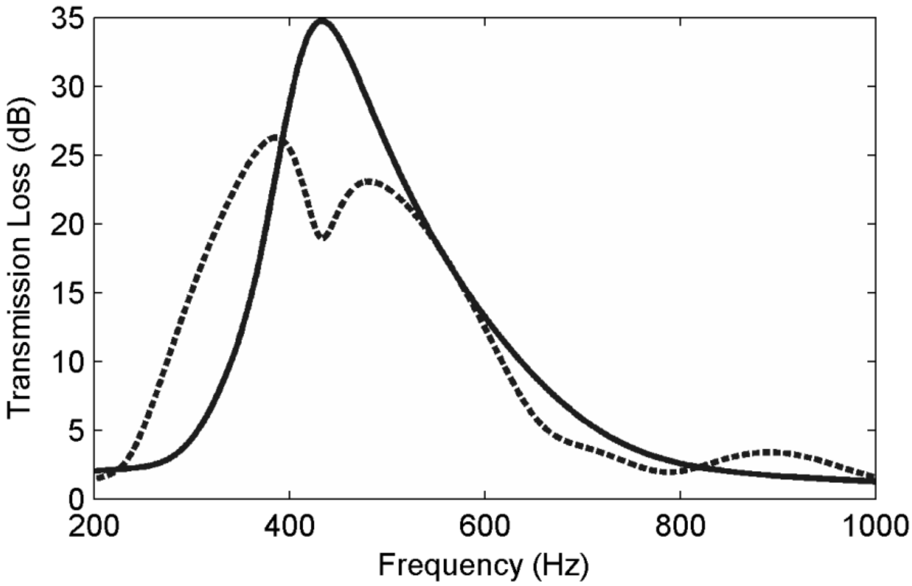

Figure 5-15 Transmission loss of a duct with three periodic micro-perforated mufflers. The distance between two mufflers *d* is set at 0 (solid line) and 0.3 m (dotted line).

The above predicted transmission loss at different periodic distance demonstrates that the Bragg resonance as a result of the periodic structure has a modulation effect on the transmission loss of the micro-perforated muffler. The characteristics of the periodic structure are very useful for the design of the periodic micro-perforated mufflers. By selecting an appropriate periodic distance, these characteristics can contribute to the control of lower frequency noise within a broader frequency range and achieve higher transmission loss around the resonant frequency.

5.4 Summary

This chapter presents a detailed examination of the acoustic attenuation of a periodic array of micro-perforated tube mufflers. Owing to its sub-millimeter perforation, the micro-perforated muffler can provide considerable sound attenuation for duct noise without using absorptive materials. When such mufflers are loaded periodically in a duct, the periodic structure produces peculiar dispersion characteristics in the overall transmission loss.

The periodic distance has an important effect on the sound attenuation performance. The combination of the Bragg reflection due to the periodic structure and the resonance of the micro-perforated muffler can result in different transmission loss. The theoretical results fit well with the FEM simulation and the experimental data. This study indicates that the length of the periodic cell can influence the sound attenuation performance of micro-perforated mufflers.

Compared to a single micro-perforated muffler, the proposed periodic placement of micro-perforated mufflers can provide lower frequency noise control within a broader frequency range or enhance transmission loss around the resonant frequency. The periodic structure provides a way of modifying the transmission loss of the single micro-perforated muffler by inserting uniform ducts provided that the space is not limited and has a potential application in muffler design.

Chapter 6

Conclusion and Suggestions for Future Work

6.1 Conclusion

The effects of the periodic arrangement on the transmission loss of the mufflers including the simple expansion chamber muffler and the micro-perforated muffler have been investigated in this thesis. The attenuation performance of the periodic mufflers is different from the single muffler and the effects of the distance between periodic mufflers has a potential application in muffler design. The theoretical study has been validated with finite element method and experiments carried out at The Hong Kong Polytechnic University.

First of all, the side branch resonator muffler has been investigated. The side branch elements attached to ducts are very common devices for suppressing tonal noise in ductwork system. The sound energy is conserved and the energy is distributed among the duct and the side branch depending on the relative impedances of the junctions. The side branch resonator functions at the frequencies where the impedance of the side branch is relatively low and the side branch is equivalent to a short circuit which suppressing the sound power transmitted to the downstream duct. The performance of the side branch Helmholtz resonator is given with the lumped-parameter model from the existing literature. The performance of the resonator is fixed once the resonator is made. In order to adapt to the environmental changes, a semi-active resonator via the control of the termination impedance of the resonator is used. A theoretical study is conducted to investigate the effect of flow on the semi active Helmholtz resonator in a low Mach number flow duct.

Secondly, a Helmholtz resonator with a spiral neck is proposed. The performance of the Helmholtz resonator is restricted with its geometries including the cross sectional area and the length of the neck and the volume of the cavity. The resonator will be bulky when the lower frequency noise is required to be controlled. In order to make the neck as long as possible, a spiral duct takes the place of the traditional short neck of the HR. The curved structure lengthens the neck without requiring a large space. The wave propagation in the spiral duct neck is analyzed and the acoustic impedance formulated based on the transfer matrix method. The results show that the resonance frequency of the HR can be reduced by using the spiral neck, which has potential applications in tonal noise control in a limited space. More turns for the spiral neck can shift the resonance frequency much lower. Apart from its low-frequency performance, the proposed resonator also has several resonance frequencies at higher frequencies because of its long neck.

Thirdly, a theoretical study of the acoustic attenuation of periodic expansion chamber mufflers has been conducted. The expansion chamber muffler is an effective device for noise reduction in duct systems. The transmission loss of the single expansion muffler has a periodic character that is often used for the periodic noise control. The use of multiple mufflers is often a way used to improve the sound attenuation performance of the mufflers. When the mufflers are periodically mounted on the duct, the transmission loss of the periodic mufflers is determined by the characteristics of both the muffler itself and the periodic structure. The Bloch wave theory and the transfer matrix method are used to study the wave propagation in periodic expansion chamber mufflers and the dispersion characteristics of periodic expansion chamber mufflers. The influence of the distance between periodic expansion chamber mufflers has been investigated. The theory is validated against finite element method simulation. Compared to a single expansion chamber muffler, the stopbands of the finite periodic structure is mainly due to its dispersion characteristics of the Bloch wave. With different configuration, the results indicate that the periodic structure can enhance the transmission loss within a narrower frequency range or change effective noise control frequency ranges with different distance between mufflers. Investigation of the influence of the distance between periodic mufflers has revealed that when the distance between mufflers is the same as the length of the expansion chamber, the transmission loss of periodic expansion chamber mufflers has the same period in frequencies and is largely enhanced within a narrowed frequency range. For other cases, the transmission loss of periodic expansion chamber mufflers is no longer a periodic function and the frequencies of peak transmission loss change with different distance between periodic mufflers. In general, unlike with a single expansion chamber muffler, the stopbands of the periodic structure are mainly due to the dispersion characteristics of the Bloch waves. A different configuration can enhance the transmission loss within a narrow frequency range or shift the stopbands. The study on the wave propagation in such periodic structures provides how the periodic structure influences the performance of the mufflers which can contribute to the design of the periodic mufflers.

Finally, the wave propagation in the periodic micro-perforated mufflers has been investigated. Because of the high acoustic resistance and low mass reactance due to the sub-millimeter perforation, the micro-perforated muffler can provide considerable sound attenuation of duct noise. The wave propagation in periodic micro-perforated mufflers is studied theoretically, numerically and experimentally. The periodic distance has an important effect on the sound attenuation performance. The micro-perforation is studied based on the plane wave assumption in both the duct and the outer chamber. The impedance model proposed by Maa is used to relate the sound pressure between the two sides of the micro-perforation and then the transfer matrix of the periodic micro-perforated muffler is derived. The theoretical results agree well with the FEM simulation and the experiment. In the experiment. the transmission loss of the three periodic micro-perforated mufflers was measured with the two-load method. This study indicates that the combination of the Bragg reflection due to the periodic structure and the resonance of the micro-perforated muffler can result in different transmission loss. The proposed periodic placement of micro-perforated mufflers can provide lower frequency noise control within a broader frequency range or enhance transmission loss around the resonant frequency. The periodic structure provides a way of modifying the transmission loss of the single micro-perforated muffler by inserting uniform ducts provided that the space is not limited and has a potential application in muffler design.

6.2 Suggestions for Future Work

On the basis of the present studies, future theoretical and experimental work are recommended as follows:

1. The chapter on the Helmholtz resonator with a spiral neck could develop a more accurate model of the spiral neck. In the present work, the spiral neck is modeled as a straight duct with equivalent cross sectional area and length and it is effective when the plane wave assumption is satisfied. In other cases, if the wave in the spiral neck is not a plane wave, the present model is not applicable. Besides, an experimental work is required to be compared with the theory and the FEM simulation.

2. This thesis only provides a study of the effect of periodic arrangement on the mufflers under plane wave assumption. However, in practice, higher-order modes effect cannot be neglected. Because of the larger cross sectional area than the inlet

duct, the higher-order modes can be excited at the expansion chamber even the frequency is below the cut-off frequency of the inlet duct. Therefore, the wave propagation in the periodic mufflers should take into account the higher-order mode effects.

3. Flow effect should be considered to investigate the effect of the periodic arrangement of the mufflers. Flow is inevitable in heating, ventilating and air conditioning system. Therefore, wave propagation of the periodic mufflers under flow condition can be investigated and compared with that under no flow condition.

4. This thesis has only considered the periodic arrangement of one type muffler such as the expansion chamber muffler of the micro-perforated muffler. A study of the periodic arrangement of two or more types mufflers may be considered in future work.

References

[1] M. L. Munjal, *Acoustics of ducts and mufflers with application to exhaust and ventilation system design* (Wiley, New York, 1987).

[2] P. M. Morse, "The transmission of sound inside pipes," J. Acoust. Soc. Am. **11**(2), 205-210 (1939).

[3] R. Scott, "The propagation of sound between walls of porous material," Proceedings of the Physical Society **58**(4), 358 (1946).

[4] D. D. Davis Jr, G. M. Stokes, D. Moore, and G. L. Stevens Jr, "Theoretical and experimental investigation of mufflers with comments on engine-exhaust muffler design," NACA Report No. 1192, (1954).

[5] S. H. Ko, "Theoretical analyses of sound attenuation in acoustically lined flow ducts separated by porous splitters (rectangular, annular and circular ducts)," J. Sound Vib. **39**(4), 471-487 (1975).

[6] B. Nilsson and O. Brander, "The propagation of sound in cylindrical ducts with mean flow and bulk-reacting lining I. modes in an infinite duct," IMA Journal of Applied Mathematics **26**(3), 269-298 (1980).

[7] A. Cummings and I. J. Chang, "Sound attenuation of a finite length dissipative flow duct silencer with internal mean flow in the absorbent," J. Sound Vib. **127**(1), 1-17 (1988).

[8] K. S. Peat, "A transfer matrix for an absorption silencer element," J. Sound Vib. **146**(2), 353-360 (1991).

[9] C.-N. Wang, "Numerical decoupling analysis of a resonator with absorbent material," Appl. Acoust. **58**(2), 109-122 (1999).

[10] R. J. Astley and A. Cummings, "A finite element scheme for attenuation in ducts lined with porous material: comparison with experiment," J. Sound Vib. **116**(2), 239-263 (1987).

[11] K. S. Peat and K. L. Rathi, "A finite element analysis of the convected acoustic wave motion in dissipative silencers," J. Sound Vib. **184**(3), 529-545 (1995).

[12] A. F. Seybert, R. A. Seman, and M. D. Lattuca, "Boundary element prediction of sound propagation in ducts containing bulk absorbing materials," J. Vib. Acoust. **120**(4), 976-981 (1998).

[13] A. Selamet, I. J. Lee, and N. T. Huff, "Acoustic attenuation of hybrid silencers," J. Sound Vib. **262**(3), 509-527 (2003).

[14] T. D. Rossing, *Springer handbook of acoustics* (Springer, New York, 2007).

[15] F. J. Fahy, *Foundations of engineering acoustics* (Academic Press, New York, 2000).

[16] D. A. Bies and C. H. Hansen, *Engineering noise control: theory and practice* (CRC Press, New York, 2009).

[17] G. W. Stewart, "Influence of a branch line upon acoustic transmission of a conduit," Physical Review **26**(5), 688 (1925).

[18] G. W. Stewart, "Acoustic transmission with a Helmholtz resonator or an orifice as a branch line," Physical Review **27**(4), 487 (1926).

[19] U. Ingard, "On the theory and design of acoustic resonators," J. Acoust. Soc. Am.

25(6), 1037-1061 (1953).

20 M. Alster, "Improved calculation of resonant frequencies of Helmholtz resonators," J. Sound Vib. **24**(1), 63-85 (1972).

21 P. K. Tang and Sirignan.Wa, "Theory of a generalized Helmholtz resonator," J. Sound Vib. **26**(2), 247-262 (1973).

22 R. L. Panton and J. M. Miller, "Resonant frequencies of cylindrical Helmholtz resonators," J. Acoust. Soc. Am. **57**(6), 1533-1535 (1975).

23 R. C. Chanaud, "Effects of geometry on the resonance frequency of Helmholtz resonators," J. Sound Vib. **178**(3), 337-348 (1994).

24 R. C. Chanaud, "Effects of geometry on the resonance frequency of Helmholtz resonators .2.," Journal of Sound and Vibration **204**(5), 829-834 (1997).

25 P. Lueg, *Process of silencing sound oscillations*, 1936, US Patent 2,043,416.

26 H. F. Olson and E. G. May, "Electronic sound absorber," J. Acoust. Soc. Am. **25**(4), 829 (1953).

27 W. Conover, "Fighting noise with noise," Noise control **2**(2), 78–82 (1956).

28 K. Eghtesadi and H. G. Leventhall, "Active attenuation of noise - the chelsea dipole," J. Sound Vib. **75**(1), 127-134 (1981).

29 M. A. Swinbanks, "The active control of sound propagation in long ducts," J. Sound Vib. **27**(3), 411-436 (1973).

30 M. J. M. Jessel and Mangiant.Ga, "Active sound absorbers in an air duct," J. Sound Vib. **23**(3), 383-& (1972).

31 G. Canevet, "Active sound absorption in an air conditioning duct," J. Sound Vib.

58(3), 333-345 (1978).

[32] B. Widrow, J. R. Glover, Jr., J. M. McCool, J. Kaunitz, C. S. Williams, R. H. Hearn, J. R. Zeidler, Eugene Dong, Jr., and R. C. Goodlin, "Adaptive noise cancelling: principles and applications," Proceedings of the IEEE **63**(12), 1692-1716 (1975).

[33] J. C. Burgess, "Active adaptive sound control in a duct: a computer simulation," J. Acoust. Soc. Am. **70**(3), 715-726 (1981).

[34] G. Chaplin and R. Smith, "Waveform synthesis-the essex solution to repetitive noise and vibration," in *Inter-noise 83. Proceedings of 1983 International Conference on Noise Control Engineering*, Edinburgh, UK (1983).

[35] A. Roure, "Self-adaptive broadband active sound control system," J. Sound Vib. **101**(3), 429-441 (1985).

[36] L. Eriksson, M. Allie, and R. Greiner, "The selection and application of an IIR adaptive filter for use in active sound attenuation," Acoustics, Speech and Signal Processing, IEEE Transactions on **35**(4), 433-437 (1987).

[37] W. Neise and G. H. Koopmann, "Reduction of centrifugal fan noise by use of resonators," J. Sound Vib. **73**(2), 297-308 (1980).

[38] J. S. Lamancusa, "An actively tuned, passive muffler system for engine silencing," in *Proceedings of Noise-Con 87*, The Pennsylvania State University, PA (1987).

[39] T. Izumi and T. Narikiyo, "Muffler system controlling the volume of resonant cavity," Trans Acoust Soc Japan **46**, 479-485 (1990).

[40] T. Izumi, H. Takami, and T. Narikiyo, "Muffler system controlling an aperture neck of a resonator," Journal of the Acoustical Society of Japan **47**(9), 647-652 (1991).

[41] H. Matsuhisa, B. S. Ren, and S. Sato, "Semiactive control of duct noise by a volume-variable resonator," Jsme International Journal Series III-Vibration Control Engineering Engineering for Industry **35**(2), 223-228 (1992).

[42] S. Sato and H. Matsuhisa, "Semi-active noise control by a resonator with variable parameters," in *Inter-noise 90; Proceedings of the International Conference on Noise Control Engineering*, Goteborg, Sweden (Aug. 13-15 1990).

[43] J. M. deBedout, M. A. Franchek, R. J. Bernhard, and L. Mongeau, "Adaptive-passive noise control with self-tuning Helmholtz resonators," J. Sound Vib. **202**(1), 109-123 (1997).

[44] K. Nagaya, Y. Hano, and A. Suda, "Silencer consisting of two-stage Helmholtz resonator with auto-tuning control," J. Acoust. Soc. Am. **110**(1), 289-295 (2001).

[45] S. J. Estève and M. E. Johnson, "Adaptive Helmholtz resonators and passive vibration absorbers for cylinder interior noise control," J. Sound Vib. **288**(4-5), 1105-1130 (2005).

[46] Y. Okamoto, H. Bodén, and M. Åbom, "Active noise control in ducts via side - branch resonators," J. Acoust. Soc. Am. **96**(3), 1533-1538 (1994).

[47] C. Radcliffe and C. Birdsong, "An electronically tunable resonator for noise control," in *Proceedings of the 2001 Noise and Vibration Conference*, (2001).

[48] M. Utsumi, "Reduction of noise transmission in a duct by termination impedance control of a sidebranch resonator," J. Vib. Acoust. **123**(3), 289-296 (2001).

[49] J. Yuan, "Active Helmholtz resonator with positive real impedance," J. Vib. Acoust. **129**(1), 94-100 (2007).

[50] D. Zhao and A. S. Morgans, "Tuned passive control of combustion instabilities using multiple Helmholtz resonators," J. Sound Vib. **320**(4-5), 744-757 (2009).

[51] S. Singh, C. Howard, and C. Hansen, "Tuning a semi-active Helmholtz resonator," in *ACTIVE 2006*, Adelaide, Australia (2006).

[52] H. Kook, L. Mongeau, and M. A. Franchek, "Active control of pressure fluctuations due to flow over Helmholtz resonators," J. Sound Vib. **255**(1), 61-76 (2002).

[53] C. E. Bradley, "Time harmonic acoustic Bloch wave propagation in periodic waveguides. Part I. Theory," J. Acoust. Soc. Am. **96**(3), 1844-1853 (1994).

[54] C. E. Bradley, "Time harmonic acoustic Bloch wave propagation in periodic waveguides. Part II. Experiment," J. Acoust. Soc. Am. **96**(3), 1854-1862 (1994).

[55] N. Sugimoto and T. Horioka, "Dispersion characteristics of sound waves in a tunnel with an array of Helmholtz resonators," J. Acoust. Soc. Am. **97**(3), 1446-1459 (1995).

[56] X. Wang and C. M. Mak, "Wave propagation in a duct with a periodic Helmholtz resonators array," J. Acoust. Soc. Am. **131**(2), 1172-1182 (2012).

[57] X. Wang and C. M. Mak, "Acoustic performance of a duct loaded with identical resonators," J. Acoust. Soc. Am. **131**(4), EL316-EL322 (2012).

[58] D. J. Mead and A. S. Bansal, "Mono-coupled periodic systems with a single disorder: Free wave propagation," J. Sound Vib. **61**(4), 481-496 (1978).

[59] J. N. Munday, C. B. Bennett, and W. M. Robertson, "Band gaps and defect modes in periodically structured waveguides," J. Acoust. Soc. Am. **112**(4), 1353-1358 (2002).

[60] X. Wang and C.-M. Mak, "Disorder in a periodic Helmholtz resonators array," Appl. Acoust. **82**(0), 1-5 (2014).

[61] K. U. Ingard, *Notes on acoustics* (Infinity Science Press, Hingham, Massachusetts, 2008).

[62] D. P.O.A.L, "Practical flow duct acoustics," J. Sound Vib. **124**(1), 91-115 (1988).

[63] A. Cummings, "The effects of grazing turbulent pipe-flow on the impedance of an orifice," Acta Acustica United with Acustica **61**(4), 233-242 (1986).

[64] *COMSOL 4.3a, Acoustics Module Application Library Manual*, 2012.

[65] A. Selamet and I. Lee, "Helmholtz resonator with extended neck," J. Acoust. Soc. Am. **113**(4), 1975-1985 (2003).

[66] A. Selamet, M. B. Xu, I.-J. Lee, and N. T. Huff, "Helmholtz resonator lined with absorbing material," J. Acoust. Soc. Am. **117**(2), 725-733 (2005).

[67] C. J. Nederveen, "Influence of a toroidal bend on wind instrument tuning," J. Acoust. Soc. Am. **104**(3), 1616-1626 (1998).

[68] S. Felix, J.-P. Dalmont, and C. J. Nederveen, "Effects of bending portions of the air column on the acoustical resonances of a wind instrument," J. Acoust. Soc. Am. **131**(5), 4164-4172 (2012).

[69] J. S. Lamancusa, "The transmission loss of double expansion chamber mufflers with unequal size chambers," Appl. Acoust. **24**(1), 15-32 (1988).

[70] A. Selamet, F. D. Denia, and A. J. Besa, "Acoustic behavior of circular dual-chamber mufflers," J. Sound Vib. **265**(5), 967-985 (2003).

[71] Z. Tao and A. F. Seybert, "A review of current techniques for measuring muffler

transmission loss," (2003).

[72] M. L. Munjal, *Acoustics of ducts and mufflers*. 2nd ed (Wiley, New York, 2014).

[73] D. Y. Maa, "Theory and design of microperforated panel sound-absorbing constructions," Sci. China Math. **18**(1), 55-71 (1975).

[74] C. Wang, L. Cheng, J. Pan, and G. Yu, "Sound absorption of a micro-perforated panel backed by an irregular-shaped cavity," J. Acoust. Soc. Am. **127**(1), 238-246 (2010).

[75] P. Cobo, J. Pfretzschner, M. Cuesta, and D. K. Anthony, "Hybrid passive–active absorption using microperforated panels," J. Acoust. Soc. Am. **116**(4), 2118-2125 (2004).

[76] T. Bravo, C. Maury, and C. Pinhède, "Vibroacoustic properties of thin micro-perforated panel absorbers," J. Acoust. Soc. Am. **132**(2), 789-798 (2012).

[77] C. N. Wang, "Numerical decoupling analysis of a resonator with absorbent material," Appl. Acoust. **58**(2), 109-122 (1999).

[78] D. Y. Maa, "Potential of microperforated panel absorber," J. Acoust. Soc. Am. **104**(5), 2861-2866 (1998).

[79] F. Asdrubali and G. Pispola, "Properties of transparent sound-absorbing panels for use in noise barriers," J. Acoust. Soc. Am. **121**(1), 214-221 (2007).

[80] M. Q. Wu, "Micro-perforated panels for duct silencing," Noise Control Eng. J. **45**(2), 69-77 (1997).

[81] L. Xiang, S. Zuo, M. Zhang, J. Hu, and G. Long, "Study of micro-perforated tube mufflers with adjustable transmission loss," J. Acoust. Soc. Am. **134**(5), 4217-4217

(2013).

[82] A. Selamet, I. Lee, Z. Ji, and N. Huff, "Acoustic attenuation performance of perforated absorbing silencers," SAE Technical Paper 2001-01-1435 (2001).

[83] A. Selamet, M. B. Xu, I. J. Lee, and N. T. Huff, "Analytical approach for sound attenuation in perforated dissipative silencers," J. Acoust. Soc. Am. **115**(5), 2091-2099 (2004).

[84] J. W. Sullivan and M. J. Crocker, "Analysis of concentric‐tube resonators having unpartitioned cavities," J. Acoust. Soc. Am. **64**(1), 207-215 (1978).

[85] S. Allam and M. Åbom, "A new type of muffler based on microperforated tubes," J. Vib. Acoust. **133**(3), 031005-031005-8 (2011).

[86] X. N. Wang, Y. S. Choy, and L. Cheng, "Hybrid noise control in a duct using a light micro-perforated plate," J. Acoust. Soc. Am. **132**(6), 3778-3787 (2012).

[87] Y. Liu, Y. S. Choy, and Y. K. Chiang, "Performance of multiple micro-perforated panels in a duct," in *Proceedings of Internoise 2014*, Melbourne, Australia (2014).

[88] ASTM E2611-09 Standard test method for measurement of normal incidence sound transmission of acoustical materials based on the transfer matrix method (American Society for Testing and Materials, Philadelphia, 2009)